Measurement of the Charge Asymmetry in the Decay $K_L^o \to \pi \mu \nu$

Contents

Measurement of the Charge Asymmetry in the Decay $K_L^o \to \pi \mu \nu$

Robert Lane McCarthy

November 1971

ABSTRACT

If $\Gamma_\pm$ = Rate($K_L^o \to \pi^\mp \mu^\pm \nu$), the $K_{\mu 3}^o$ charge asymmetry is defined to be $\delta = (\Gamma_+ - \Gamma_-)/(\Gamma_+ + \Gamma_-)$. This number has been measured to be $(2.1 \pm 1.0) \times 10^{-3}$ at the Lawrence Berkeley Laboratory's Bevatron. The error is meant to be interpreted as one standard deviation and contains both a statistical and a systematic contribution. The systematic contribution is a measure of the accuracy with which a neutron-induced background has been excluded.

I. Introduction - The Physical Meaning of ε

Prior to the writing of this dissertation, in the fall of 1971, CP violation[1] has been observed in only one system in nature, the neutral K meson system. This system consists[2] of a particle-antiparticle pair K^0 and $\bar{K}^0$. These states are defined to be the eigenstates of strangeness of eigenvalue +1 and -1, and in fact strangeness is the only quantum number differentiating them. Hence, the non-conservation of strangeness in weak interactions makes the neutral K meson system unique in nature for it allows particle and antiparticle to communicate virtually.

$$K^0 \rightleftarrows \pi\pi \rightleftarrows \bar{K}^0$$

This communication in turn implies that K^0 and $\bar{K}^0$ are not states with definite lifetimes.[3] Instead the particle states of the K meson system (states with definite lifetimes) must be superpositions of K^0 and $\bar{K}^0$. If CP were rigorously conserved, the K meson states with definite lifetimes would necessarily be eigenstates of CP.[4] Hence they would be:

$$|K_1^0\rangle = \frac{1}{\sqrt{2}}\left(|K^0\rangle + |\bar{K}^0\rangle\right) \qquad CP = +1$$

$$|K_2^0\rangle = \frac{1}{\sqrt{2}}\left(|K^0\rangle - |\bar{K}^0\rangle\right) \qquad CP = -1$$

This was believed to be the case before 1964. The short-lived component of the neutral K meson was found to decay to two pions ($CP = +1$)[5] and was therefore thought to be K_1^0. This meant that the long-lived component was K_2^0 with $CP = -1$. But in 1964

---

[1] For definition of the operators C and P see Appendix 1.

[2] We assume there is no third K meson.

[3] M. Gell-Mann and A. Pais, "Behavior of Neutral Particles under Charge Conjugation," Phys. Rev. 97, 1387 (1955).

[4] This statement is not obvious. It is proved in Appendix 2. Note that it is not true for CPT.

[5] See Appendix 1.

Christenson et. al.[6] discovered that the long-lived component also decayed to two pions. This is a violation of CP. Hence it was necessary to consider the possibility that this violation occurs in the neutral K meson states themselves, i.e. that the particle states are not eigenstates of CP but rather the CP mixtures

$$|K_S^o\rangle = \frac{1}{\sqrt{1 + |\varepsilon|^2}} (|K_1^o\rangle + \varepsilon|K_2^o\rangle)$$

$$|K_L^o\rangle = \frac{1}{\sqrt{1 + |\varepsilon|^2}} (|K_2^o\rangle + \varepsilon|K_1^o\rangle)$$

where S and L denote the short-lived and long-lived components. These superpositions are the most general ones consistent with CPT invariance.[7] Thus ε is the CP mixture parameter of the neutral K meson particle states and $|\varepsilon|$ represents the amount of CP violation in these states.

Two other important CP parameters are defined as follows:

$$\eta_{+-} \equiv \frac{\langle \pi^+\pi^- |H_w| K_L^o\rangle}{\langle \pi^+\pi^- |H_w| K_S^o\rangle} \simeq \varepsilon + \varepsilon'$$

$$\eta_{oo} \equiv \frac{\langle \pi^o\pi^o |H_w| K_L^o\rangle}{\langle \pi^o\pi^o |H_w| K_S^o\rangle} \simeq \varepsilon - 2\varepsilon'$$

The approximate expressions for η_{+-} and η_{oo} in terms of ε and ε' were first pointed out by Wu and Yang.[8] One can grasp the significance of ε' by considering the case in which $\varepsilon = 0$ and hence in which there is no CP violation in the neutral K meson states. Then the observed CP violation in the $\pi\pi$ decays would be entirely due to the decay interaction Hamiltonian.

---

[6] Christenson, Cronin, Fitch and Turlay, "Evidence for the 2π Decay of the K_2^o Meson," Phys. Rev. Lett. 13, 138 (1964).

[7] T. D. Lee and C. S. Wu, Chapter 9: "Decays of Neutral K Mesons," in Annual Review of Nuclear Science, Palo Alto, 1966, Vol. 16, P. 524.

[8] T. T. Wu and C. N. Yang, "Phenomenological Analysis of Violation of CP Invariance in Decay of K^o and $\bar{K}^o$," Phys. Rev. Lett., 13, 380 (1964).

In this case, if one defines $\eta_{+-} \equiv \varepsilon'$, then one can show using isotopic spin invariance of the strong interactions that $\eta_{oo} = -2\varepsilon'$. So ε' represents the contribution of the decay Hamiltonian to the CP violation in $K_L^o \to \pi\pi$.

On the other hand, if the decay interaction is CP invariant then from the definition of K_L^o and K_S^o (since only K_1^o can decay to $\pi\pi$)

$$\eta_{+-} = \eta_{oo} = \varepsilon \qquad\qquad \varepsilon' = 0$$

These equations hold for any theory which predicts that the entire CP violation resides in the neutral K meson states. This is true in particular of the superweak theory of Wolfenstein in which the source of CP violation is postulated to be a new interaction, much weaker than even weak interactions.[9]

Our experiment is designed to measure the real part of ε via δ_μ the $K_{\mu 3}^o$ charge asymmetry.

$$\text{If} \quad \Gamma_\pm \equiv \text{Rate}\ (K_L^o \to \pi^\mp \mu^\pm \nu)$$

$$\text{then} \quad \delta_\mu = \frac{\Gamma_+ - \Gamma_-}{\Gamma_+ + \Gamma_-}$$

A similar definition holds for the electronic charge asymmetry. Then for $\ell = \mu$ or e, assuming that these leptonic decays proceed by first order weak interaction only and that this interaction is CPT invariant, one can show that

$$\delta_\ell = 2\,\mathrm{Re}\varepsilon \left\{ \frac{1 - |x_\ell|^2}{|1 - x_\ell|^2} \right\}$$

where $x_\ell = 0$ if the $\Delta S = \Delta Q$ rule holds in weak interactions.[10] A nonzero x_ℓ is the mechanism by which the $K_{\mu 3}^o$ and K_{e3}^o charge

---

[9] L. Wolfenstein, "Violation of CP Invariance and the Possibility of Very Weak Interactions," Phys. Rev. Lett., 13, 562 (1964).

[10] See Appendix 3 for a derivation and discussion of this expression for δ_ℓ as well as a definition of x_ℓ.

asymmetries could differ. However, the factor $\frac{1 - |x_e|^2}{|1 - x_e|^2}$ has been measured for the electronic decay to be $.96 \pm .05$.[11] If the $\Delta S = \Delta Q$ rule is valid this factor is 1 and

$$\delta_\ell = 2 \, \mathrm{Re}\varepsilon$$

In this case if the CP violation is entirely in the K meson state

$$\delta_\ell = 2 \, |\eta_{+-}| \cos (\arg \eta_{+-})$$

and we can predict the value of the charge asymmetry using the measured values[12, 13]

$$|\eta_{+-}| = (1.92 \pm .05) \times 10^{-3}$$

$$\arg \eta_{+-} = (45.2 \pm 4.0)^\circ$$

Inserting these values we find

$$\delta_\ell = (2.71 \pm .20) \times 10^{-3}$$

if the $\Delta S = \Delta Q$ rule holds and the CP violation is entirely in the neutral K meson states.

The superweak theory predicts[13] that

---

[11] Bennett at. al., "$K_S - K_L$ Regeneration Amplitude in Copper at 2.5 Gev/c and Phase of η_{+-}," Physics Letters, 29B, 317 (1969).

[12] $|\eta_{+-}| = (1.92 \pm .05) \times 10^{-3}$ from A. Barbaro-Galtieri et. al., Rev. Mod. Phys., 42, 87 (1970). This is a world average. Best value is $|\eta_{+-}| = (1.91 \pm .06) \times 10^{-3}$ from Fitch et. al., "Studies of $K_2^\circ \to \pi^+ \pi^-$ Decay and Interference," 164, 1711 (1967).

[13] $\mathrm{Arg}\, \eta_{+-} = (45.2 \pm 4.0)^\circ$ from Aronson et. al., "Precise Determination of the $K_L - K_S$ Mass Difference By the Gap Method," Phys. Rev. Lett., 25, 1057 (1970). This paper also gives

$$\tan^{-1} 2\Delta m \tau_S = (43.2 \pm 0.4)^\circ = (\arg \varepsilon)_{\text{superweak}}$$

where Δm is $(K_L^\circ - K_S^\circ)$ mass difference and τ_S is the K_S° lifetime.

$$\arg \eta_{+-} = \arg \varepsilon = (43.2 \pm 0.4)^{\circ}$$

The fact that this number is consistent with the measured value of $\arg \eta_{+-}$ is strong evidence in support of the superweak theory. If we insert this number for $\arg \eta_{+-}$ in the above calculation we find that

$$\delta_{\ell} = (2.80 \pm .07) \times 10^{-3}$$

if the superweak postulate and the $\Delta S = \Delta Q$ rule are both valid.

II. DESIGN OF THE EXPERIMENT

A. Beam

Our experiment was located at the end of the second channel of the external proton beam at the Bevatron. We normally took about 6×10^{11} protons per Bevatron pulse on a 5-inch copper target. Our neutral beam (see Figure 1) was defined by our first collimator to have a solid angle of approximately 0.2 millisteradians about the production angle of 7^{o}. The first collimator was four feet long and had horizontal faces made of brass, but vertical faces made of uranium. It commenced 51 in. from the target. The second and third collimators followed at 153 in. and 177 in. from the target and were respectively 24 in. and 57 in. long. They were made entirely of brass. All three collimators were tapered such that the rear two collimators were in the shadow of the first collimator.

Charged particles were swept from the beam by four sweeping magnets. The first magnet was actually a steering magnet for the external proton beam and was situated between the target and the first collimator. Its field integral was typically 400 kilogauss-inches. The remaining three sweeping magnets were placed as indicated on Figure 1. Their field integrals were 865, 200, and 250 kG-in. All magnets were oriented such that they swept protons to the east. Shielding filled the volume outside the beam line (to a distance of at least eight feet from the beam) from the upstream edge of the second collimator to the experimental area. The first ten feet of this shielding was iron. The remainder (about fifteen feet) was concrete.

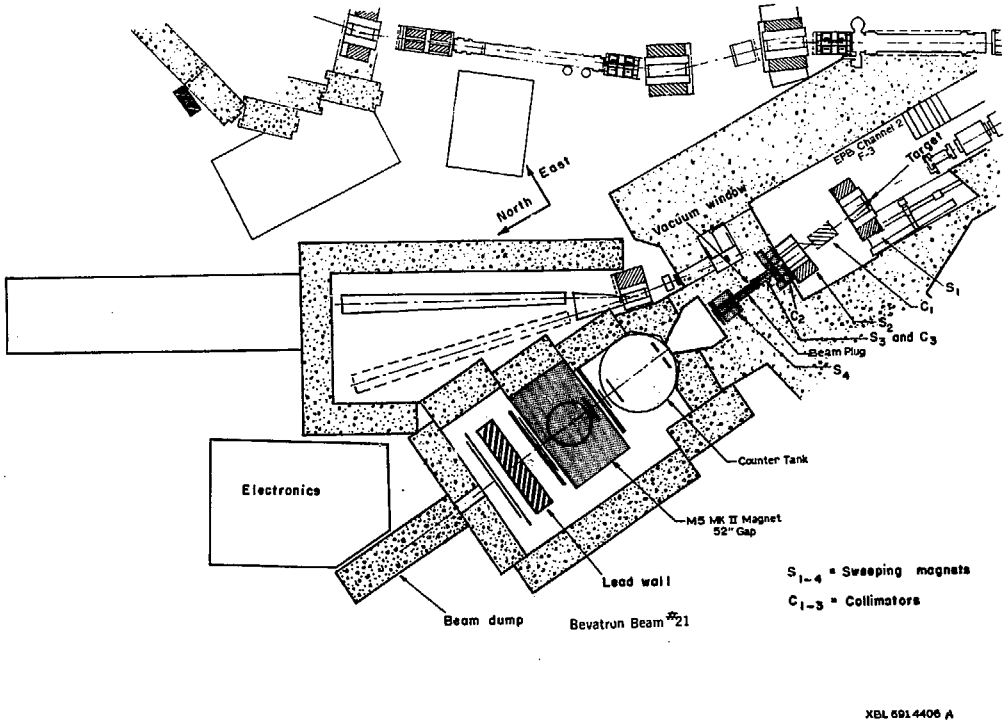
East
North
Vacuum window
EPB Channel 2
F-3
Target
S_1
C_1
C_2
S_2
S_3 and C_3
Beam Plug
S_4
Counter Tank
Electronics
M5 MK II Magnet
52" Gap
Lead wall
Beam dump
Bevatron Beam #21
S_{1-4} = Sweeping magnets
C_{1-3} = Collimators
XBL 6914406 A

Figure 1

B. Counters and Their Functions

The detection apparatus consisted of 154 scintillation counters monitored by a PDP-9 computer. The important counter banks are labeled in Figure 2. K_L^o decays were identified by an up-down coincidence of the large trigger counters labeled P situsted outside the neutral beam. The $K_{\mu 3}^o$ component of these decays was identified by filtering muons from pions through the use of a 24-inch-thick lead wall. Muons were required to traverse the lead wall and count in banks L and M. In addition, the muons traversed 2 in. of steel just downstream of the T counters and 2 in.of steel between banks L and M. Those muons reaching the N bank traversed a third 2 in.steel plate. However, the N bank was not required for a $K_{\mu 3}^o$ signature. The system was up-down symmetric. The muon could be up with the pion down or vice versa.

The system was designed to accept most of the $K_{\mu 3}^o$ decays which had a vertex in the decay volume and produced a muon with sufficient momentum to penetrate the lead wall, but yet also produced both a muon and a pion with sufficient transverse momentum to get out of the beam (i.e. cross over the beamside edge of the appropriate P counter). In order to accept these muons the counter banks increased dramatically in size from the upstream end of the experiment to the downstream end (see Figures 2, 3, and 4). This progression culminated in the L and M banks which had active areas of 8 feet (height) by 14 feet (width). A Monte Carlo calculation shows that we succeeded in accepting 95% of these muons. The Monte Carlo also shows that the P counters

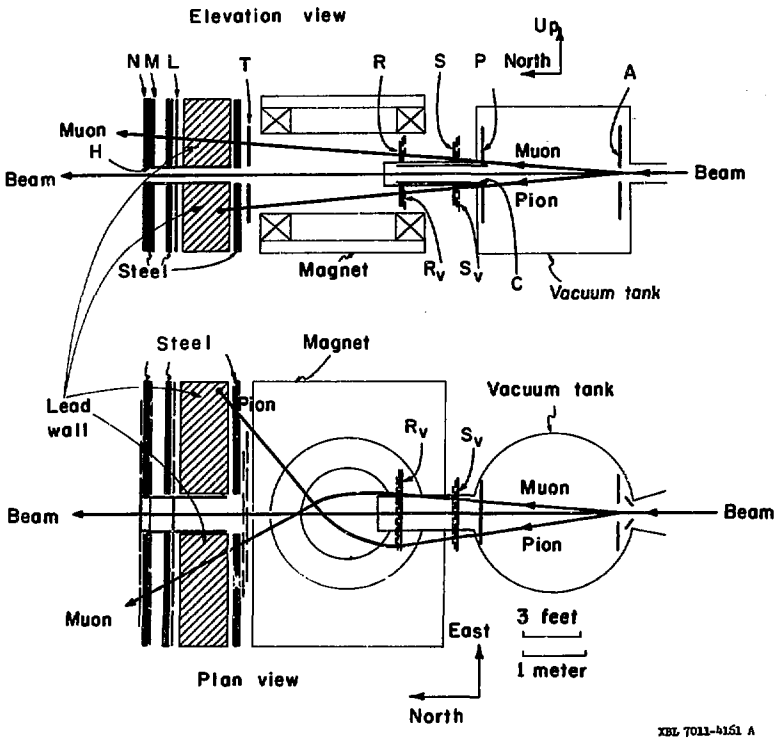
Elevation view
Up
North
N M L
T
R
S
P
A
Muon
H
Beam
Muon
Beam
Pion
Steel
Magnet
R_v
S_v
C
Vacuum tank
Steel
Magnet
Lead wall
Pion
Vacuum tank
R_v
S_v
Muon
Beam
Beam
Pion
Muon
East
3 feet
1 meter
Plan view
North
XBL 7011-6151 A

Figure 2

S-R-T BINNING

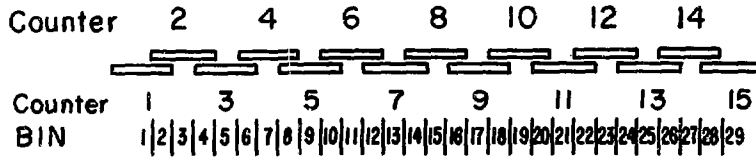

BINNING CRITERIA

EVEN BINS: BIN 14 IS ON IF AND ONLY IF COUNTERS 7 AND 8 ARE ON

ODD BINS: BIN 13 IS ON IF AND ONLY IF COUNTER 7 IS ON BUT COUNTERS 6 AND 8 ARE OFF

DETAILS

ALL DIMENSIONS IN INCHES

BANK IS UP OR DOWN

Bank	Number of Counters	Number of Bins	Height of Counter	Width of Counter	Thickness of Counter	Width of Bin
S	13	25	12	4.5	.25	1.5
R	15	29	15	4.5	.25	1.5
T	8	15	25	18	.50	6

XBL 7110-4581

Figure 3

W BINNING

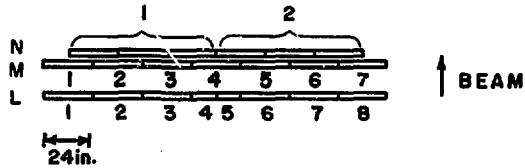

W BIN REQUIREMENTS

W	L ON	LMN BINS M ON	N ON		L ON	LM BINS M ON	N OFF	W
	Required	*Required*	*Required*		*Required*	*Required*	*Required*	
				STRAIGHT				
1	1	1	1		1	1	1	23
2	2	2	1		2	2	1	24
3	3	3	1		3	3	1	25
4	4	4	1		4	4	1,2	26
5	5	4	2		5	4	1,2	27
6	6	5	2		6	5	2	28
7	7	6	2		7	6	2	29
8	8	7	2		8	7	2	30
				DIVERGING				
9	2	1	1		2	1	1	31
10	3	2	1		3	2	1	32
11	4	3	1		4	3	1	33
12	5	5	2		5	5	2	34
13	6	6	2		6	6	2	35
14	7	7	2		7	7	2	36
				CONVERGING				
15	1	2	1		1	2	1	37
16	2	3	1		2	3	1	38
17	3	4	1		3	4	1	39
18	4	4	2		8	4	2	40
19	5	4	1		7	5	2	41
20	6	4	2		8	6	2	42
21	7	5	2					
22	8	6	2					

EACH BANK 48 IN. HIGH X .5 in. THICK

UP AND DOWN BANKS BUTTED TOGETHER TO FORM SOLID SURFACES
EXCEPT HOLE CUT FOR BEAM 24 in. HIGH X 48 in. WIDE

XBL7110-4583

Figure 4

were large enough to accept about 90% of the above pions. Thus the expected muon track would contain P, S, R, T, L, M and perhaps N counts. The pion, however, could indicate its presence by a lone P count or, if it stayed close to the beam, it might produce counts further downstream.

The charge-resolving magnet was named the M5. It had circular pole faces 63 in. in diameter and a gap of 52 in. The field pointed up or down. The M5 was run at ±1300 amperes with a typical field integral of 670 kG-in. and thus imparted a typical transverse momentum of 500 Mev/c to particles passing through it. Since the maximum transverse momentum a muon can acquire in $K^{o}_{\mu 3}$ decay is 216 Mev/c, negatively charged muons were given a complete angular separation from positively charged muons. One method of charge determination was simply to observe whether the position of the muon at the L bank was east or west of the center of the bank. In the absence of multiple scattering in the lead wall this method of charge determination would have been completely unambiguous. But because of the multiple scattering, we decided to determine the charge also by looking at the direction of the muon curvature in the M5. This determination was accomplished via the S, R and T banks. The method used to bin the muon position in the S, R and T banks is depicted in Figure 3. Similar information is presented for the L, M and N banks in Figure 4. For the purpose of binning, the L, M and N banks form one logical bank which we will call W.

An unpleasant fact of life in a neutral beam at the Bevatron is that the ratio of high energy neutrons to long-lived K mesons is large——on the order of two hundred to one. In order to

avoid contamination of our K sample by neutron interactions, all mass was removed from our neutral beam in the region accepted by our trigger counters. The geometrical details are illustrated in Figure 5. The vertical beam profile is indicated showing both the umbra and our large penumbra which was a result of the necessity of collimating close to the target. The anti counter (labeled A in Figure 2) was actually a set of six counters which acted as a shield against charged particles coming from upstream. It was logically equivalent to a single large counter with a hole in it slightly bigger than the beam. The vertical separation of the upper and lower portions is indicated on Figure 5 along with the positions of the P counters. An event was accepted only if counts were observed in both P counters but not in the anti counter. Thus, an event originating at a vertex must have originated downstream of the intersection of the two lines L_1 and L_2 defined by the edges of the A and P counters. In this manner, our decay volume was defined without putting any mass into the beam. The geometrical details of the A and P counters are also presented in Figure 5.

The entire decay volume was held at vacuum (typically 10^{-5} atmospheres). The beam passed into the vacuum through a thin window (.01 in. aluminum) just downstream of the last sweeping magnet. As indicated by Figure 1, eighty-eight inches downstream of the vacuum window but ten inches upstream of the beginning of our acceptance (intersection of L_1 and L_2 in Figure 5) our vacuum chamber was broadened horizontally to include the entire horizontal dimension of our acceptance, outside of the beam as well as in the beam. Hence with two exceptions which will be described

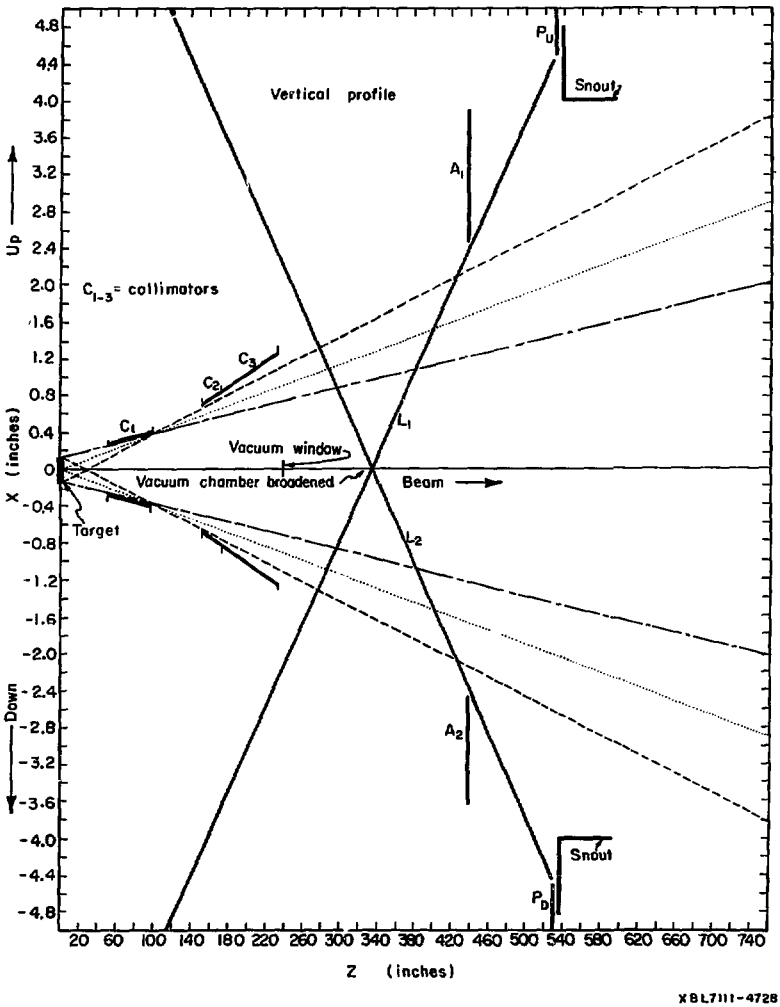

XBL7111-4728

Figure 5a

Geometry of A and P counters (inches)

Counters	Height	Width	Thickness	Defining apertures (separation of 2 counters) Vertical	Horizontal
A_1 and A_2	22	17	0.5	4.75	—
A_3 and A_4	40	22	0.5	--	—
A_5 and A_6	24	12	0.25	—	12.0
P_U and P_D	22.5	45	0.5	9.0	—

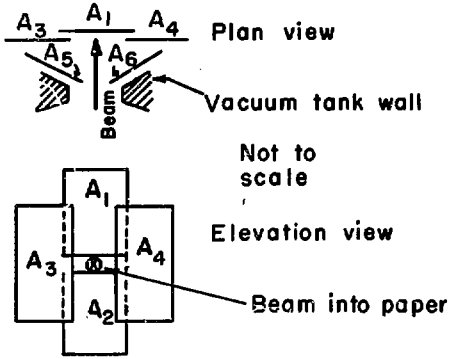

XBL7111-4731

Figure 5b

shortly, we are confident that all vertices which we accepted originated in vacuum. Figure 5 also shows that any single track which originated in the collimator and was accepted must have exited the last collimator at a depth greater than one inch into the collimator face. We note that two such tracks, if correlated and not forming a vertex but converging from deep within opposite faces of the collimator, could have fooled our trigger system. A calculation[14] based on the measured rate for a single muon track leads us to believe such events are negligible (less than 10^{-4} of our total number of events).

The S_V and R_V Counters shown on Figure 2 were installed to give us some vertical resolution. Their geometry is presented in Figure 6. For events in which the pion reached the R bank we were able to use these vertical resolution counters in conjunction with the S and R banks to reconstruct the decay vertices. Each vertex position was taken to be at the point of closest approach of muon and pion trajectories. If extra counters were on, the combination with the smallest distance of closest approach was used. Figure 7b shows the distributions of the horizontal and vertical distances of closest approach. The vertical resolution was much better than the horizontal resolution because the muon and pion were diverging vertically but not necessarily horizontally. Also, effects of the magnetic field between the S and R banks were neglected even for the pions, thus causing further deterioration of the horizontal resolution. These curves suggest that the longitudinal resolution was about ±20 in. in the decay volume. Figure 7a shows the vertex distribution. Due to randoms and scattering

[14] See Appendix 4 for the calculation.

Geometry of S_V and R_V counters (inches)
for up and down counters

Counters	Height	Width	Thickness
S_{V1}	2.5	40	0.5
2	4.5	40	0.25
3	4.5	40	0.25
4	3.5	40	0.25
R_{V1}	2.5	48	0.5
2	4.5	48	0.25
3	7.0	48	0.25
4	7.0	48	0.25

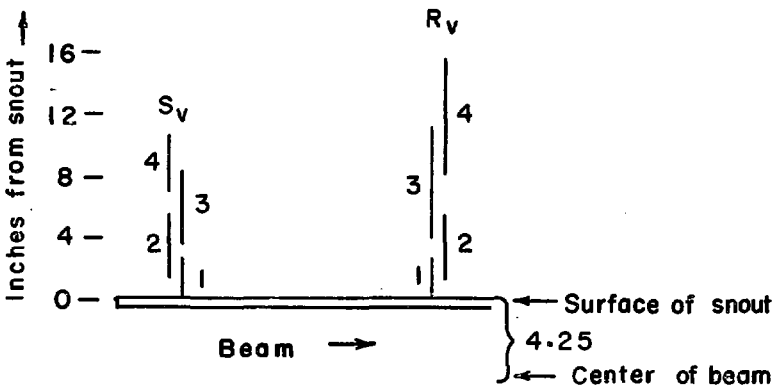

XBL7111-4729

Figure 6

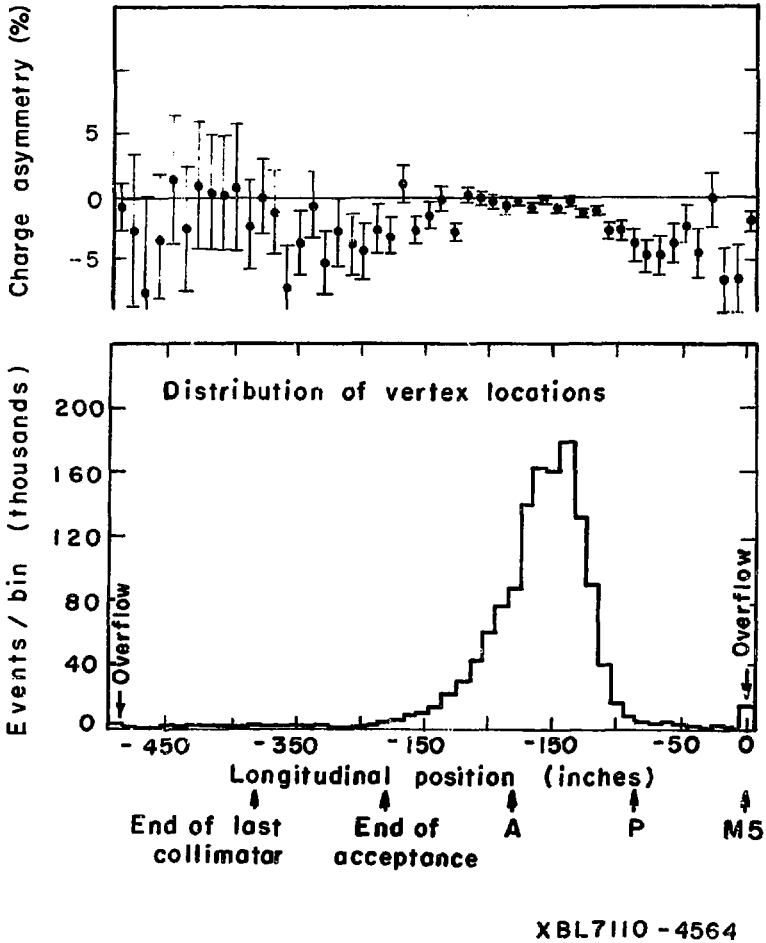
Charge asymmetry (%)
5
0
-5
Distribution of vertex locations
Events / bin (thousands)
200
160
120
80
40
0
Overflow
Overflow
-450
-350
-150
-150
-50
0
Longitudinal position (inches)
End of last collimator
End of acceptance
A
P
M5
XBL7110-4564

Figure 7a

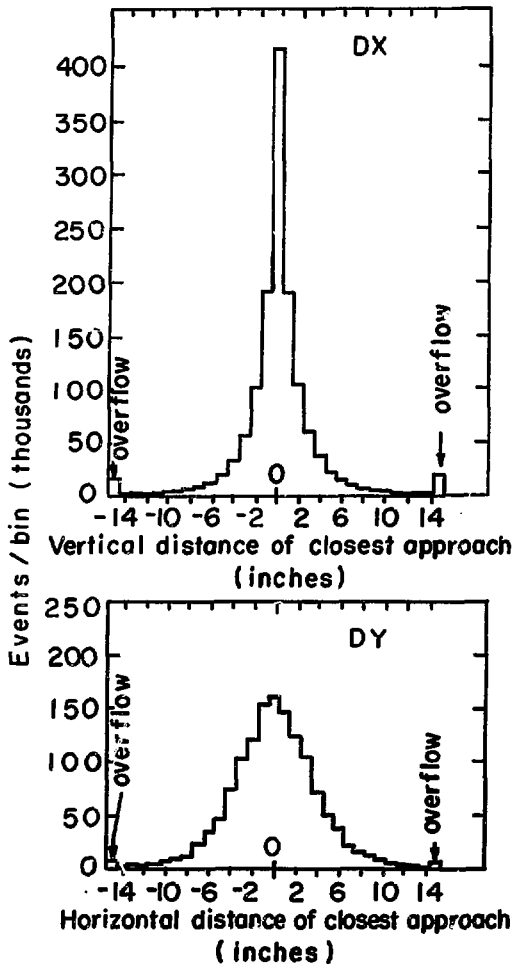

XBL7110-4563

Figure 7b

on the pion side, we expect the long tail extending upstream. Thanks to the pion interactions we also expect these events to have a charge asymmetry. But we note that the events upstream of -300 in. only change the charge asymmetry of the whole sample by 3×10^{-4}. Hence the vertex distribution supports our contention that the upstream acceptance is well understood. We note again, however, that only the events with the pion reaching the R bank are included in this plot which is discussed further in IV-C.

As indicated on Figure 2, the A and P counters were entirely contained in a cylindrical vacuum tank. The tank was 10 feet in diameter and 10 feet high. The beam entered the tank from the upstream vacuum system through a large rectangular hole, the sides of which were well outside the A-P acceptance. In order to keep neutron interactions as far as possible from the P counters the beam was brought out of the vacuum tank into a vacuum snout which extended well into the M5. The walls of the snout were .25 in. aluminum but they had exterior ribs in order to withstand the vacuum load. The internal dimensions were 8 in. (height) by 22 in. (width). The vacuum window on the downstream end of the snout was .025 in. aluminum. The decay products accepted by the A-P system exited from the vacuum tank through an aluminum plate 1.75 in. thick which also supported the snout.

The two flaws in the trigger system mentioned earlier will now be discussed. First, neutrons in the halo around the beam could have interacted in the anti counter itself. If the charged particles emanating from such an interaction were produced sufficiently close to the downstream counter edge, they would not have traveled far enough in the counter to count. Hence, the event would have

been accepted by the A-P system if these charged particles had counted in both P's. The correction for this effect will be discussed in IV-C-4. The second flaw in the above trigger system is that it does not take into account neutron backscatter. Specifically, halo neutrons could have interacted in the walls of the snout and sprayed low energy particles backward into both P counters. In order to measure the number and charge asymmetry of such events we lined the horizontal walls of the snout with counters, one up and one down. We also placed counters below P_{up} and above P_{down} to detect interactions in the P's themselves. The geometry of these guard counters labeled C is presented in Figure 8. Note that for a neutron interaction to have backscattered from the snout into both P's, both an upper C and a lower C must have counted. This is true also if the interaction occurred in a C counter. (The possibility of C counter inefficiency will be discussed later.) The two S_V counters nearest the beam also turned out to be quite useful in detecting neutron interactions.

After leaving the snout, the neutral beam passed into a bag of helium which extended through a hole in the lead wall to a point about three feet downstream of the N counters. Here the neutral beam entered a shielded air passage way which extended to a point twenty feet downstream of the N counters where the neutrons were dumped into uranium blocks. The L, M and N counters were well shielded from this beam dump.

The hole in the lead wall allowed us to get rid of the neutral beam in a reasonably clean manner but also opened a path by which pions could penetrate the lead wall. In order to get rid of some of these pions, the hole in the wall was lined with a steel beam

Geometry of C counters

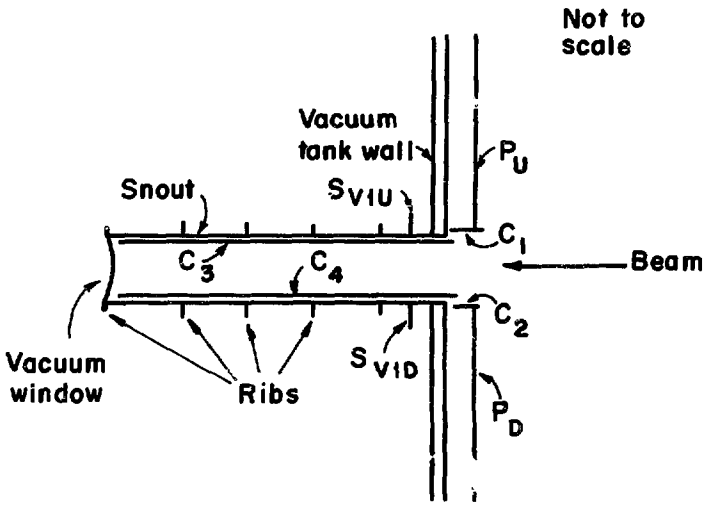

Counters	Length	Width	Thickness
C_1 and C_2	525	38	0.250
C_3 and C_4	48	22	0.375

XBL7111-4730

Figure 8a

Geometry of H counters

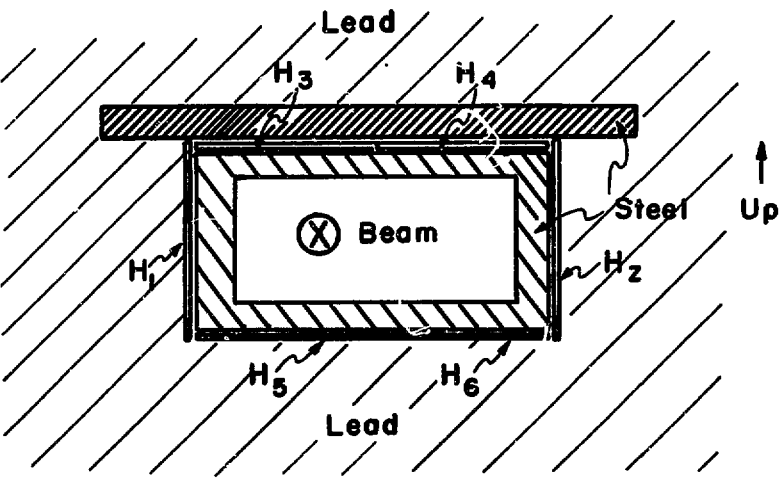

Dimensions (inches)

Counters	Length	Width	Thickness
H_{1-2}	44	21.5	0.5
H_{3-6}	44	18.0	0.5

H counters extended from 2 in downstream of upstream lead wall surface to the M bank

XBL7111-4732

Figure 8b

conduit which extended from 4 in. upstream of the start of the lead wall, through the wall and holes in the L,M, and N banks, and into the shielding wall downstream of the N counters. The conduit had horizontal walls 3 in. thick and vertical walls 4 in. thick. Then the conduit in turn was lined with counters in order to detect the remaining particles passing through the conduit. These counters are labeled H. Their geometry is also described in Figure 8.

All of the A,P, and C counters were run in vacuum. This presented a development problem since normal tube bases break down at low pressures due to the increased mean free path of an electron. We tried various potting compounds unsuccessfully but finally arrived at a solution by putting the phototubes and tube bases in sealed containers and attaching these containers to the outside air via tygon tubing.

Just before and after taking data the beam line and crucial vertical positions of the A and P counters were surveyed. The beam line was found to be in order and the A and P positions were correct $\pm 1/32$ in. The S,R,T,S_V, and R_V positions were measured also before and after data-taking to an accuracy of $\pm$ 1/8 in. The L,M, and N positions were surveyed only before taking data but are believed to be correct to $\pm$ 1/4 in.

C. Electronics

The electronics system used for this experiment has been described elsewhere.[15] Only an abbreviated description will be presented here. The basic component of our system was the MECL (Motorola Emitter Coupled Logic) system developed at the Lawrence Berkeley Laboratory. Figure 9 shows the treatment of a typical counter under this system. The photomultiplier anode signal was first discriminated and then, if it survived discrimination, stretched to a uniform 20±1 nanoseconds. The ECR bit then determined whether the pulse from the counter was to proceed or not. During the tuning phases of the experiment this bit could be controlled either manually or by the computer. It was very useful for diagnostic purposes. However, during the data-taking phase, the information from each counter was always allowed to proceed. After the ECR gate two pulses were produced for use in the fast external logic. One such use was the formation of a pulse called the prompt strobe (Fig. 10) which signified that the event under consideration had passed our acceptance criteria on the counter banks upstream of the lead wall. Only when such a strobe was generated did counter information get stored. A third pulse following the ECR gate for a typical counter was then sent into a coincidence

---

15 R.M.Craven et al., "An On-Line Scintillation Counter Control System", UCRL-20635, Lawrence Berkeley Laboratory internal report, to be published.

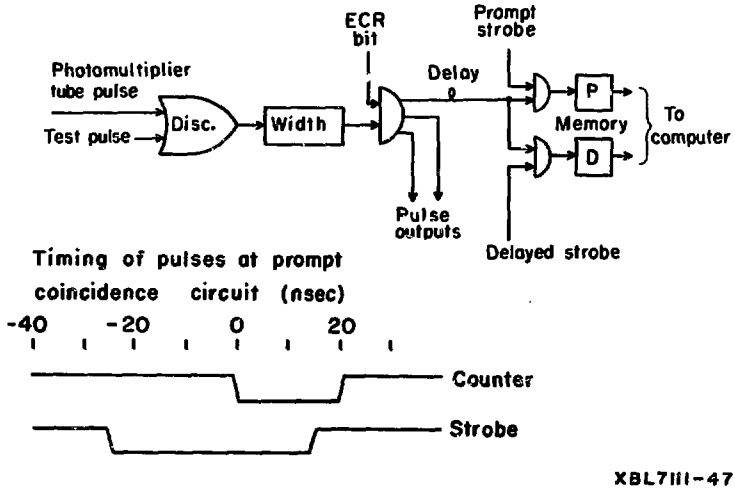
ECR
bit
Prompt
strobe
Photomultiplier
tube pulse
Delay
Test pulse
Disc.
Width
P
Memory
To
computer
D
Pulse
outputs
Delayed strobe
Timing of pulses at prompt
coincidence circuit (nsec)
-40
-20
0
20
Counter
Strobe
XBL7111-4733

Figure 9

circuit versus the prompt strobe. The resulting bit of information, whether or not the counter in question was on in time correlation with the prompt strobe, was then stored in the MECL memory bit for that counter.

The processing of each prompt strobe pulse took about one microsecond. Consequently, to prevent interruption of this processing, the strobe logic turned itself off for a microsecond after each output pulse. One function performed during this period was the generation of a delayed strobe pulse precisely one Bevatron revolution (403 nsec) after the prompt strobe. This delayed strobe then inquired whether or not each counter was on in random time correlation with the prompt strobe. The reason for waiting one Bevatron revolution was to insure that both time slots sampled the same beam structure. The delayed counter information was then stored in the MECL memory delayed bits.

The MECL discriminators had many advantages over commercially available discriminators. They were smaller by a factor of 10 or more in weight, volume and cost. However, they did have a deadtime. Immediately after an output pulse, the discriminator would not respond to an input pulse for 20 nsec. In the presence of a charge asymmetric random background (which we had in several banks), such an inefficiency could have been disastrous. Our solution (as indicated on Figure 9) was to use a strobe of which the leading edge arrived at the MECL coincidence circuit 25 nsec before an in-time counter. This meant that a counter pulse arriving up to 45 nsec before the in-time counter would turn on the bit for that counter. So it would make no difference that the discriminator was inefficient for an in-time counter. However,

this made the resolving time for each MECL coincidence circuit a very long 60 nsec. This meant an increase by a factor of three in random rates over the corresponding rates with a 20 nsec resolving time.

Because of this problem the C and H counters were fed into Chronetics discriminators run in a deadtimeless mode. Then for each such counter a short-resolving-time coincidence test was made versus the strobe and the output pulse was sent to the proper MECL discriminator. The A and P counters were also sent into Chronetics discriminators for the purpose of generating the strobe in a deadtimeless fashion.

A simplified diagram of the electronics appears in Figure 10. As indicated only the A, P, S, R, and T counters are involved in the strobe logic. The symbol S really stands for 26 counters, 13 up and 13 down.

The final decision as to whether or not the event causing the prompt strobe was to be recorded by the computer was made in a MECL slow logic box called the Matrix. In this box slow, cheap coincidence circuits were used on the bit information from the L, M, and N counters. In this way very complex acceptance cirteria could be used to decide whether or not a muon had penetrated the lead wall. This was useful in the tuning phases of the experiment when our random rates were high, but the final Matrix acceptance criterion turned out to be very simple. If the Matrix decided the event was accepted, it informed the PDP-9 that the event was to be read out and turned off the strobe logic for one millisecond, the time needed to transfer the data to the computer. (This time would have been much shorter if we

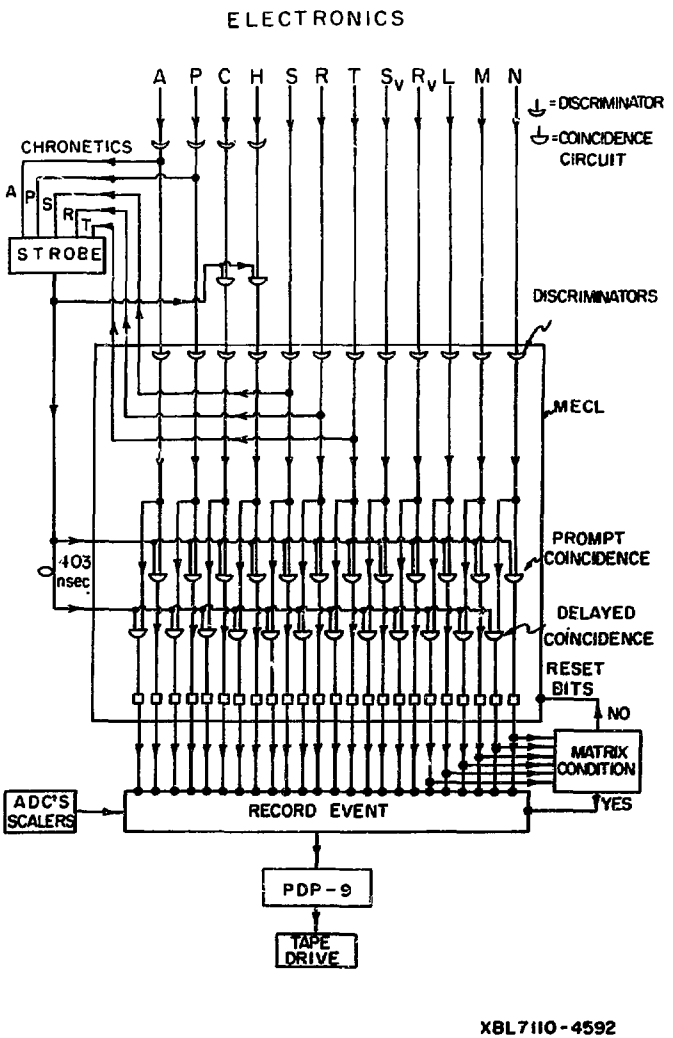
ELECTRONICS
A P C H S R T S_V R_V L M N
= DISCRIMINATOR
= COINCIDENCE CIRCUIT
CHRONETICS
A P S R T
STROBE
DISCRIMINATORS
MECL
PROMPT COINCIDENCE
403 nsec
DELAYED COINCIDENCE
RESET BITS
NO
MATRIX CONDITION
YES
ADC'S SCALERS
RECORD EVENT
PDP-9
TAPE DRIVE
XBL7110-4592

Figure 10

had not been using scalers meant for use with a typewriter.) After the event had been transferred to the computer, it was written onto magnetic tape at the end of the Bevatron pulse. If the Matrix criterion was not satisfied, the MECL bits were reset off and the strobe logic was allowed to continue looking for another event.

We will now discuss the strobe and Matrix logic, i.e., the trigger. First we define several symbols:

$\bar{A}$ = lack of an A count

$\textcircled{P}$ = P counter delayed 403 nsec

U,D = up, down

$P_U P_D$ = coincidence of P_U and P_D .

We also define the symbol OR to mean the logical-electronic operation using two bits of information to form a third such that (A OR B) is on if A is on or B is on. A similar definition applies to the symbol AND (the operation performed by a simple coincidence circuit.)

Then if

$$V_D \equiv (\bar{A}P_U P_D \quad \text{OR} \quad \textcircled{\bar{A}P_U} \; P_D)$$

$$V_U \equiv (\bar{A}P_U P_D \quad \text{OR} \quad \textcircled{\bar{A}P_D} \; P_U)$$

the prompt strobe was

$$\bar{A}V_D \; S_D \; (R_D T_D) \quad \text{OR} \quad \bar{A}V_U \; S_U \; (R_U T_U) \quad .$$

This pulse was generated by a set of Chronetics coincidence circuits as indicated by the strobe logic diagram, Figure 11. Here S_D denotes the OR of 13 S-down counters. When possible the S, R, and T counters were removed from the strobe. The only purpose of including them was to decrease the strobe rate at high beam intensities to a

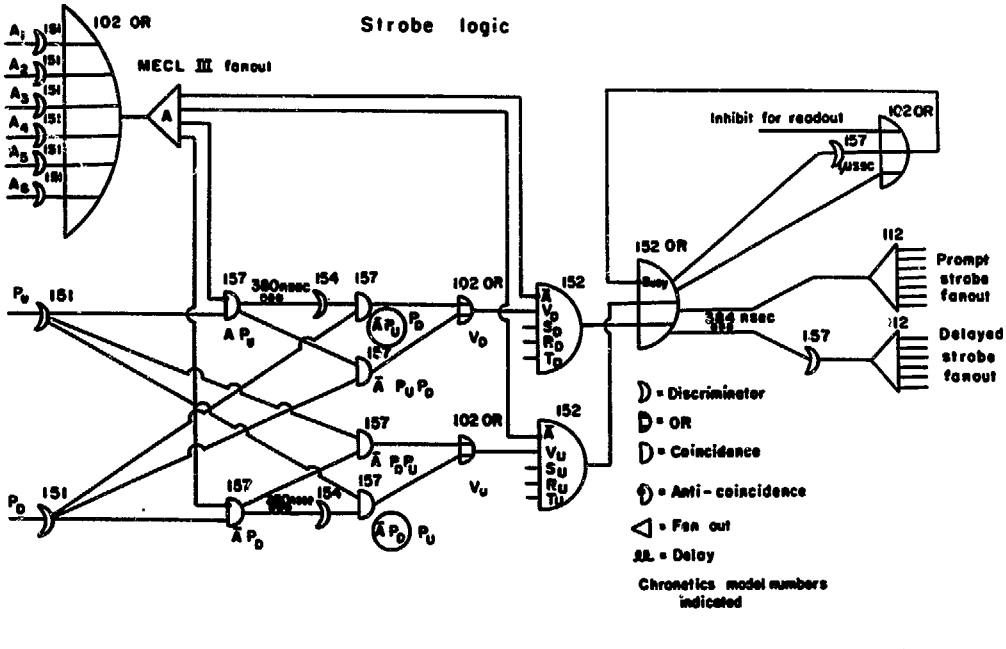
Strobe logic
102 OR
MECL III fanout
A
Inhibit for readout
102 OR
157
μsec
152 OR
Busy
112
Prompt strobe fanout
Delayed strobe fanout
380 nsec
154
157
102 OR
152
Discriminator
OR
Coincidence
Anti-coincidence
Fan out
Delay
Chronetics model numbers indicated
XBL7111—4734

Figure 11

level tolerable to our computer (110 events/pulse). By including one of these banks in the strobe we effectively caused that bank's discriminators to operate with deadtime again since they controlled the strobe. However, in the section discussing randoms we will show that since the T's were in the strobe only for a few special runs, this caused no problem. The R and T are shown in parentheses since the most common strobe only included the S's. Occasionally, however, all three banks were removed or the R's were included. The anti was included in the strobe at two stages so that prompt and delayed events could be treated symmetrically. The anti is required twice for strobes with a delayed P.

If L denotes the OR of all L counters, both up and down, then the Matrix condition was simply

LM OR (LM)

Thus the system was triggered on real events as well as on the two random configurations which we believed would be important: a muon track with a random pion P, and an $\bar{A}VS$ with a random LM signal. Note that the (LM) refers to the Matrix logic and hence the delayed MECL bits while the (AP) refers to the strobe logic. Therefore, the time slots associated with these counts differ by 806 nsec. The (LM) count occurred 403 nsec after the prompt strobe while the (AP) count occurred 403 nsec before it.

The system also contained six analog to digital converters. These were used to do pulse height analysis and time to pulse height analysis of the various counters. Each TPH analysis was done on the prompt strobe versus a selected MECL OR output. Each PHA was done on the sum of the dynode signals within a given bank. An active adder was used to form the sum for each bank. In this

way we could analyze up to 62 counters at one time. If a PHA of S_{1D} were desired, we could select events for which S_{1D} was the only S_D on. The PHA's were actually pulse area analyses, but we will follow established convention and retain the H.

Once each week the entire electronics system was tested beginning at the discriminators. The strobe logic was tested by hand with an oscilloscope and a pulser. The entire MECL system, including the Matrix, was tested under computer control using the ECR bits and an internal pulser (which produced the test pulse of Figure 9). This testing included data transfers to the computer, which checked the incoming information.

III. DATA ANALYSIS

A. General Analysis

The data from the experiment consists of approximately 200 reels of magnetic tape. The off-line analysis was done on the Lawrence Radiation Laboratory's CDC 6600 B. In the first analysis pass the raw data, MECL bit counter information, was turned into bin information and both types of data were written onto a device for mass storage of data, the IBM photodigital chipstore. This device writes with a light beam onto film chips for permanent storage. The data is in turn read with a light beam and a photomultiplier tube. With the aid of this device, we were able to scan large masses of compacted data with one computer job at a rapid rate (100,000 events/ minute of central processor time).

The $K^0_{\mu 3}$ signature required in the analysis programs was much more restrictive than the trigger requirement. The signature requirements for prompt, delayed Matrix, and delayed P events were as follows:

prompt: $\bar{A}P_D P_U S_U R_U T_U W_U$ OR $\bar{A}P_U P_D S_D R_D T_D W_D$

delayed Matrix:

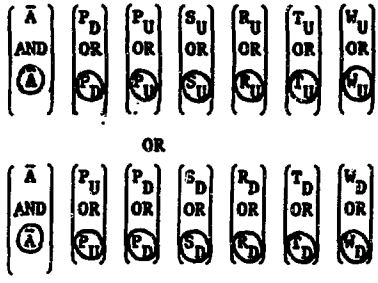

delayed P: $\bar{A}P_U S_U R_U T_U W_U$ OR $\bar{A}P_D S_D R_D T_D W_D$

Here (P_D) signifies the delayed bit of P_D. $\bar{A}$ signifies the bit which we sent to the computer telling whether or not the anti was on. Thus for a delayed Matrix event, we formed the OR of real and delayed bits for each counter (the $\bar{A}$ bit requires special treatment) before performing the same signature test as carried out on prompt events. Hence if a delayed T count was associated with a delayed W, this information was preserved. W_U signifies one of the bins of L_U, M_U and perhaps N_U liated in Figure 4.

We could not require the (P) bit for the delayed P events because actually the time slot associated with the $(\bar{A}P_D)$ count of an $(\bar{A}P_D)$ P_U prompt strobe was 403 nsec earlier than the prompt strobe. Similarly the information of which counters were on in correlation with such an $(\bar{A}P_D)$ was lost. This loss was not serious since the pion was only required once. A bit was sent to the computer telling us whether a given strobe was due to a prompt or delayed P. We used this bit to decide which signature criterion to use. In the case of delayed P events, we relied on the strobe logic to tell us that the pion P had actually been on in the proper time slot. The MECL bits were examined to determine whether an event satisfied the prompt or delayed Matrix condition.

The first pass analysis program also calculated and binned the following quantities characterizing the muon trajectory: decay angle, projected position at the anti, bend angle in the M5, and scattering angle in the lead wall. Figure 12 illustrates these calculations. The position of a muon at a given bank was

MUON TRAJECTORY CHARACTERISTICS

YA	PROJECTED POSITION AT ANTI
DKA	TANGENT OF DECAY ANGLE
SCA	TANGENT OF SCATTERING ANGLE IN LEAD WALL
BA	TANGENT OF BEND ANGLE IN MS

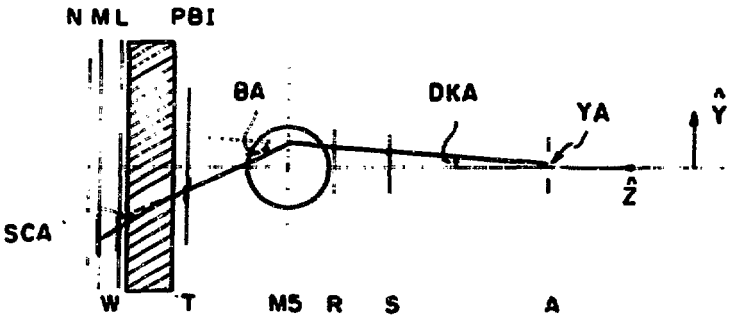

$$YMS = YS + (YR - YS) * \left(\frac{ZMS - ZS}{ZR - ZS}\right) \qquad TA = (YT - YMS)/(ZT - ZMS)$$

$$YPBI = YMS + (YT - YMS) * \left(\frac{ZPBI - ZMS}{ZT - ZMS}\right) \qquad PBA = (YW - YPBI)/(ZW - ZPBI)$$

$$YA = YR + (YR - YS) * \left(\frac{ZR - ZA}{ZR - ZS}\right)$$

$$DKA = (YR - YS)/(ZR - ZS)$$

$$SCA = (PBA - TA)/(1 + PBA * TA)$$

$$BA = (TA - DKA)/(1 + TA * DKA)$$

XBL7110-4589

Figure 12

taken to be the center of its bin in that bank. The muon decay angle was then simply the difference in R and S y-coordinates divided by the difference of R and S z-coordinates. Hence we neglected effects of the magnetic field between the R and S counters. The denominators in the expressions for the bend angle and scattering angle are due to the fact that we are actually taking the difference of tangents of angles. This factor becomes important only when the angles involved are large.

The second-pass analysis program then made cuts on all four of these quantities. Events which did not contain a muon trajectory with reasonable values of all four of them were excluded from further analysis. The first-pass analysis and a Monte Carlo calculation were used to determine the points at which to make the cuts. Figure 13 shows the distributions of these four quantities after the second pass cuts had been made. The cuts appear to be quite liberal as they must be.

Approximately 24 million events were recorded on tape during the data-taking phase. About 9 million of these events satisfied a $K^{\circ}_{\mu 3}$ signature criterion. Most of the events which failed the signature tests were randoms. The dominant type of random was of the form $\overline{\text{APPS}}$ (LM), i.e., the R and T banks (not required in the trigger) were missing. Such events are weighted twice in the above 24 million events since the random LM signal could have occurred in prompt or delayed time. These events could have been eliminated by requiring the R and T banks on the muon side in the strobe, but for reasons which we have indicated and will further discuss in Section IV-D,

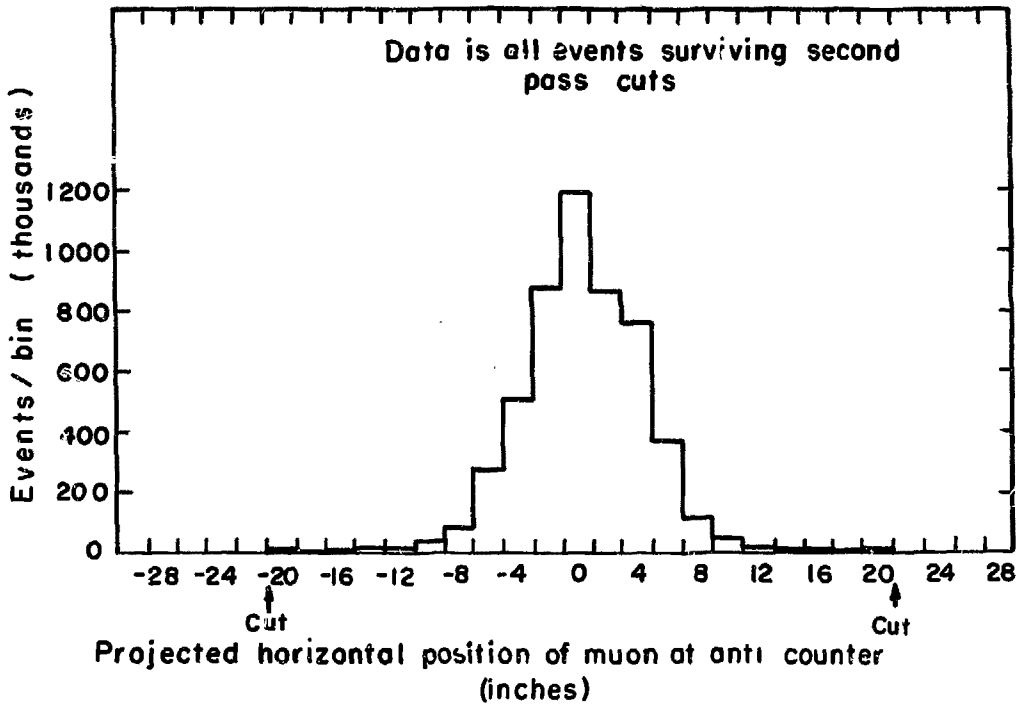

XBL7110-4579

Figure 13a

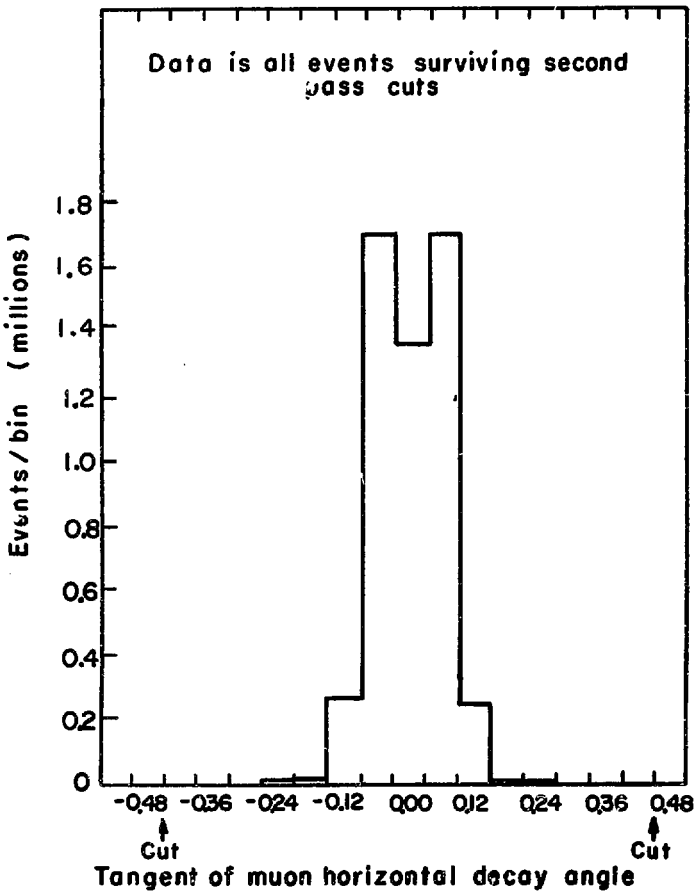
Data is all events surviving second pass cuts
Events/bin (millions)
1.8
1.6
1.4
1.2
1.0
0.8
0.6
0.4
0.2
0
-0.48 -0.36 -0.24 -0.12 0.00 0.12 0.24 0.36 0.48
Cut
Cut
Tangent of muon horizontal decay angle
XBL7110-4570

Figure 13b

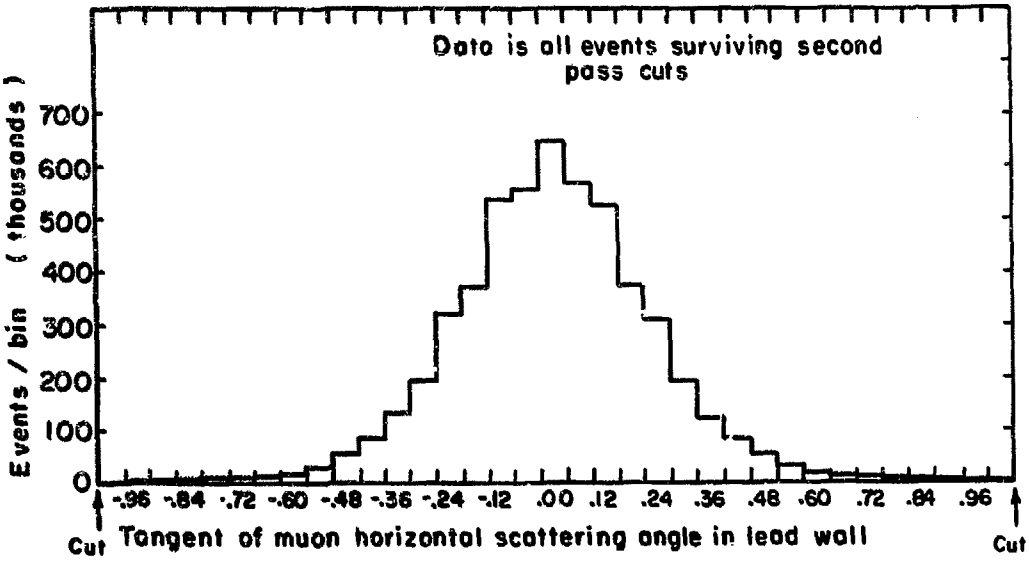

XBL7110-4569

Figure 13c.

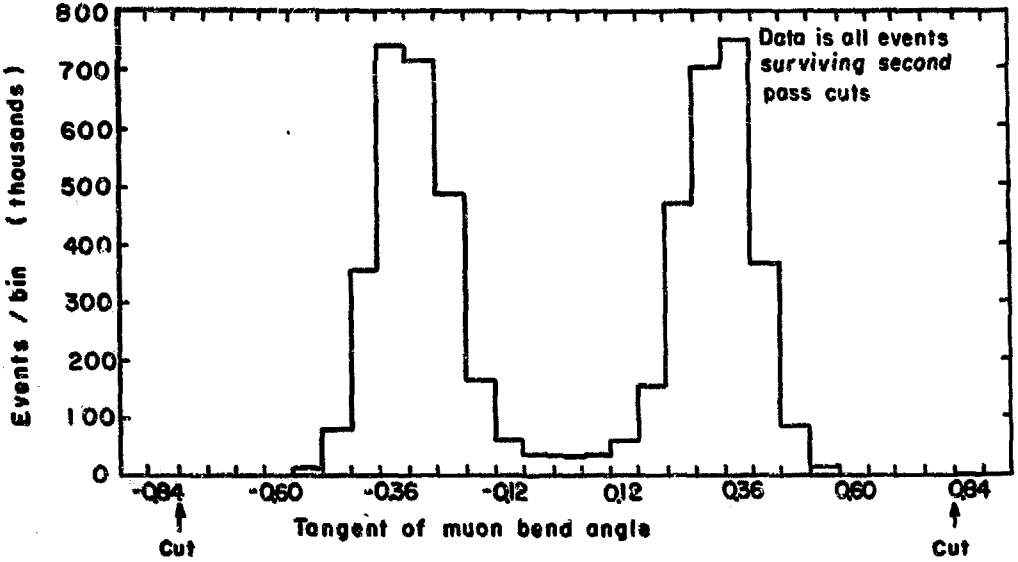

XBL7110-4568

Figure 13a

we chose to keep the strobe loose. These events were examined for any possible systematic errors introduced by their exclusion. We could find none at levels important to the experiment.

Another type of random which occurred often among the events failing the signature criteria involved L and M counts which did not line up, i.e. did not form a W bin. These events were written on tape as a result of our very lax Matrix requirement. Such events were also examined before being excluded. An interesting effect was found in this sample involving crossover events. A crossover event is one possessing an L_U and a time correlated M_D, i.e. a muon which scatters sufficiently to cross over to the pion side between the L and M banks. In a sample corresponding to 394,000 events which passed the second pass cuts 3672 prompt crossover events were found which contained 143 asymmetric events (number of μ^+ minus number of μ^-). In the same sample there were 1094 delayed Matrix and delayed P crossovers with 142 asymmetric events. Hence the change in the total charge asymmetry from excluding such events is $(0.00 \pm 0.17) \times 10^{-3}$.

It is possible for an event to be none of the three normal types - prompt, delayed Matrix, or delayed P. For example, an event might have both a prompt and a delayed P. Events which were abnormal in this manner were considered data for a second order randoms correction which we did not need to make. Hence, they were excluded from the data after the first analysis pass. They will be discussed further in the section on randoms. The number of these events was studied and is well understood

in terms of the rates for more normal events and the singles rates of various counters.

An additional 9% of the data was excluded by the second-pass cuts. Most of these excluded events were randoms, especially of the type $\bar{A}$PSRT(W) (weighted twice) where the trajectory indicated by the S, R, and T did not line up with the W bin. Only about 2% of the real events were excluded by these cuts. However, a significant number of these real events which did not point back sufficiently well to the hole in the anti counter are thought to be neutron interactions in the snout. They have a large positive charge asymmetry and will be discussed in the section dealing with beam interactions. They form the major background in this experiment. After the neutron cut (Section IV-C) the second-pass cuts only changed the charge asymmetry by -0.15 %.

The second pass analysis program also excluded events which had W bin requirements satisfied both up and down because of the consequent confusion in muon identification. In a sample corresponding to 4.4 million events which passed the second-pass cuts, 4,101 such double W events actually had a complete muon track on one side only. The asymmetry of these events, for which the muon really could be identified, was $(1.1 \pm 1.5) \times 10^{-2}$. The change in the charge asymmetry resulting from their exclusion was then $(1.0 \pm 1.5) \times 10^{-5}$, so they can be safely excluded. The true double penetration events, which contained complete tracks both up and down, will be discussed in Section IV-B.

B. Monte Carlo

The Monte Carlo program for this experiment was written in order to perform several important calculations and in general to test and enhance our understanding of the experiment. Every effort was made to make the Monte Carlo conform to reality before comparison with the data. Then comparison with the data pointed out the aspects of the experiment which we could not predict without resorting to variation of uncertain input parameters such as the K_L^o momentum spectrum.

The $K_{\mu 3}^o$ events were generated in the K meson rest frame in accordance with the V - A theory as given by Okun'.[16] K_{e3}^o events (used in the pion-decay-in-flight calculation) were generated in the same manner as $K_{\mu 3}^o$ events by merely changing the lepton mass. The form factors for these leptonic decays and the Dalitz plot for the $K_{\pi 3}^o$ decays were chosen in agreement with recent experimental information.[17,18]

The K_L^o mesons were given a momentum distribution in accord with a recent measurement at the Bevatron[19] done at a production

---

16. L. Okun', "Strange Particles: Decays", in Annual Review of Nuclear Science, Palo Alto, 1959, Vol. 9, p.89

17. For the leptonic decays we took $\lambda_+ = \lambda_- = 0.08$ and $\xi(0) = -0.26$ as is plausible from C.-Y. Chien et al., Physics Letters 33B, 627(1970).

18. For the $K_{\pi 3}^o$ decays we took $a_o = -0.257$ and $\beta_o = -0.023$ as in C. D. Buchanan et al., Physics Letters 33B, 623(1970).

19. Rolland P. Johnson, private communication. The apparatus used for this measurement is discussed in A. R. Clark et al., Physical Review Letters 26, 1667(1971).

angle of 3.7°. This spectrum was extrapolated to our production angle of 7° using a well known prescription.[20] The same prescription was used to describe the dependence of the momentum spectrum on production angle across our acceptance. Effects of the finite size of our target (12 in. x 1/4 in. x 1/4 in.) in conjunction with our collimation system were calculated in the geometrical approximation. (A K_L^o was assumed to be lost if it entered a collimator surface.) Attenuation in the copper target of both the primary protons and the K_L^o's was included with absorption lengths of 4.7 in. and 9.4 in. respectively.

Each K_L^o was then allowed to decay at a distance from the target picked in accordance with the distribution proper for its momentum. The resulting muon and pion were then Lorentz transformed from the K meson rest frame to the laboratory and propagated through the experimental apparatus. The pion was traced only as far as a P counter, but the muon was followed all the way to the M or N bank. The magnetic field was approximated by a cylindrical grid with two inch radial and vertical spacing. Muons were propagated through matter in steps of length two inches or less. In each step the energy loss was calculated using a linear approximation (correct to 2%) to a recent version[21]

---

[20] The angular dependence was assumed to be $\exp(-3.9\ P\ \theta)$ where P is the K_L^o momentum in Gev/c and Θ is the production angle, as given by George Trilling, 200 Bev Accelerator: Studies on Experimental Use 1964-1965, Vol. 1, p. 38, UCRL-16830, Lawrence Radiation Laboratory.

[21] Peter M. Joseph, "Range Energy Tables for High Energy Muons," CLNS-52, Laboratory of Nuclear Studies, Cornell University, May, 1969

of the muon energy loss tables. Energy loss straggling was also calculated at each step using linear approximations to the theory of Symon as given by Rossi.[22] This theory extrapolates between the Gaussian and Landau limiting cases. Multiple scattering was included in the Gaussian approximation using a formula also given by Rossi[23] which allows simultaneous calculation of both the resultant direction and position after traversing an absorber. Single scattering was not included for two reasons. First, for a 2 in. lead or steel absorber, calculations showed that single scattering would be swamped by the tail of the Gaussian out to scattering angles dominated by the nuclear form factor. Second, there is no known way to calculate the joint distribution of the scattered position and direction if the more complete theory is used.[24]

Approximately ten thousand $K^{o}_{\mu 3}$ events were generated with this Monte Carlo. The distributions of Figure 13 are shown again in Figure 27 after various refinements on the data. The Monte Carlo predictions for these distributions are compared with the refined data. Statistical error bars are shown for the Monte Carlo predictions only when they are bigger than the corresponding points. Agreement is good between the predicted and actual distributions of the muon projected position at the anti. The Monte Carlo was quite successful in predicting the left-right asymmetry of this distribution. It was also quite successful in predicting the distribution of the

---

22. Bruno Rossi, High Energy Particles (Prentice-Hall, Inc., Engle wood Cliffs, New Jersey,1952), p. 32

23. Ibid., p. 71

24. William T. Scott, "The Theory of Small-Angle Multiple Scattering of Fast Charged Particles", Reviews of Modern Physics 35,272(1963)

muon decay angle. However, the Monte Carlo was unable to predict the distribution of the muon scattering angle in the lead wall. Apparently a more complete multiple scattering theory is required for this purpose such as the one developed by Cooper and Rainwater.[25] In this case, as has been indicated, a correct treatment of the problem is very difficult.[26] Since the Monte Carlo seemed sufficiently accurate to do the required calculations, such a proper treatment was not attempted.

There are also some differences between the predicted and actual distributions of the muon bend angle. These differences are partially due to the Monte Carlo's underestimation of the multiple scattering. Muons with a large bend angle and hence a low momentum are more likely to stop in the lead wall due to an increase in multiple scattering than muons with higher momentum because they are nearer to the threshold momentum for penetrating the wall. They also have a longer path length in the lead since their angle of incidence is further from normal. Hence a shift of the actual data toward smaller bend angles is to be expected.

---

[25] Leon N. Cooper and James Rainwater, "Theory of Multiple Coulomb Scattering from Extended Nuclei," Phys. Rev. 97, 492 (1955)

[26] Agreement between a Monte Carlo and data has been found for a similar problem as related by Michael A. Paciotti, "Charge Asymmetry in the Muonic Decay of the K^0_2," Ph.D. dissertation, University of California, Berkeley (1970) p. 27, and private communication. However, he calculated the displacement incorrectly - directly from the scattering angle instead of using the joint distribution. He was measuring the true scattering angle defined to be the angle between initial and scattered trajectories. Hence his measurements, unlike ours, were independent of the scattered position.

Uncertainties in the K_L^o momentum spectrum may also explain the differences. However, some of the excess events in the central bins are due to neutron interactions and will be discussed in Section IV-C.

In Figure 14 we present the Monte Carlo predictions for the muon and pion momentum spectra occurring in the events we accepted. The muon spectrum is probably somewhat low as has been indicated.

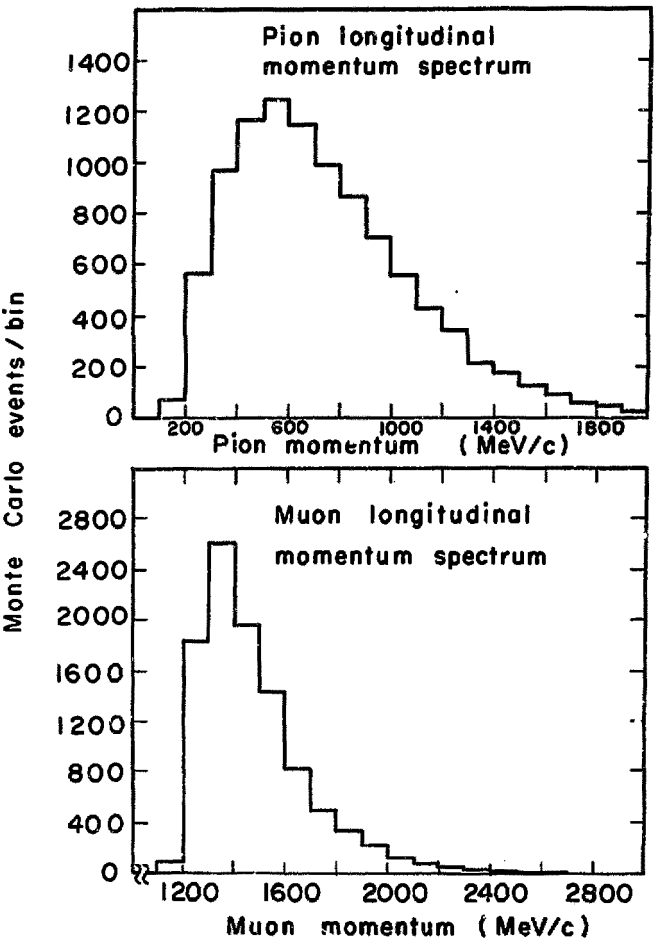

XBL7110-4566

Figure 14

IV. PROBLEMS - SOLUTIONS - CORRECTIONS

In this section we shall discuss the determination of the charge asymmetry. A correction to the charge asymmetry will be considered negligible if it is less than 10^{-4} in magnitude and error (one standard deviation). The term "good events" will be defined in part C. These events make up the relatively uncontaminated portion of our data remaining after a certain cut has been employed to free the data of neutron interactions. The term "uncorrected good events" refers to these events after the neutron cut has been made but before any other corrections have been applied (including the knock-on correction which is associated with the neutron cut).

The randoms correction is discussed in part D. In all histograms, event lists, and calculations outside of part D the delayed Matrix and delayed P random-trigger events have been subtracted(bin by bin where applicable) unless otherwise noted. This statement applies to the histograms already presented in Figure 13.

A. Experimental Technique ~ Reversal of the Magnetic Field

Frequent reversal of the charge-resolving magnetic field is the cornerstone of the experimental technique required to do this experment. We define:

$N \equiv$ total number of K_L^o which decayed to $\pi\mu\nu$ downstream of our last collimator during the experiment.

$\eta_R \equiv$ efficiency for detecting these $K_{\mu 3}^o$ events if the muon bent right.

$\eta_L \equiv$ efficiency for detecting these $K_{\mu 3}^o$ events if the muon bent left.

$N_+ \equiv$ number of $K_{\mu 3}^o$ in N having a μ^+

$N_- \equiv$ number of $K_{\mu 3}^o$ in N having a μ^-

$n_+ \equiv$ number of $K_{\mu 3}^o$ detected having a μ^+

$n_- \equiv$ number of $K_{\mu 3}^o$ detected having a μ^-

Then the true charge asymmetry in $K_{\mu 3}^o$ decays (within the statisical error on N) is

$$\delta = \frac{N_+ - N_-}{N_+ + N_-} \pm \frac{1}{\sqrt{N}}$$

If we had kept the magnetic field pointing up throughout the experiment we would have measured

$$\delta = \frac{n_+ - n_-}{n_+ + n_-} = \frac{N_+\eta_R - N_-\eta_L}{N_+\eta_R + N_-\eta_L} = \frac{\delta + a}{1 + a\delta}$$

where $$a = \frac{\eta_R - \eta_L}{\eta_R + \eta_L}$$

is the asymmetry of the efficiencies. Thus in order to have made a proper measurement we would have required that η_R equal

η_L to one part in 10^4. Geometrical alignment problems alone make such a requirement completely untenable.

Consequently we frequently reversed the magnetic field. If "↑" and "↓" denote events taken with the field up and down respectively, then

$$N^{\uparrow} + N^{\downarrow} = N$$

$$\delta^{\uparrow} = \frac{N_+^{\uparrow} - N_-^{\uparrow}}{N_+^{\uparrow} + N_-^{\uparrow}} \qquad \delta^{\downarrow} = \frac{N_+^{\downarrow} - N_-^{\downarrow}}{N_+^{\downarrow} + N_-^{\downarrow}}$$

and the measured charge asymmetry is

$$\delta_{\text{measured}} = \frac{1}{2}\left[\frac{n_+^{\uparrow} - n_-^{\uparrow}}{n_+^{\uparrow} + n_-^{\uparrow}} + \frac{n_+^{\downarrow} - n_-^{\downarrow}}{n_+^{\downarrow} + n_-^{\downarrow}}\right] = \frac{1}{2}\left[\frac{\delta^{\uparrow} + a^{\uparrow}}{1 + a^{\uparrow}\delta^{\uparrow}} + \frac{\delta^{\downarrow} - a^{\downarrow}}{1 - a^{\downarrow}\delta^{\downarrow}}\right]$$

where we have included the possibility that the efficiencies might depend upon the sign of the magnetic field. Now the δ's and a's are all less than 10^{-2}, so to an accuracy of 10^{-4} of the charge asymmetry

$$\delta_{\text{measured}} = \frac{\delta^{\uparrow} + \delta^{\downarrow}}{2} + \frac{a^{\uparrow} - a^{\downarrow}}{2} = \delta + \frac{a^{\uparrow} - a^{\downarrow}}{2}$$

since $\delta^{\uparrow}$ and $\delta^{\downarrow}$ are both equal to δ(within the small statistical error on N_+ and N_-).

The geometric bias[27] is defined to be

$$\Lambda \equiv \frac{1}{2}\left[\frac{n_+^{\uparrow} - n_-^{\uparrow}}{n_+^{\uparrow} + n_-^{\uparrow}} - \frac{n_+^{\downarrow} - n_-^{\downarrow}}{n_+^{\downarrow} + n_-^{\downarrow}}\right]$$

---

[27] This definition is in accord with J. Marx et. al., "Charge Asymmetry in K_{e3} Decay and Ree," Physics Letters, 32B, 222 (1970)

Again to an accuracy of 10^{-4} of A

$$A = \frac{\delta^{\uparrow}-\delta^{\downarrow}}{2} + \frac{a^{\uparrow} + a^{\downarrow}}{2} = \frac{a^{\uparrow} + a^{\downarrow}}{2} = a$$

the geometric bias is equal to the average asymmetry of the efficiencies.

Another expression may be used to define the measured charge asymmetry as follows:

$$\delta_{\text{measured-2}} = \frac{n_+^{\uparrow} - n_-^{\uparrow} + n_+^{\downarrow} - n_-^{\downarrow}}{n_+^{\uparrow} + n_-^{\uparrow} + n_+^{\downarrow} + n_-^{\downarrow}}$$

$$= \frac{(\delta^{\uparrow} + a^{\uparrow})N^{\uparrow} + (\delta^{\downarrow} - a^{\downarrow})N^{\downarrow}}{(1 + a^{\uparrow}\delta^{\uparrow})N^{\uparrow} + (1 - a^{\downarrow}\delta^{\downarrow})N^{\downarrow}}$$

So to an accuracy of 10^{-4} of $\delta_{\text{measured-2}}$

$$\delta_{\text{measured-2}} = \delta + \frac{a^{\uparrow} - a^{\downarrow}}{2} + \left(\frac{a^{\uparrow} + a^{\downarrow}}{2}\right)\alpha$$

$$= \delta + \frac{a^{\uparrow} - a^{\downarrow}}{2} + A\alpha$$

where $$\alpha \equiv \frac{N^{\uparrow} - N^{\downarrow}}{N^{\uparrow} + N^{\downarrow}}$$

is zero if an equal number of events are taken with the field up and down. The measured value of α is

$$\alpha_{\text{measured}} = \frac{n_+^{\uparrow} + n_-^{\uparrow} - n_+^{\downarrow} - n_-^{\downarrow}}{n_+^{\uparrow} + n_-^{\uparrow} + n_+^{\downarrow} + n_-^{\downarrow}} = \frac{\alpha + a\delta}{1 + a\alpha\delta} \simeq \alpha$$

In our experiment, for uncorrected good events,

$$A = -2.4 \times 10^{-3} \qquad \alpha = +1.0 \times 10^{-4}$$

so $$A\alpha = -2.4 \times 10^{-7}$$

and the two expressions for the measured charge asymmetry are equivalent. We will generally use the second expression in discussing the dependence of the charge asymmetry on various

parameters. It offers computational convenience and is somewhat more transparent than the first prescription since the charge asymmetry may be expressed as the ratio of the asymmetric events to the total number of events.

From the expressions for the measured charge asymmetry we can see that it is crucial that the efficiencies must not have depended on the sign of the magnetic field. A difference in the efficiency asymmetries with the field up and down enters directly into the measured charge asymmetry. There are two ways that the efficiencies might have depended on the sign of the field: via the counting efficiency of the detectors, and via the geometrical efficiency of the volume occupied by the detectors. These two possibilities will be considered in turn shortly.

The reason for reversing the magnetic field frequently is to cancel out the effect of a possible slow, long-term variation of the efficiency asymmetry. Such a variation, even if it were not correlated with the sign of the field could cause a systematic error if the field were not reversed sufficiently often. Our magnetic field was reversed approximately every 45 minutes for a total of about 600 reversals during the data-taking phase of the experiment. The runs were paired such that the beam monitor counts with the field up and with the field down were equal ±2% within each pair. The data consists of 206 such pairs in the main data sample and 81 pairs in the sample with mass added in various parts of the system to study systematic effects. Figure 15 shows the distribution of the charge asymmetry of the uncorrected good events within each pair of the main sample.

Each asymmetry is expressed as a difference from the total uncorrected charge asymmetry (5.03×10^{-3}) in units of its own statistical error, so that the distribution should approximate a Gaussian. It does so fairly well.

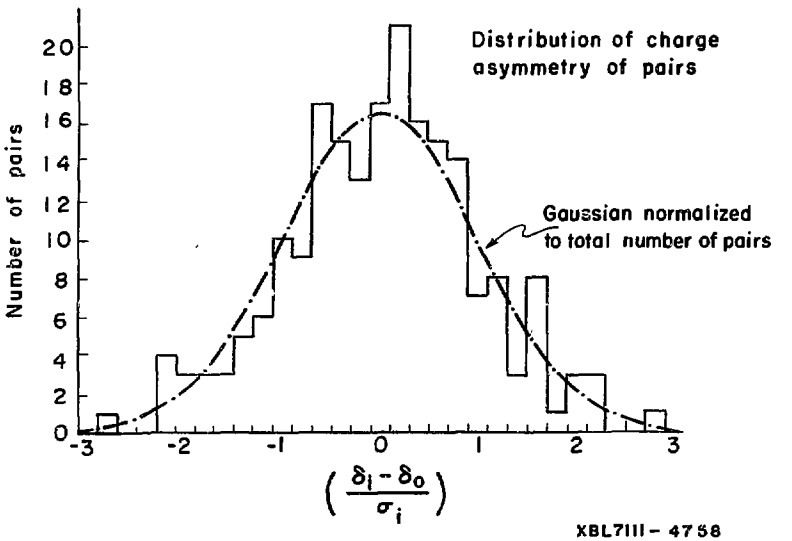
Distribution of charge asymmetry of pairs
Gaussian normalized to total number of pairs
Number of pairs
20
18
16
14
12
10
8
6
4
2
0
-3
-2
-1
0
1
2
3
$\left(\frac{\delta_i - \delta_o}{\sigma_i}\right)$
XBL7111-4758

Figure 15

1. Counting Efficiency

A major advantage of having performed this experiment with counters rather than spark chambers is that we were able to measure our counting efficiency very accurately and can state that it did not change with the magnetic field reversals to an accuracy of one part in 10^4. All counters in the A,P,S,R,T,L, M,N, and H banks were tested in an auxiliary beam of 2.8 Gev/c π^- before their use in the main experiment. Each counter was placed in the π^- beam in the midst of four smaller counters, two on each side, which formed a telescope. A counter was deemed inefficient for a given π^- if all four members of the telescope counted but the counter in question did not. Each counter had its high voltage set at a level such that the inefficiency at the worst spot on the counter was less than 10^{-4} with the output pulse attenuated by a safety factor of two. After the high voltage level was set for each counter, an oscilloscope photograph was taken of the anode pulse for minimum-ionizing particles.

During the data-taking phase of the experiment the counter pulse heights were periodically monitored visually with an oscilloscope. In order to decrease the random rates of the counters behind the lead wall, the safety factor for the L, M, and N counters was cut from 2 to 1.25. The safety factor for the other banks remained at 2. During the course of the experiment many of the counter pulse heights deteriorated due to crazing of the scintillator, deterioration of the photomultiplier tube, breakage of the scintillator to light pipe joint, etc.

When this pulse height deterioration was discovered, the phototube high voltage was raised until the miminum-ionizing pulse height was at its value from the auxiliary beam test. At no time was the pulse height of any counter required in the $K^{o}_{\mu 3}$ signature discovered to have sunk so low that its inefficiency became greater than 10^{-4} considering the above safety factors. This statement includes the realization that the width of the band of minimum-ionizing particles increased as a counter deteriorated.

We also did pulse height analyses of every counter (except the anti) required in the $K^{o}_{\mu 3}$ signature on muons from the prompt events. The peak channel in the spectrum could generally be determined $\pm$ 7% of itself. Analyses taken with the field up and down were compared with the result that the peak position never shifted with the reversal of the magnetic field beyond the limits set by the margin of error in determining the peak. Figure 16 shows pulse height analyses of R_{6U} with the field up and down. The peak channels were independently determined by eye to be channel 29 $\pm$ 2.

Thus we have shown that our counter pulse heights did not shift with reversal of the magnetic field to an accuracy of $\pm$ 7%. Since the margin of safety on all counters required in the signature was far greater than 7% before reaching an inefficiency of 10^{-4}, we believe that our counting efficiency was constant under field reversal to $\pm 10^{-4}$.

The most ominous threat to the stability of the counters

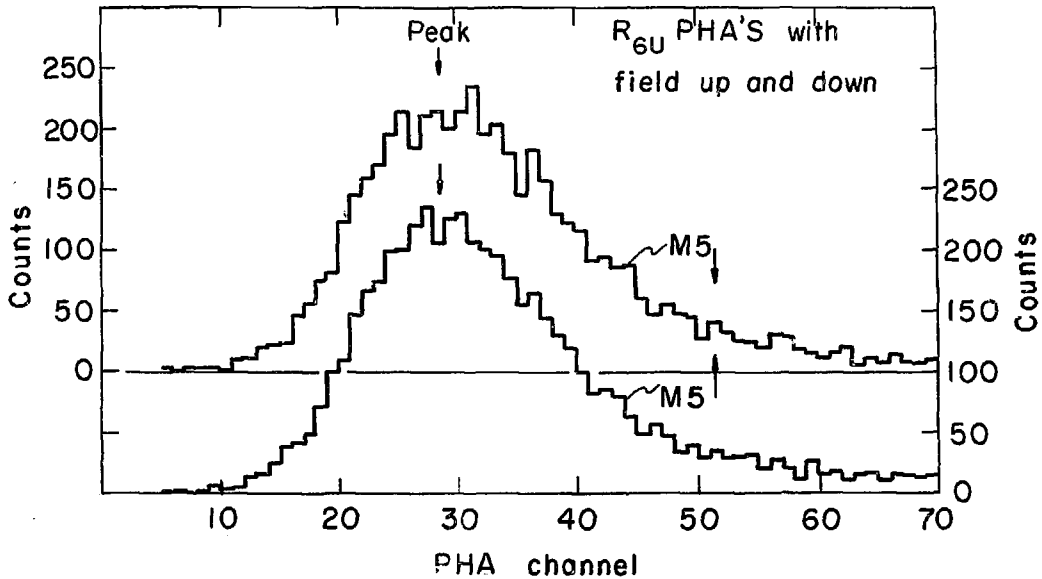

XBL7110-4565

Figure 16

under field reversal was the field of the M5 itself. Great care was needed to keep the fringe field from disturbing the phototubes. They can be adversely affected by fields as small as 0.5 gauss. No phototubes were located in a position where the field was more than 100 gauss before shielding. In order to satisfy this requirement the R counters had light pipes six feet long. Then the phototubes were shielded by successive concentric cylinders of iron (1/2 in. thick), iron (1/8 in. thick), and μ-metal ($\sim$ 1/16 in. thick). We note that the L, M, and N counters which had the smaller safety factor above were far from the magnet and in a magnetic field of only $\sim$10 gauss before shielding.

The diagnostic C, S_V, and R_V, counters were treated far more mundanely than the counters required in the $K^o_{\mu 3}$ signature. Because of their positions the two large C counters lining the snout were plateaued on cosmic rays. Hence we can only prove that their inefficiencies were less than 5%, but they were probably much lower. The two small C counters were plateaued in our vacuum tank but with the aid of a counter telescope. Their inefficiencies were less than 5×10^{-3} under testing conditions greatly inferior to those of the auxiliary beam. The S_V and R_V counters had their voltages set with an oscilloscope triggered on a PSRT coincidence.

All counting rates were checked $\sim$ once every two hours while taking data with the aid of the PDP-9. No counter required in the $K^o_{\mu 3}$ signature ever failed. Several vertical resolution counters did fail and were fixed before taking further data.

2. Geometrical Efficiency - Reversibility of the Field

The most obvious way that the geometrical efficiency of our counters could have changed with field reversal is that the field may have indeed not quite reversed. Let us suppose that with the field down the vertical component of the field at some central position was -B, but with the field up it was B+ΔB. Since the magnitude of the field would then have been greater with the field up, more muons would have been bent outside the region subtended by the T bank, resulting in a loss of efficiency with the field up. But this effect alone would still not have caused a change in the measured charge asymmetry since η_R and η_L would have changed by equal amounts. Only a change in the efficiency asymmetry affects our measurement. However, such an irreversal of the field could have combined with misalignments or the horizontal asymmetry of the beam to produce a change in the efficiency asymmetry. The experiment was designed such that the major $K^o_{\mu 3}$ acceptance cuts were made by the A - P system, before the magnetic field, so that the efficiency asymmetry would be insensitive to field irreversal.

The magnet current was set with a Leeds and Northrup potentiometer which measured the voltage drop across an accurately measured resistance in one of the cables between the magnet and its power source, a motor-generator. The accuracy with which the current could be set was 2×10^{-3} but the repeatability was 10^{-3}. The latter quantity is the important consideration in field reversal. The magnet current was also

measured by a transductor placed around one of the cables to the magnet. After each Bevatron pulse the output voltage from this transductor was recorded on magnetic tape. The transductor voltage also showed that the magnet current was generally reversed to an accuracy of 10^{-3}.

The PDP-9 checked the transductor output voltage for each pulse and typed out an alarm if the reading strayed by more than 5×10^{-3} from the intended value. Such bad pulses were thrown out of the data sample by the analysis program. The motor-generator generally regulated the magnet current to an accuracy better than 10^{-3}. Occasionally, however, due to a malfunction of the regulator, large (2%) fluctuations of the current would occur. These fluctuations were immediately detected by the computer and the data-taking was halted while the regulator was repaired.

The field was monitored by three coils which were flipped pneumatically from the electronics shack approximately once every four hours. The measurements of these devices were found to repeat to an accuracy of 2×10^{-4} (±2 gauss) when measuring the central field of the M5. Hence their accuracy in detecting possible irreversal of a magnetic field parallel to the axis of the coil is taken to be ±2 gauss. One flip coil was placed near the center of the upper pole face to monitor the central field. This field was found to reverse $\pm 10^{-3}$, the accuracy with which the current was set. Another flip coil was placed in the upstream end of the magnetic field near the S counters. The field here also reversed $\pm 10^{-3}$. The third flip coil was used to monitor the magnetic field in the 2 in. steel plate just downstream of the T counters.

In order to measure the vertical component of the field in the plate, this coil was placed at the top of the plate where the field was only 50 gauss. Consequently, since the accuracy of the coil was ±2 guass, we were only able to determine that this field reversed to an accuracy of ±4%. Since the field integral in the plate was ∿3% of the total field integral, the net effect of the plate on the total integral could be an irreversibility of at most $\sim 10^{-3}$. Consequently, we can claim that the total field integral reversed to an accuracy of 2×10^{-3}.

In order to study the effects of a possible irreversal of the total field integral we took a series of runs in sets of four each. Each set contained two pairs of runs, one with the magnet current normal and one with the magnet current set 2% low. The following list gives the charge asymmetries found for the sums of the uncorrected good events of each type.

	$M5^{\downarrow}$ (in %)	$M5^{\uparrow}$
current 2% low	1.15 ± 0.30	0.34 ± 0.30
current normal	0.61 ± 0.30	0.28 ± 0.30

Since we are considering the effects of field irreversal we assume

$$a^{\uparrow} = a^{\downarrow} = a = A$$

that the efficiency asymmetry is independent of the sign of the current but depends upon its magnitude. Then for a 2% drop in the current, the change in the efficiency asymmetry is

$$\Delta a = (-2.4 \pm 3.0) \times 10^{-3}$$

The Monte Carlo predicts that all known muon loss mechanisms provide a linear dependence of the efficiency asymmetry on magnet current for changes less than 2%. Therefore, for a current drop

of 2×10^{-3} (the accuracy with which the field is known to reverse)

$$\Delta a = (-2.4 \pm 3.0) \times 10^{-4}$$

The corresponding change in the charge asymmetry if the current was set systematically low for one sign of the field is

$$\Delta\delta_{\text{measured}} = \frac{\Delta a}{2} = (-1.2 \pm 1.5) \times 10^{-4}$$

This is the largest correction we could make for a systematic irreversal of the magnetic field. It is nearly negligible. Since any possible field irreversal seems to be due to the accuracy with which the current could be set and seems therefore to be random, no correction will be made.

Another way that the geometrical efficiency of our counters could have changed with field reversal is that the counters may have actually moved when the field was reversed. We do not think that this is possible since the only steel pieces connected to the counters (the phototube shields) were securely bolted in place. There were eddy current forces on the aluminum foil wrapping of the counters when the current was changed, but these forces do not depend upon the sign of the field.

B. Charge Resolution

Neither method of charge determination used in this experiment was without fault. The L counters could provide the wrong answer for a small fraction of the muons. They could also provide no answer at all if the W bin criteria were satisfied both on the west side and on the east side. The S-R-T determination was never wrong if it was used on a real muon but was often ambiguous if an extra S, R, or T counter were on or if the track under consideration had a high momentum. We will use the word "track" to describe a combination of S, R, T, and W bins which represents a trajectory surviving the second pass cuts. If an event had more than one muon track, the S-R-T charge determination was plus or minus if and only if all tracks were plus or all tracks were minus. If the S-R-T or L charge determination were neither plus nor minus, it was set to zero. The following table shows the number of events possessing each possible type of charge determination. Only the normal data are shown omitting the data taken with extra mass. The results are presented for four data samples: all events surviving the second pass cuts; the first sample excluding events with a C counter up-down coincidence; the first sample excluding events with magnitude of bend angle less than .21; and the first sample with both exclusions. Both of these exclusions preferentially cut out neutron interactions. The third sample is nearly the uncorrected good event sample. The fourth sample will be labeled "good-NCC". It will be used to calculate the $K^{o}_{\mu 3}$ charge asymmetry.

Table I - Types of Charge Determination

		S - R - T		
		-	0	+
Bend Angle <.21 Included - C-Coincidence Events Included				
	-	2,543,596	81,485	19,542
L	0	888	975	1,512
	+	10,467	82,362	2,600,556
	Total		5,341,383	
Bend Angle <.21 Included - C-Coincidence Events Excluded				
	-	2,201,340	57,406	10,807
L	0	784	629	1,057
	+	8,764	49,116	2,226,765
	Total		4,556,668	
Bend Angle <.21 Excluded - C-Coincidence Events Included				
	-	2,368,662	1,390	10,184
L	0	735	202	816
	+	8,249	1,328	2,396,811
	Total		4,788,377	
Bend Angle <.21 Excluded - C-Coincidence Events Excluded				
	-	2,055,651	854	7,169
L	0	624	143	706
	+	7,032	744	2,076,950
	Total		4,149,873	

The charge resolution is seen to be quite good. As a fraction of the uncorrected good events:

6×10^{-4} fail S-R-T determination
3×10^{-4} fail L determination
4×10^{-5} fail both
4×10^{-3} have S-R-T and L disagreement

The S-R-T method is used to determine the muon charge when possible. Where the S-R-T method fails, the L method is used. Assuming that the failure of the S-R-T method is uncorrelated with the wrong decision of the L method, only for 2×10^{-6} of the good events is the wrong charge chosen. Thus the total number of good events for which the correct charge is not chosen is completely negligible.

The reason the charge resolution is so good is that all the problems have been excluded in the bend angle cut. The S-R-T method fails mainly for events with a small bend angle for two reasons. First, it cannot resolve a straight track. Second, an event with two tracks of opposite charges is likely to have one track with a small bend angle (where the charge of the trajectory changes). As explained in the next section, the track with the smallest bend angle is chosen to represent a multiple track event.

The large charge asymmetry of the events for which the methods disagree is undoubtedly due to neutron interactions. Note that this charge asymmetry is absent in the fourth data sample.

We have not included in the above data samples the double

penetration events which possess two complete muon tracks, one up and one down. Both methods of charge determination fail for these events because the muon cannot be identified. These events comprise $(0.22 \pm 0.01)\%$ of the data. The Monte Carlo predicts $(0.21 \pm 0.03)\%$ of the data are such events with double penetrations due to pion decay in flight from $K^{o}_{\mu 3}$. (This latter error is statistical only.) Hence we believe that all of these events are due to pion decay in flight and that they can safely be ignored.

We note that although the Monte Carlo is not successful in describing a muon's multiple scattering in the lead wall, it is reasonably successful in predicting a muon's ability to penetrate the wall. If we count up the number of muons which do not count in the N bank, we find:

$$\frac{LM}{ALL} = \underset{\substack{\text{from data (all events surviving the second pass cuts)}}}{(.297 \pm .0002)} \simeq \underset{\text{from Monte Carlo}}{(.286 \pm .004)}$$

where the statistical error of the Monte Carlo is indicated. Hence the Monte Carlo's decay-in-flight predictions seem fairly believable.

C. Beam Interactions

This section will speak chiefly of neutron interactions but the results are valid for the sum of all components of the beam. Thus the anti mass extrapolation in part 3 corrects for both K_S^o regeneration and neutron interactions in the anti.

Figure 17 shows the neutron and K_L^o momentum spectra[28,19] at the Bevatron. We see that the neutron spectrum is peaked at very high momentum and thus unfortunately can produce very high momentum secondaries. One type of neutron interaction which we could have accepted involves low energy spray to trigger the P's and a fast strongly interacting particle to penetrate the lead wall. This strongly interacting particle might be expected to need a very high momentum in order to penetrate the wall. Another type of neutron interaction which would not require that a hadron penetrate the wall would involve instead decay in flight of a fast pion. This latter process would produce muons in the same momentum range as those from $K_{\mu 3}^o$ decay. If the first process occurred, the second process can be expected to have occurred at some level.

The anti counter is one of the counters which we claim (IV-A-1) was efficient to 1 part in 10^4 throughout the experiment. In order to double check this we retested the anti in its final

---

[28] M.N.Kreisler, "Neutron-Proton Elastic Scattering from 1 to 6 Gev," SLAC-66, and Ph.D. dissertation, Stanford Univ. (1966), P.83. Formulas from the reference in footnote 20 were used to extrapolate to our beam energy.

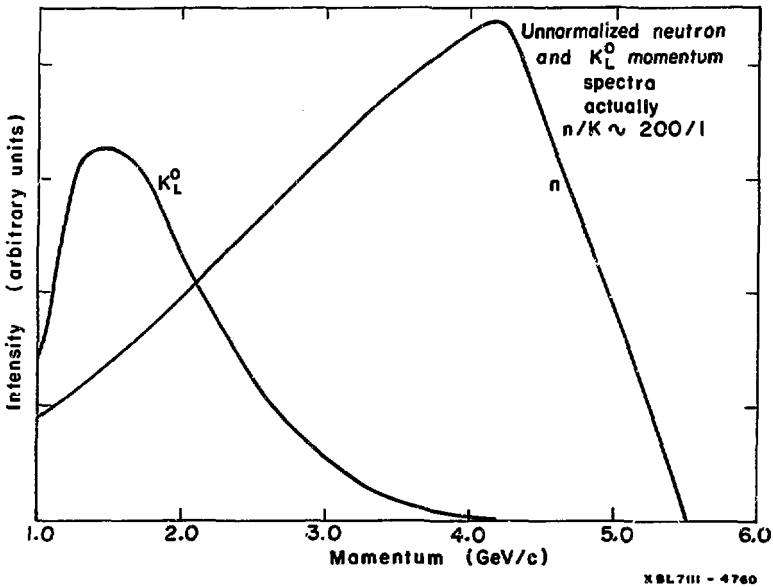
Unnormalized neutron and K_L^0 momentum spectra actually n/K ∿ 200/1
K_L^0
n
Intensity (arbitrary units)
1.0
2.0
3.0
4.0
5.0
6.0
Momentum (GeV/c)
XBL 7111 - 4760

Figure 17

position immediately before taking data. We found that its inefficiency was less than 5×10^{-4} under testing conditions greatly inferior to those in the auxiliary beam.

We took some data with the anti requirement removed from the trigger. We then found that for events satisfying a $K^{o}_{\mu 3}$ signature requirement with exception of the anti requirement, after the neutron cut, the ratio of the number of everts with anti on to anti off was(1.1) . The charge asymmetry of the events with the anti on was $(0.4 \pm 0.9)\%$. Thus the maximum contribution to the measured charge asymmetry due to anti inefficiency is 4×10^{-7} using an inefficiency of 10^{-4}.

We also checked the efficiency of the anti electronics by doing a TPH analysis on the sum of the anti discriminators versus the prompt strobe when the anti requirement was included in the strobe. The analysis was done on 1.66 million good events and we did find an apparent inefficiency of 2×10^{-4}. However, at this level we tend to believe the anti electronics in preference to the TPH circuitry. Even if this inefficiency were real, it would produce a negligible change in our charge asymmetry.

Hence we believe that the anti counter worked and therefore as we have indicated in Section II-B, we believe that neutron interactions triggered our system from only two places: the snout area and the anti itself. These two possibilities will be discussed in parts 1 and 4. The knock-on correction associated with the neutron cut will be treated in part 2. For the sake of completeness we discuss interactions with residual air in the vacuum tank in part 3.

In the treatment of neutron interactions we neglect interactions which originated far enough downstream of the snout to miss a C counter before triggering the P's. This procedure is reasonable because the magnetic field of the M5 protected the P's from such interactions. This assertion is supported by Figure 7a, the vertex distribution. If any such events contaminated our data, about half of them (the ones with a particle going through the pion R and S banks on its way to a P) would be in the downstream overflow bin of this plot. The net effect of this bin on the charge asymmetry of the total sample represented in Figure 7a is -2×10^{-4}. We attribute this asymmetry to pion interactions and not neutron backscatter but it is small in any case. Extrapolated to the set of all events surviving the second pass cuts it amounts to -1×10^{-4}.

The data sample represented in Figure 7a consists of all events surviving the second pass cuts with a single muon track but with the additional requirement that S, R, S_V, and R_V banks have counts both on the muon and pion sides. The conclusions drawn from Figure 7a are however, independent of any restrictions to the good events or to the events without a C coincidence. It also makes no difference if events with a multiple muon track are included. The negative charge asymmetry in the bins between -100 in. and -50 in. is believed to be due to pion interactions in the vacuum tank wall (1.75 in. aluminum). The charge asymmetry of these events is insensitive to the C coincidence. The events for which the pion scatters appreciably can be expected to appear near the position of the S and R banks because the vertical distance separating muon and pion trajectories here is constrained.

Hence if there is no true vertex, the reconstruction program can be expected to have put an event in these bins.

1. Neutron Cut

As we have already noted, we had two means of detecting neutron interactions in the snout: the C counter up-down coincidence, and the S_V counter nearest the beam on the muon side which will be called S_{V1}. Neither means may be used as an absolute veto to exclude neutron events. S_{V1} merely detected the events coming from the most likely area of origin, the upstream portion of the snout and the vacuum tank wall near the beam. Each S_{V1} counter as shown in Figure 6 had a vertical dimension of 2.5 in. and had its beamside edge touching the outside of the snout. The S_{V1} also has the disadvantage that one third of the muons from $K^o_{\mu 3}$ passed through it. The C counter coincidence can not be used as an absolute veto mainly because pions from $K^o_{\mu 3}$ might have interacted asymmetrically in the snout before triggering the coincidence. However, there are also two possible sources of C-coincidence inefficiency:

1. neutron backscatter of neutrals which might have converted and counted in the P's
2. counting inefficiency

We believe that both of these possibilities are unlikely, but we cannot exclude them to the precision required for this experiment.

Since we have no absolute neutron veto we have adopted the philosophy of studying the data in the hope that a portion of it is free of neutrons and hence insensitive to the state of the C coincidence and S_{V1}. In order to aid us in this study

we adopt the following abbreviations:

CC ≡ events with C coincidence on

SV ≡ events with S_{V1} on

CCSV ≡ events with C coincidence and S_{V1} on

ALL ≡ all events (surviving second pass cuts)

NCC ≡ ALL events excluding CC events

NSV ≡ ALL events excluding SV events

NCCSV ≡ ALL events excluding CCSV events

These definitions will at times be restricted to refer to a subset of ALL events such as ALL single-track events. (Track is defined in IV-B).

In the following discussion we will present a series of plots versus the magnitude of the tangent of the muon bend angle in the M5 (as defined by Figure 12). This quantity will generally be referred to simply as the "bend angle". The bin size used for the bend angle will be .06. Each bin will be named after its central value (except bin .00 which extends only from .00 to .03). The relation between the bend angle, the true turning angle (in radians), and the momentum central to each bin is given by the following table.

Bend Angle	True Turning Angle	Momentum (Gev/c)
.00	.000	∞
.06	.060	8.00
.12	.119	4.03
.18	.178	2.70
.24	.235	2.04
.30	.292	1.64
.36	.347	1.38

Bend Angle	True Turning Angle	Momentum (Gev/c)
.42	.398	1.21
.48	.447	1.07
.54	.495	.97
.60	.541	.89
.66	.583	.82
.72	.624	.77
.78	.662	.73

From the geometry of our counters we calculate that our resolution was ±.12 in terms of the bend angle. Thus it is possible for an event to appear as much as two bins from its true location.

Figure 18 shows the distributions of the number of events and charge asymmetry per bend angle bin for the NCC and CC, normal, single-track events.

The statistical errors are shown if they are significantly bigger than the corresponding points. Neutron contamination is evident. There is a very large charge asymmetry in the high momentum bins where very few muons from $K^{o}_{\mu 3}$ are expected. In the region where the muons are expected the charge asymmetry drops to reasonable values. A strong correlation between the asymmetric events and the C coincidence is seen indicating that many of these events originated in the snout. The large charge asymmetry of the high momentum NCC events is mainly due to neutron interactions in the anti counter as will be demonstrated in part 4. Apparently, whether the event was made in the anti or the snout, the culprit was the same——the type of neutron

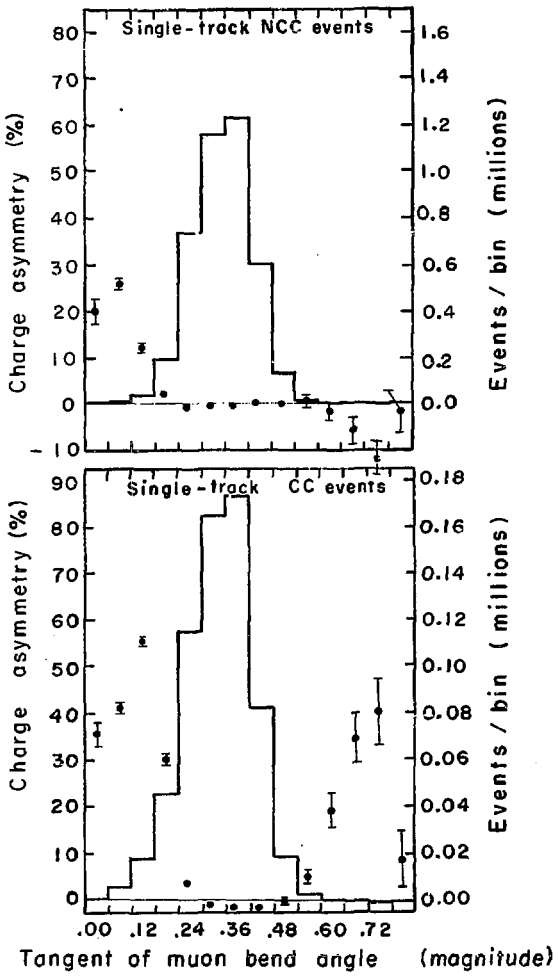
Single-track NCC events
Charge asymmetry (%)
Events / bin (millions)
Single-track CC events
Charge asymmetry (%)
Events / bin (millions)
.00 .12 .24 .36 .48 .60 .72
Tangent of muon bend angle (magnitude)
XBL7110-4587

Figure 18

interaction in which a hadron penetrated the lead wall. These events appear to have left much of the region where real muons are expected uncontaminated. We note that the charge asymmetry of the CC bin .12 is an astounding 55% which indicates that the ratio of plus to minus charges in this bin is ∿3.5/1. This figure suggests that the hadron penetrating the wall is a proton produced by inelastic charge exchange of a high energy halo neutron. In this case the background would be completely charge asymmetric. The reason the charge asymmetry falls for the highest momentum events is undoubtedly loss of charge resolution by our system.

The low momentum events also show a charge asymmetry which is correlated with the C coincidence. The nature of these events is somewhat puzzling since the minimum muon momentum penetrating to the M bank is 1075 Mev/c. One possibility is that they are neutron induced events where the neutron penetrates the lead wall and converts to form a W bin. The SRT requirement could then be satisfied by a pion, associated with the neutron, which does not penetrate the wall but happens to point to the neutron's W. We would then be measuring the charge of the pion. In any case the number of these events is very small. They will be included in the good event sample and the uncertainties associated with them will be incorporated into the systematic error of the neutron cut. In themselves, these events represent no problem. There are so few of them that the effect on the charge asymmetry is less than 10^{-4} no matter what sample we keep or exclude from the bins .60 or greater. The only problem is——how many of these events are underneath the muon peak?

Figure 19 is an expanded view of the charge asymmetries under the muon peak. There are systematic differences between the NCC and CC events throughout the plot. In bins .24 and .54 the differences are apparently due to the high and low momentum background events we have just been discussing. In bins .36 and .42 however, the NCC events have a negative charge asymmetry. There are two likely causes of this asymmetry. One is neutron interactions where the particle penetrating the lead wall is a muon from π decay in flight. The second is asymmetric interactions of $K^{o}_{\mu 3}$ pions before triggering the C coincidence. The first type of event should not be included in the charge asymmetry measurement while the second type should. Hence the net effect of these events on the charge asymmetry represents a systematic error. We tend to believe that these events are produced by neutrons since the neutron interactions in the anti counter have a negative charge asymmetry in this region as we shall see in part 4.

We study the size of the systematic error introduced by neutron interactions in Figure 20. This figure is another plot of the charge asymmetries in the muon peak region, but here we plot the asymmetries of the NCC, ALL, and NCCSV events in order to study the effect of the CC events on the charge asymmetry of each bin. We have indicated the statistical errors of the NCC points. With the sole exception of bin .24, the difference between the ALL and NCC asymmetries is about equal to or less than the NCC statistical error. This conclusion is unchanged if we use the ALL statistical error. The NCCSV curve, however, shows similar agreement with the NCC curve for all bins including bin .24. Hence the problem in bin .24 is due entirely to CCSV

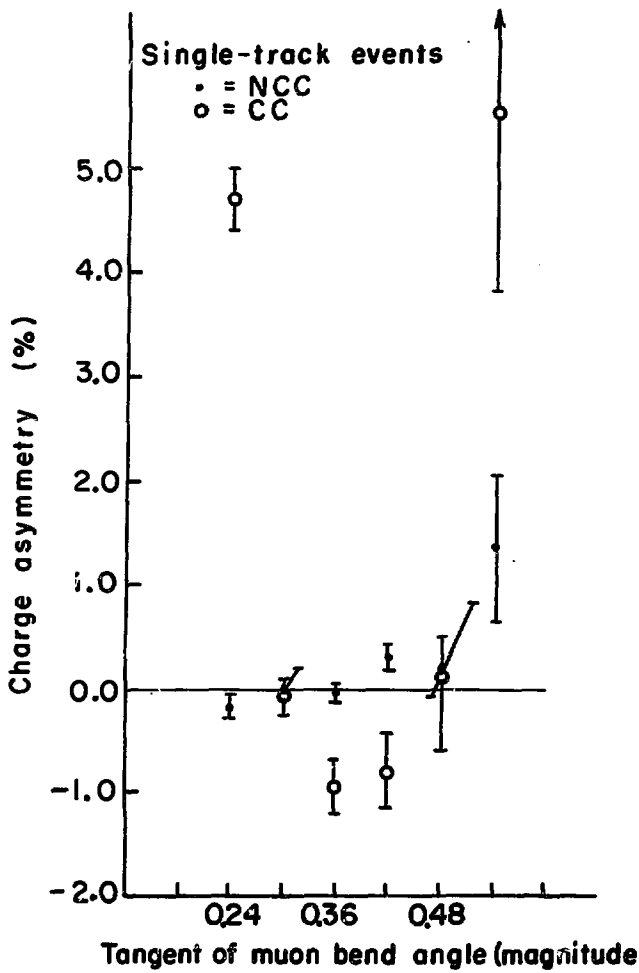
Single-track events
• = NCC
o = CC
5.0
4.0
3.0
2.0
1.0
0.0
-1.0
-2.0
Charge asymmetry (%)
0.24
0.36
0.48
Tangent of muon bend angle (magnitude)
XBL7111 - 4757

Figure 19

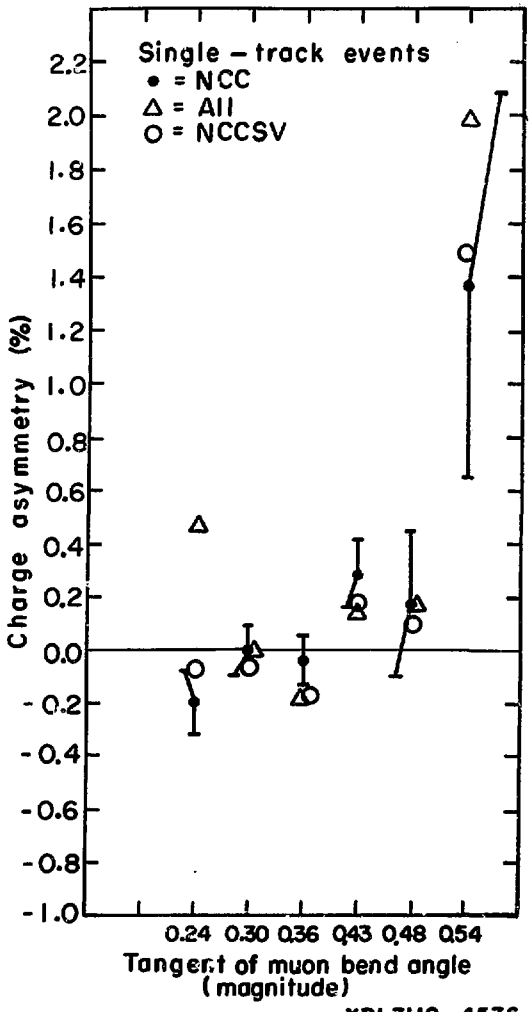
Single – track events
• = NCC
△ = All
○ = NCCSV
Charge asymmetry (%)
2.2
2.0
1.8
1.6
1.4
1.2
1.0
0.8
0.6
0.4
0.2
0.0
- 0.2
- 0.4
- 0.6
- 0.8
- 1.0
0.24 0.30 0.36 0.43 0.48 0.54
Tangent of muon bend angle
(magnitude)
XBL7110-4576

Figure 20

events, which have been labeled as neutron candidates by both means of identification. If we exclude the CCSV events from bin .24, apparently we can achieve a systematic error in excluding neutrons of about the same size as our statistical error. Thus we define the term "good events".

good events: NCCSV events with bend angle bin $\geq .24$

plus

CCSV events with bend angle bin $\geq .30$

There are 4,380,674 good, single-track events in the main data sample. Their charge asymmetry is

$$\delta \text{ (good, single-track)} = (-2.2 \pm 4.8) \times 10^{-4}$$

where the statistical error has been indicated. Events which are not good will be called, of course, "bad." The events with bend angle bin $\geq .60$ do not change the above conclusions since, as we have already noted, their effect on the charge asymmetry of good events is less than 10^{-4}. The increase of the charge asymmetry as a function of bend angle is thought to be due to knock-on electrons and will be discussed in part 2.

Through the aid of Figure 21 we discuss the neutron cut from an integral point of view. Here we have plotted the NCC, NCCSV, and ALL charge asymmetries for all bend angles greater than or equal a given value. Again the NCC statistical errors are indicated. For the total sample the CCSV events have a large effect on the charge asymmetry ($\sim$.6%). However, after bin .18 has been cut away this effect has been reduced to $\sim$.1%(two NCC standard deviations). The effect then remains at $\sim$one NCC standard deviation across the muon peak. Hence the neutron cut has been made at a reasonable place. It is made just as the dependence

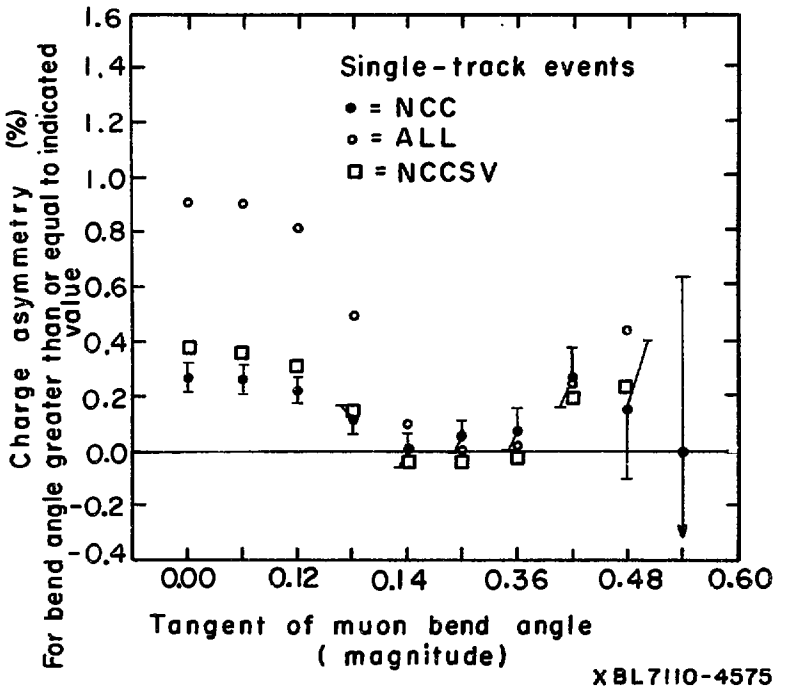
Single-track events
• = NCC
○ = ALL
□ = NCCSV
Charge asymmetry (%)
For bend angle greater than or equal to indicated value
1.6
1.4
1.2
1.0
0.8
0.6
0.4
0.2
0.0
-0.2
-0.4
0.00
0.12
0.14
0.36
0.48
0.60
Tangent of muon bend angle
(magnitude)
XBL7110-4575

Figure 21

on CCSV events reaches a minimum and just as the charge asymmetry becomes reasonably constant as a function of cut angle (before reaching the knock-on structure in bin .42). The neutron cut includes 92% of the single-track data in the good event sample. We note that the charge asymmetry of good-NCC single-track events (bend angle bin $\geq$.24) is zero and differs from the good event single-track charge asymmetry by only 2×10^{-4}.

$$\delta(\text{good-NCC, single-track}) = (-0.1 \pm 5.1) \times 10^{-4}$$

Multiple-track events constitute 10.8% of the data which passed the second pass cuts. Because of the need for a neutron cut, these events are a serious problem. If such an event had an extra S, R, or T on, there was an ambiguity in its assignment to a bend angle bin. In order to be sure to exclude the high momentum neutron-induced events, when such an ambiguity arose the track with the smallest bend angle was chosen to represent the event. This procedure, though necessary, causes serious problems in the analysis of events with knock-on electrons. Consider a μ^- which makes a knock-on in the R counters. The electron will spiral around in the magnetic field and, if it has sufficient energy, it may count in an R bin separate from that of the muon. Since the knock-on has the same charge as the μ^-, it will always spiral in the same direction as the muon bends. Hence the track including the knock-on's R count will always have a higher momentum than the real μ^- track (unless the knock-on travels so far that its track has the curvature of a μ^+). By the same reasoning a μ^+ can only produce a knock-on track of lower momentum. Hence, due to the above analysis procedure, knock-ons will shift μ^- tracks to smaller bend angles but will leave μ^+ tracks in their

proper bins. Then the neutron cut, when applied to multiple track events, will preferentially exclude μ^-.

Figure 22 presents the normal multiple-track events. The effects of knock-ons are clearly seen. However, aside from the knock-on effects, the multiple-track curves look very similar to the corresponding single-track curves (Figures 18, 19). The CC events possess a substantially higher charge asymmetry than the NCC events in the high momentum bins. The difference of the charge asymmetries becomes much smaller in bin .24, reverses sign in bin .30 and remains $\sim$ constant through bin .48.

Thus again the CC and NCC charge asymmetry curves are systematically different. The important question is then—— how important is this difference? Figure 23 answers this question for the multiple-track events in the same manner that Figure 20 answered it for the single-track events. If the same neutron cut is made on the multiple-track events, the difference between the NCC and ALL charge asymmetries is about one statistical standard deviation (of either) or less. Figure 24 then shows that the same conclusion is valid for the sum of events with single and multiple tracks. Again bins .60 and greater are unimportant since their effect on the total charge asymmetry is less than 10^{-4}.

Figure 25 presents the integral curves for all events of the main data sample and corresponds to Figure 21. The same comments apply. However, due to the general shift of the multiple-track events to the high momentum bins, the neutron cut only places 88% of the total data sample in the good event class. The uncorrected charge asymmetries for good events and good-NCC events of the main sample are as follows:

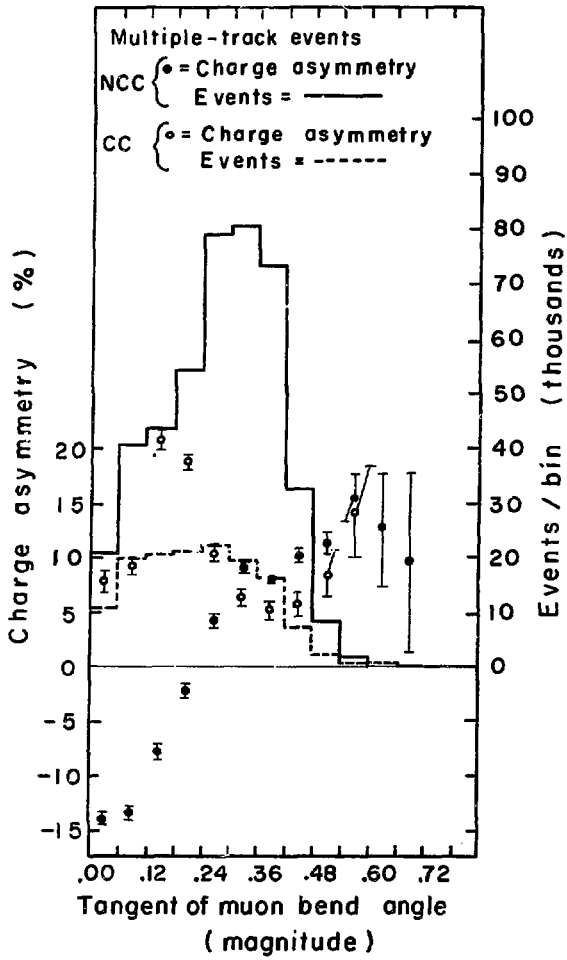
Multiple-track events
NCC { • = Charge asymmetry
Events = ——
CC { ∘ = Charge asymmetry
Events = ------
Charge asymmetry (%)
Events / bin (thousands)
20
15
10
5
0
-5
-10
-15
100
90
80
70
60
50
40
30
20
10
0
.00
.12
.24
.36
.48
.60
.72
Tangent of muon bend angle
(magnitude)
XBL7110-4574

Figure 22

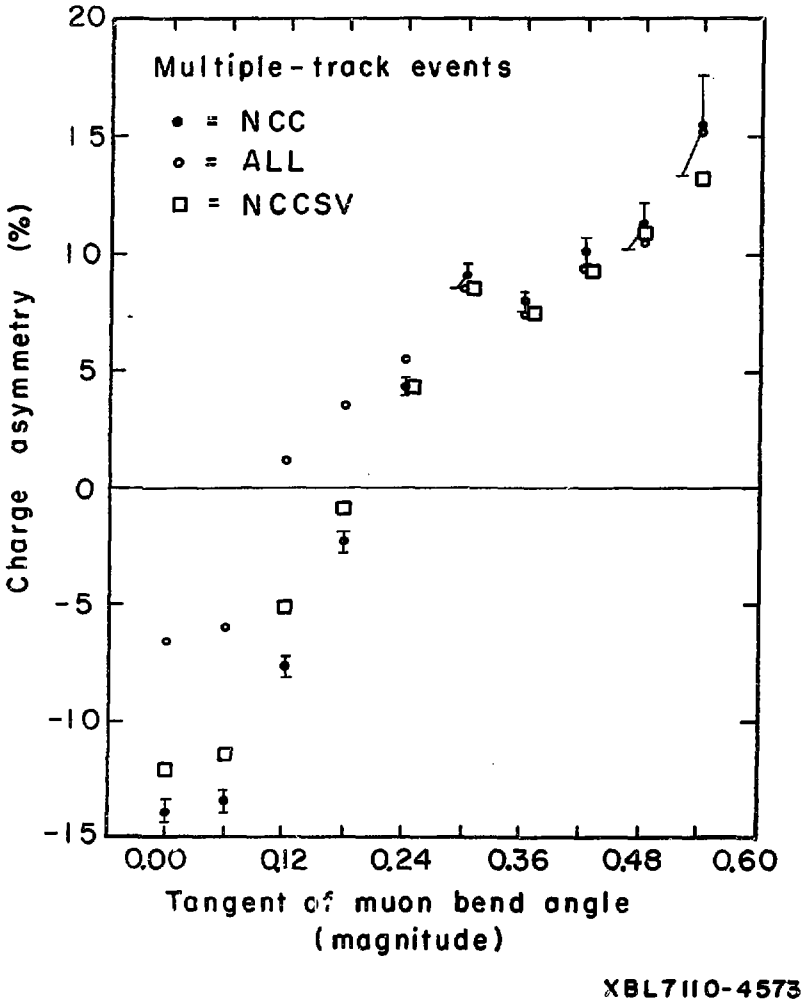
Multiple-track events
• = NCC
o = ALL
□ = NCCSV
Charge asymmetry (%)
20
15
10
5
0
-5
-10
-15
0.00
0.12
0.24
0.36
0.48
0.60
Tangent of muon bend angle
(magnitude)
XBL7110-4573

Figure 23

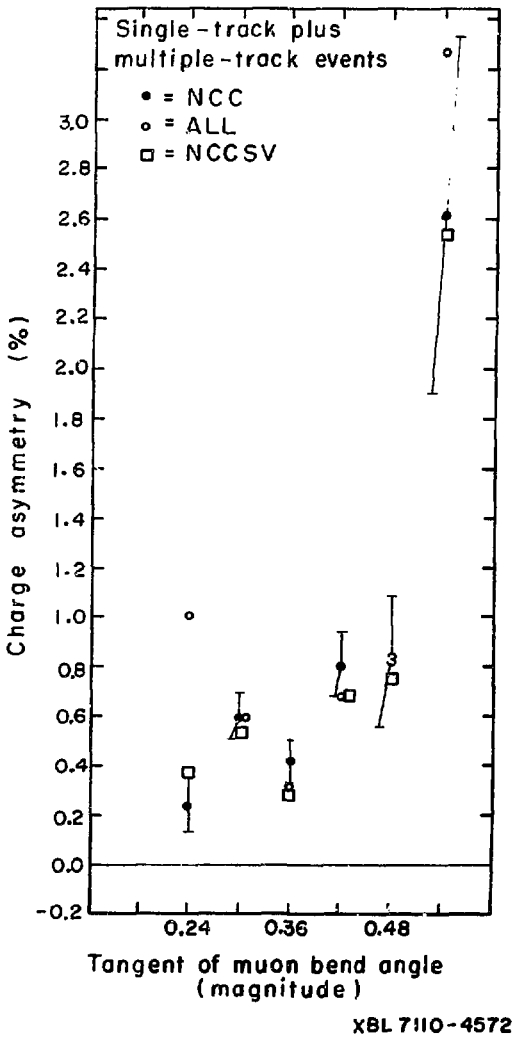
Single-track plus
multiple-track events
• = NCC
o = ALL
□ = NCCSV
Charge asymmetry (%)
3.0
2.8
2.6
2.4
2.2
2.0
1.8
1.6
1.4
1.2
1.0
0.8
0.6
0.4
0.2
0.0
-0.2
0.24
0.36
0.48
Tangent of muon bend angle
(magnitude)
XBL 7110-4572

Figure 24

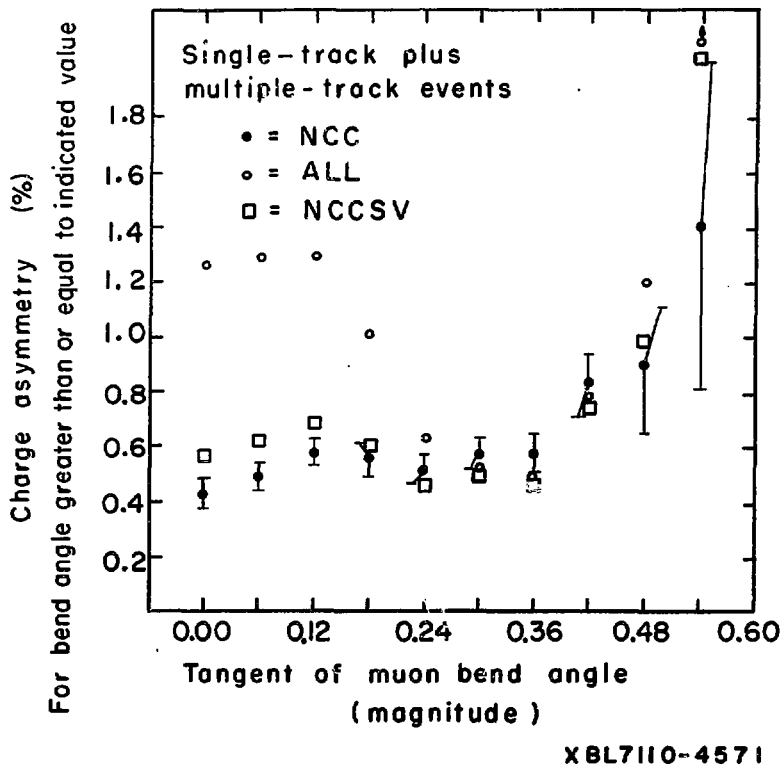
Single-track plus
multiple-track events
• = NCC
○ = ALL
□ = NCCSV
Charge asymmetry (%)
For bend angle greater than or equal to indicated value
1.8
1.6
1.4
1.2
1.0
0.8
0.6
0.4
0.2
0.00
0.12
0.24
0.36
0.48
0.60
Tangent of muon bend angle
(magnitude)
XBL7110-4571

Figure 25

$$\delta_{good} = (5.03 \pm 0.46) \times 10^{-3}$$

$$\delta_{good\text{-}NCC} = (5.16 \pm 0.49) \times 10^{-3}$$

The two numbers are essentially equivalent. The second one is our best value for the charge asymmetry before corrections. The above errors are statistical only. In accord with the previous discussion we attribute an additional systematic error of 5.0×10^{-4} to our ability to exclude the effects of neutrons with the above cut.

We have explicit evidence that the background events in the high momentum bins are caused by backscatter. Figure 26 shows two TPH's of the upper T bank versus the prompt strobe for 266,00 good and 45,000 bad events respectively. The peak is 11 nsec wide at half maximum because several of the counters were mistimed slightly. (The width for the lower T bank is 6 nsec.) The important point to notice is the early tail on the curve for the bad events. The charge asymmetry of the events in this tail from channels 51 through 80 is 13.5±1.4%. It is apparent that the T count was early for these events relative to the time of the P's (which generally controlled the strobe) because the events originated in the snout. The corresponding charge asymmetry for the good-event tail can be accounted for by single T counters on in random with the good events but slightly earlier. The reason the bad-event tail stretches out for $\sim$ 30 nsec is thought to be that the backscattered particles were often slow. The good event sample has apparently been freed of at least most of these backscattered events.

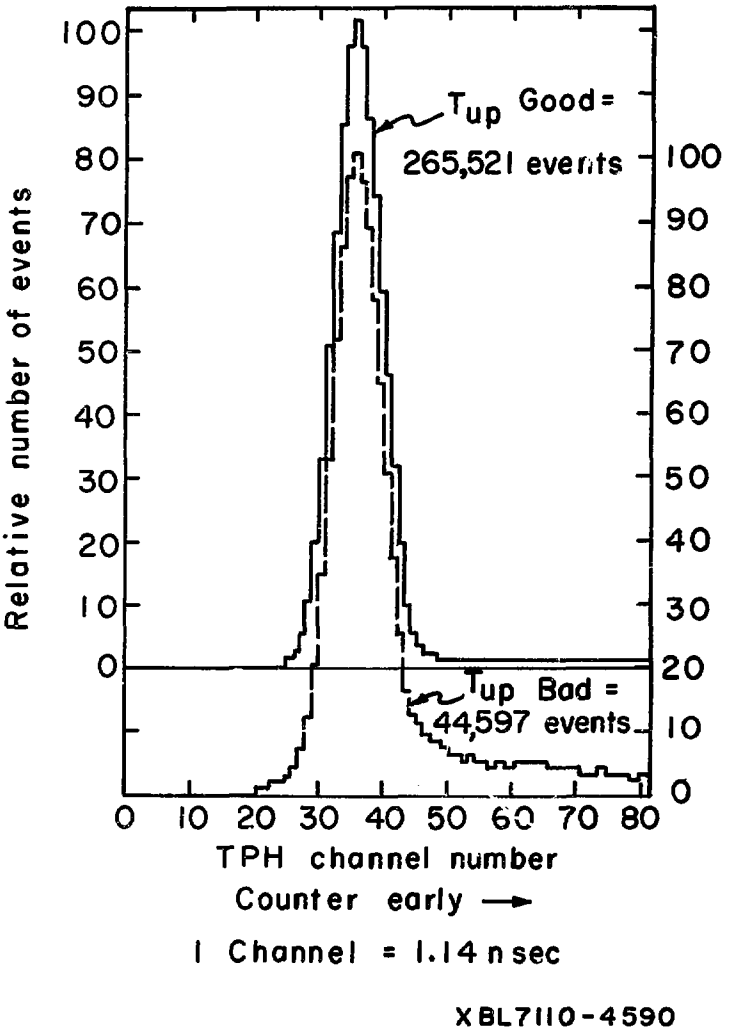
Relative number of events
100
90
80
70
60
50
40
30
20
10
0
Tup Good =
265,521 events
Tup Bad =
44,597 events
0 10 20 30 40 50 60 70 80
TPH channel number
Counter early →
1 Channel = 1.14 n sec
XBL7110-4590

Figure 26

Figure 18 indicates that a fairly reasonable estimate of the amount of our neutron contamination is given by the charge asymmetry for ALL events. It certainly gives a lower limit. Figure 25 then indicates that this contamination is $\sim$1% for ALL events but is probably $\lesssim$.1% for good events. We can obtain another estimate from the Monte Carlo via S_{V1}. The Monte Carlo prediction for the fraction of events with S_{V1} on is compared to the data below:

	Monte Carlo	ALL	Bend Angle >.21	good-NCC
$\frac{S_{V1}}{all}$ =	.325 ± .004	.349	.329	.316

The Monte Carlo error is statistical only. If the extra S_{V1} events in the ALL sample are considered to be neutrons, these figures indicate that the background neutron level in the ALL sample is $\sim$2%. After the neutron cut the level is apparently undetectable (less than 1%).

The fraction of events with a C coincidence on is .147 for ALL events but drops to .133 for events with bend angle > .21. This drop is consistent with the 1-2% neutron contamination of ALL events. Of the 13.3%, about .1% is known to be neutron contamination in bin .24 (Figure 25) and 6.3% is due to C-coincidence randoms. (The large C counters had high counting rates since they were very near the beam.) This leaves 6.9% of the events which had a C coincidence due to a knock-on electron (from the π or μ), a pion interaction or a neutron interaction. A rough calculation shows that $\sim$3% is due to knock-ons, leaving $\sim$4% which could easily be due to pion interactions entirely. Apparently the charge asymmetry of these pion interactions is less than $\sim$1% because the change in the total charge asymmetry due to their exclusion is less than 5 x

10^{-4} as we have seen. We note that it is possible that a significant neutron contamination of the good events could exist and have a charge asymmetry which just cancels that of pion interactions for each bend angle bin greater than or equal to .24. However, it is much simpler to achieve the observed C-coincidence and S_{y1} independence of the charge asymmetry if both effects are either nonexistant or charge symmetric within the observed systematic error of 5×10^{-4}. As a general rule, we will adopt the attitude that a null result means that there is no effect rather than a precise cancellation of two effects.

The known causes of multiple-track events are listed below:

	Causes of Multiple-Track Events (% of total data)				
	S	R	T	W	Sum
Randoms	0.8	1.3	1.5	0.8	4.4
Knock-ons	1.0	0.7	0.0	3.0	4.7
Sum	1.8	2.0	1.5	3.8	9.1

The randoms contributions were calculated from the known on-times. The R knock-on contribution was calculated by Monte Carlo methods but the S and W knock-on contributions were calculated roughly by hand. We expect no multiple-track knock-ons in the T bank because it is protected by the M5 magnetic field on one side and an iron plate on the other. Thus knock-ons and randoms account for most and perhaps all of the 10.8% of the data with multiple tracks.

In Figure 27 we study the effect of the second-pass cuts on

the good-NCC, single-track events. (For the bend-angle plot we use all single-track, NCC events.) The plots correspond to those of Figure 13 which were made before the neutron cut and which include multiple-track events. The exclusion of the multiple-track and bad events has considerably reduced the tails on the anti-position and decay-angle plots as well as the population of the high-momentum bins in the bend-angle plot. These effects are only partially due to the exclusion of neutron-induced events since the analysis program often chose the wrong track of a multiple-track event. The gross features of the plots are unchanged by the above two exclusions. The charge asymmetries per bin are also shown in Figure 27.

The charge asymmetries in the tails of the anti-position and decay-angle plots are large and positive. The same events are undoubtedly responsible for this behavior in both plots. The total number of asymmetric events in the tails of either plot is less than 2.5×10^{-4} of the good-NCC, single-track events. (A tail on the anti-position plot is defined to consist of the outer five bins. On the bend-angle plot the tail is the outer two bins.) Hence even if these events extend under the muon peak, their effect on the charge asymmetry is less than 5×10^{-4}, the systematic error of the neutron cut. These events could be due to neutron interactions in combination with a C-coincidence inefficiency. The asymmetric events in the outer bins of the scattering-angle plot are negative and make a contribution to the total charge asymmetry which is similarly small. They will be discussed in Section IV-F.

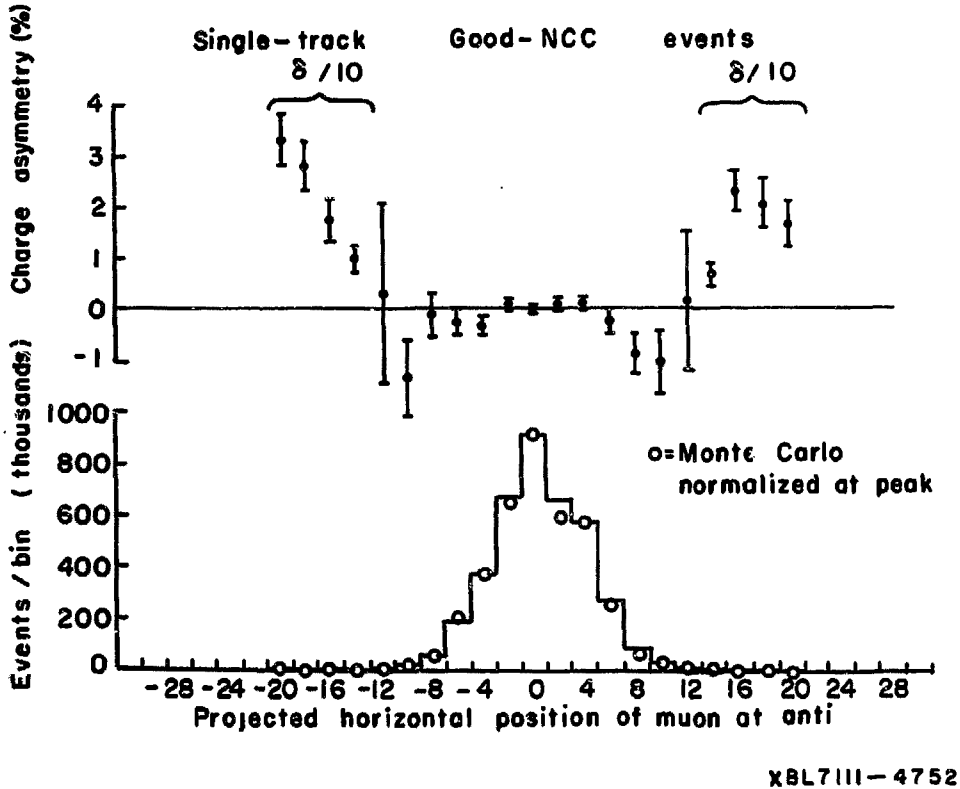
Single-track
δ/10
Good-NCC
events
δ/10
Charge asymmetry (%)
4
3
2
1
0
-1
Events / bin (thousands)
1000
800
600
400
200
0
o=Monte Carlo
normalized at peak
-28 -24 -20 -16 -12 -8 -4 0 4 8 12 16 20 24 28
Projected horizontal position of muon at anti
XBL7111-4752

Figure 27a

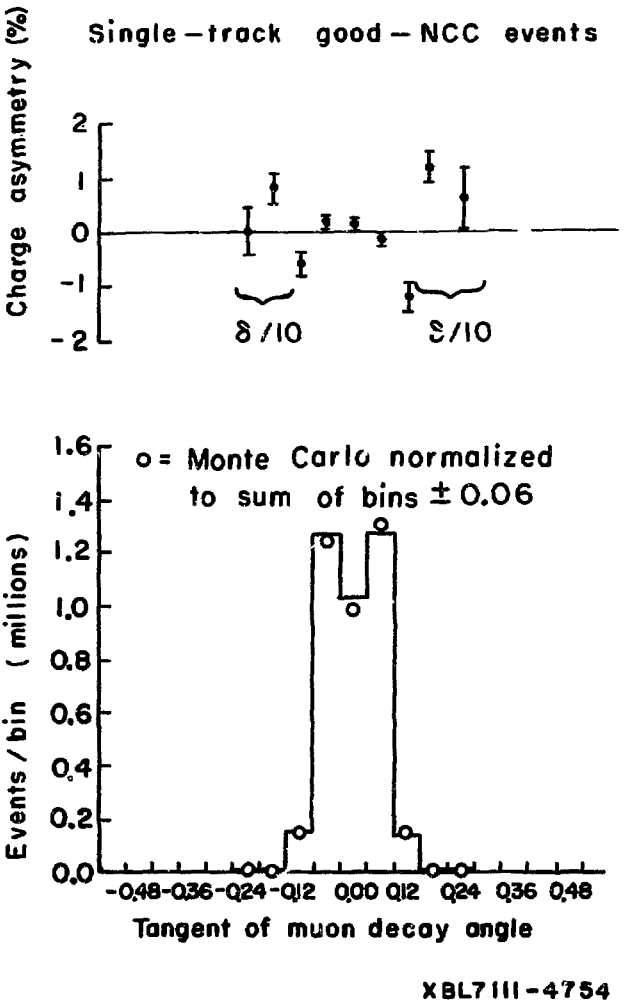
Single – track good – NCC events
Charge asymmetry (%)
2
1
0
-1
-2
δ/10
ε/10
o = Monte Carlo normalized
to sum of bins ± 0.06
Events / bin (millions)
1.6
1.4
1.2
1.0
0.8
0.6
0.4
0.2
0.0
-0.48 -0.36 -0.24 -0.12 0.00 0.12 0.24 0.36 0.48
Tangent of muon decay angle
XBL7111-4754

Figure 27b

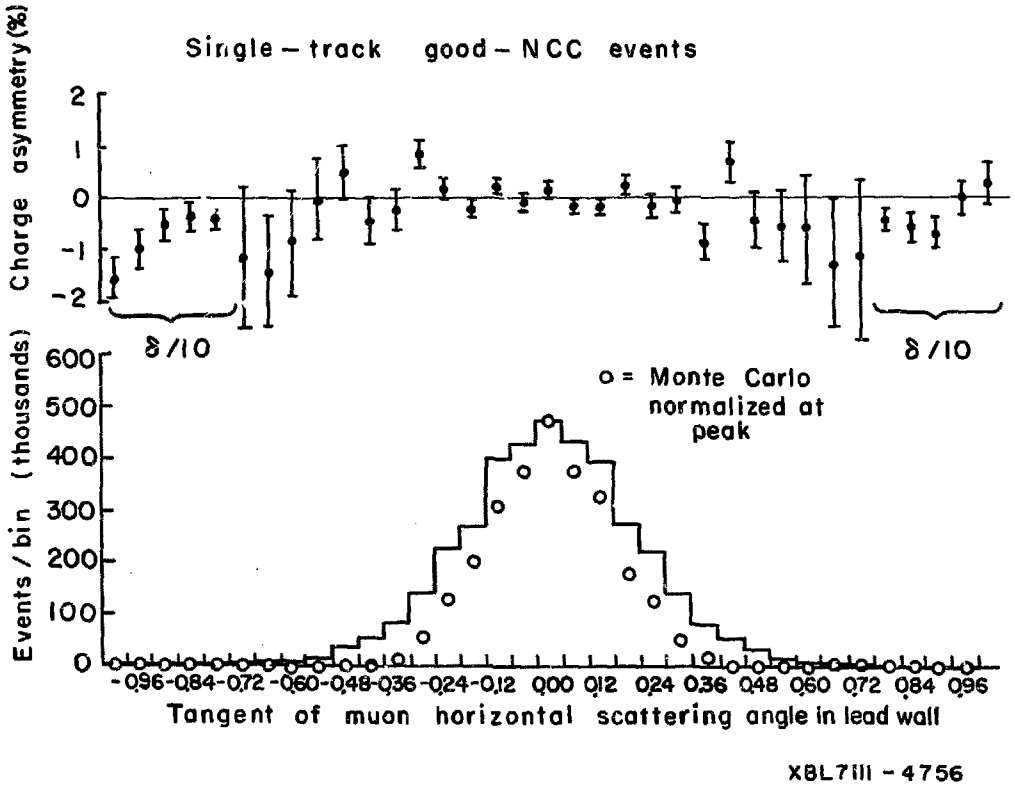
Single – track good – NCC events
Charge asymmetry (%)
2
1
0
-1
-2
δ/10
δ/10
Events / bin (thousands)
600
500
400
300
200
100
0
o = Monte Carlo normalized at peak
-0.96 -0.84 -0.72 -0.60 -0.48 -0.36 -0.24 -0.12 0.00 0.12 0.24 0.36 0.48 0.60 0.72 0.84 0.96
Tangent of muon horizontal scattering angle in lead wall
XBL7111 - 4756

Figure 27c

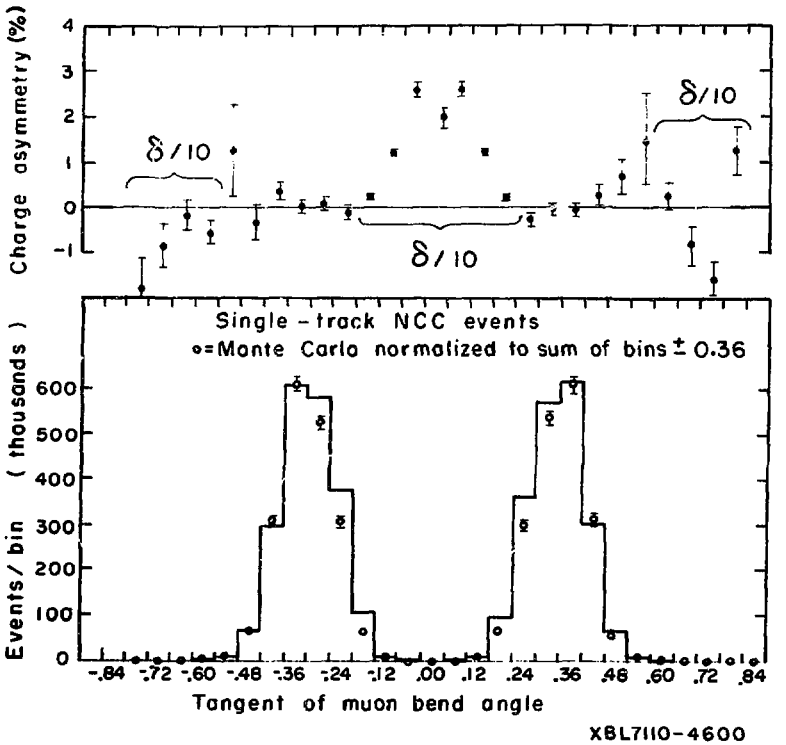
Charge asymmetry (%)
δ/10
δ/10
δ/10
Single-track NCC events
o=Monte Carlo normalized to sum of bins ± 0.36
Events/bin (thousands)
Tangent of muon bend angle
XBL7110-4600

Figure 27d

Figure 28 presents the single-track distributions of muons in the S,R,T, and W banks for good events or good-NCC events as indicated. (We show the good-NCC plots when they are available.) The Monte Carlo predictions are also shown. The agreement between the Monte Carlo and the data is generally good for the S and R banks but somewhat poorer in the T and W banks. The disagreement in the W bank is undoubtedly due to the Monte Carlo's underestimation of the multiple scattering. The systematic over-population of the even S, R, and T bins is due to randoms and knock-ons as will be discussed in IV-D-3 and IV-C-2. The systematic difference of even-bin and odd-bin charge asymmetries in the R bank is a related effect, discussed in IV-C-2. A systematic decrease in the charge asymmetry is seen in the outer bins of the T and W banks. This effect will be discussed in IV-D-3. The negative charge asymmetry of W bins 37-42 is discussed in IV-F-3.

Since we have shown that the good events and the good-NCC events are equivalent, only the good-NCC events will be considered in the discussion of the remaining corrections. If a discussion involves the entire bend-angle spectrum the NCC events will be used. However, in the case of a correction which could be expected to have dependence on the state of the C-coincidence, the good event correction will be indicated. In the case of certain corrections which are obviously independent of the C-coincidence, the good event sample will be studied simply because the corresponding study for the good-NCC events was not performed.

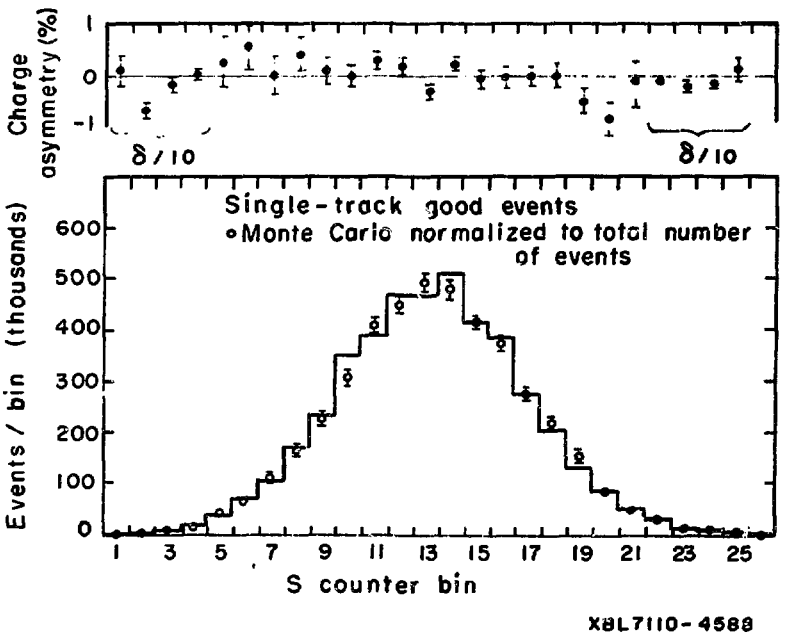
Charge asymmetry (%)
1
0
-1
δ/10
δ/10
Single-track good events
•Monte Carlo normalized to total number of events
Events / bin (thousands)
600
500
400
300
200
100
0
1
3
5
7
9
11
13
15
17
19
21
23
25
S counter bin
XBL7110-4588

Figure 28a

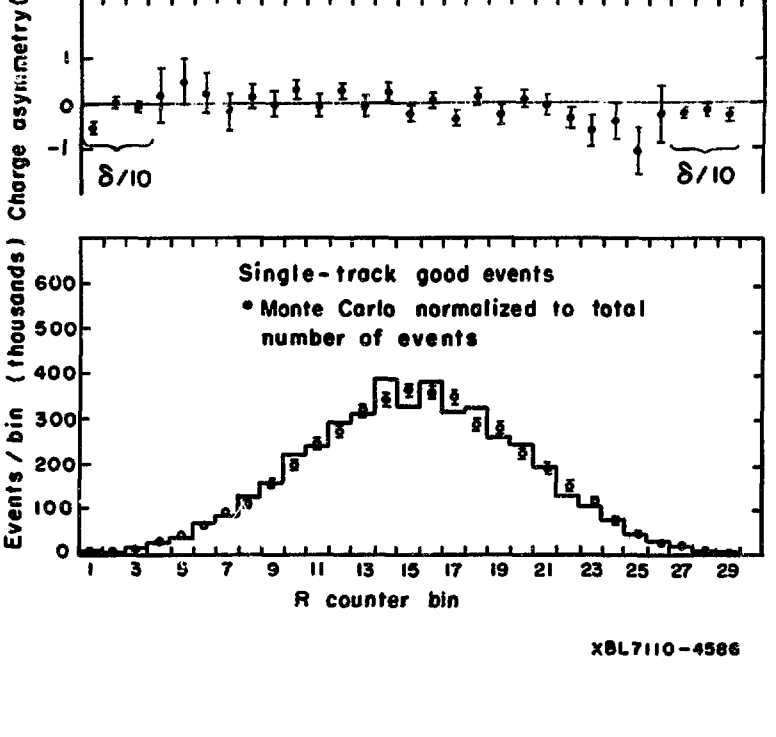
Charge asymmetry (%)
1
0
-1
δ/10
δ/10
Events / bin (thousands)
600
500
400
300
200
100
0
Single-track good events
* Monte Carlo normalized to total number of events
1 3 5 7 9 11 13 15 17 19 21 23 25 27 29
R counter bin
XBL7110-4586

Figure 28b

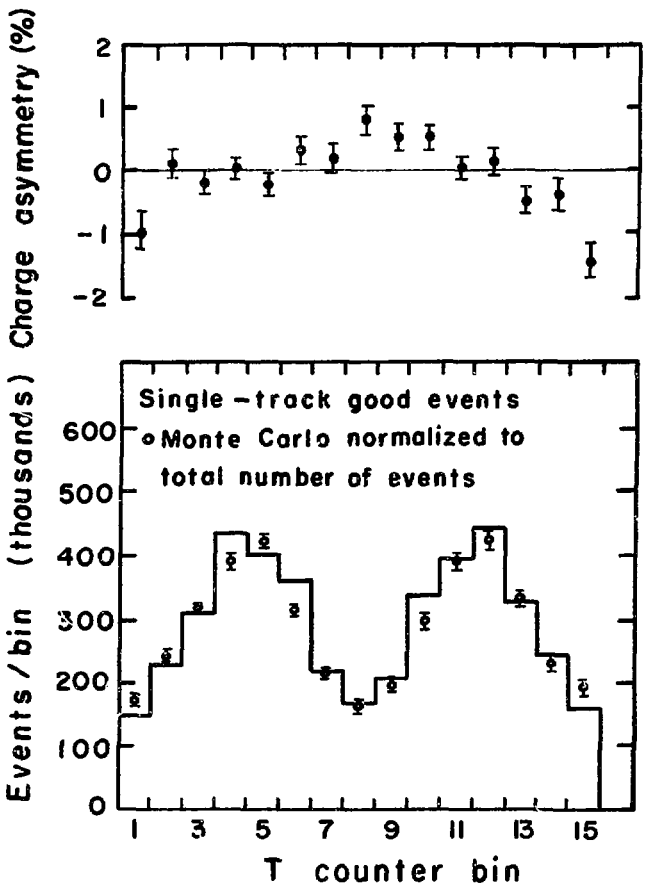
Charge asymmetry (%)
2
1
0
-1
-2
Single-track good events
Monte Carlo normalized to
total number of events
Events / bin (thousands)
600
500
400
300
200
100
0
1
3
5
7
9
11
13
15
T counter bin
XBL7110-4585

Figure 28c

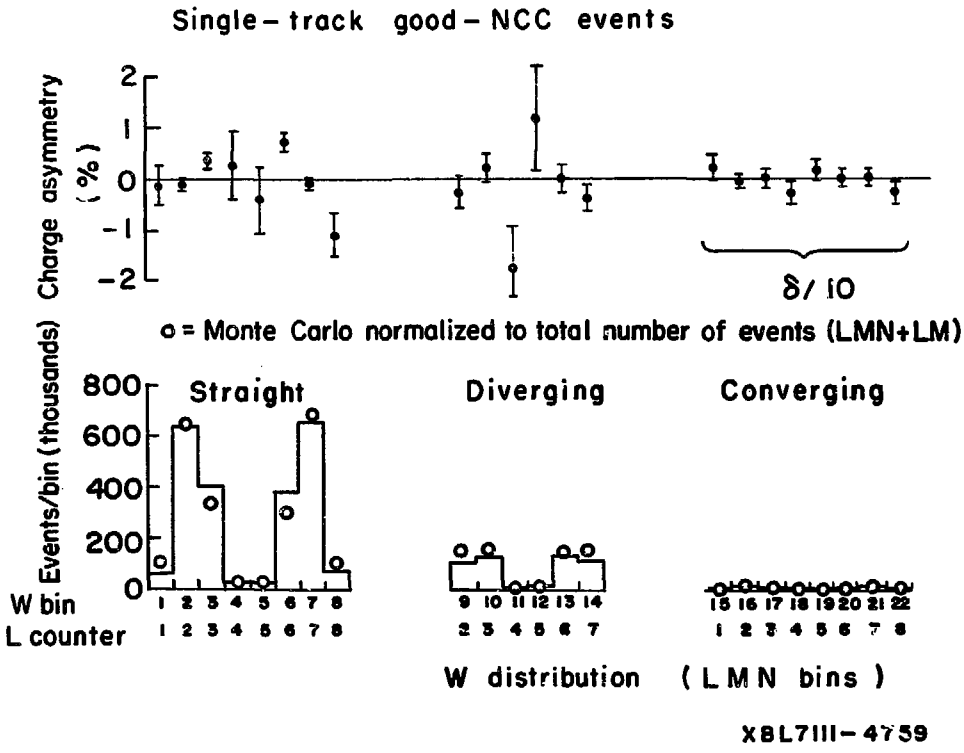
Single – track good – NCC events
Charge asymmetry (%)
2
1
0
-1
-2
δ/ 10
o = Monte Carlo normalized to total number of events (LMN+LM)
Events/bin (thousands)
800
600
400
200
0
Straight
Diverging
Converging
W bin
L counter
1 2 3 4 5 6 7 8
1 2 3 4 5 6 7 8
9 10 11 12 13 14
2 3 4 5 6 7
15 16 17 18 19 20 21 22
1 2 3 4 5 6 7 8
W distribution (LMN bins)
XBL7111-4759

Figure 28d

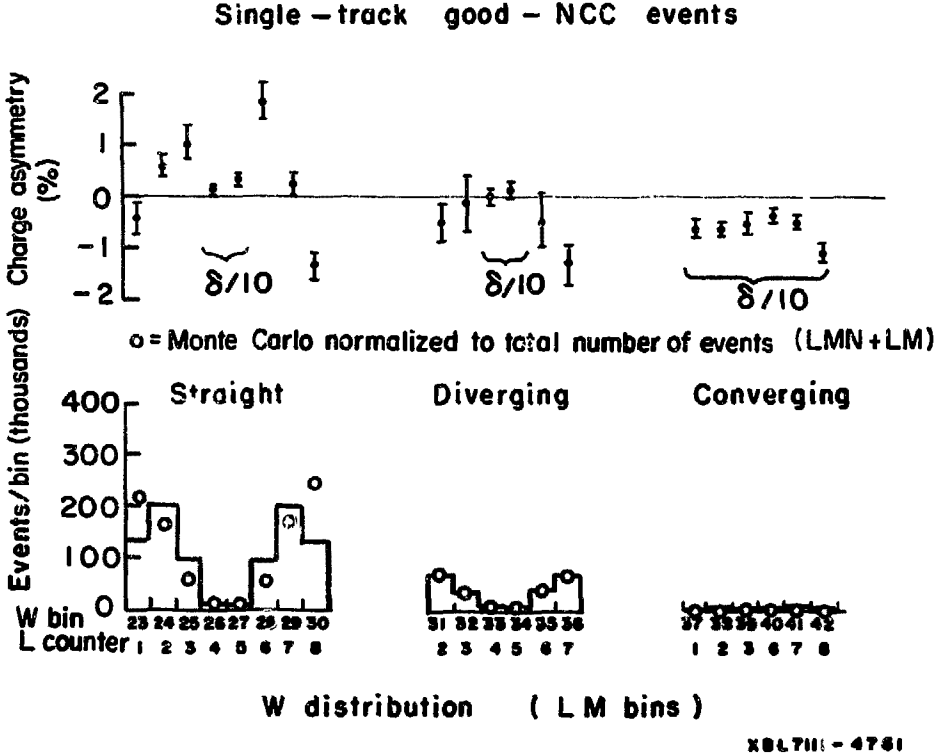
Single – track good – NCC events
Charge asymmetry (%)
2
1
0
-1
-2
δ/10
δ/10
δ/10
o = Monte Carlo normalized to total number of events (LMN+LM)
Events/bin (thousands)
400
300
200
100
0
Straight
Diverging
Converging
W bin
L counter
23 24 25 26 27 28 29 30
1 2 3 4 5 6 7 8
31 32 33 34 35 36
2 3 4 5 6 7
37 38 39 40 41 42
1 2 3 6 7 8
W distribution (L M bins)
XBL 7111 - 4781

Figure 28e

2. Knock-On Correction

Figure 29 illustrates the different ways in which a knock-on can affect an event. The 2-bin knock-ons are the most obvious type in which the electron merely causes a second bin to be on. However, due to the idiosyncrasies of our binning scheme, a knock-on can cause three bins to be on or can shift the apparent muon position with or without the turning on of a second bin. A 3-bin knock-on can occur only if the muon bin is even. A shift of the muon position can occur only if the real muon bin is odd.

The knock-on correction was studied both from the data and from the Monte Carlo events. A pass was made through the ten thousand $K^{o}_{\mu 3}$ Monte Carlo events and a file was created containing the quantities required for each event in order to perform the knock-on study. Then twenty-five passes were made through this new file with the knock-on probabilities multiplied by ten in order to generate the knock-on spectrum produced by about 2.5×10^{6} muons from $K^{o}_{\mu 3}$ decay. The knock-ons were generated at the exact muon position in the R_V or R banks according to the energy distribution given by Rossi.[29] The probability of generating a knock-on from this distribution with energy greater than a given value contains a logarithm. In order that the knock-on energy distribution would be accurate to one per cent, this log term was retained. The kinematic maximum knock-on energy

---

[29] Bruno Rossi, High Energy Physics (Prentice Hall, Inc. Englewood Cliffs, New Jersey, 1952), P. 16

Types of knock-ons

2 BIN

3 BIN

1 BIN SHIFT

2 BIN SHIFT

μ-e BIN DIFFERENCE	EFFECT: μ BIN EVEN	μ BIN ODD
0	NONE	NONE
1	NONE	1 BIN SHIFT
2	2 BIN	1 BIN SHIFT
3	2 BIN	2 BIN SHIFT
4	3 BIN	2 BIN
MORE	2 BIN	2 BIN

XBL7110-4578

Figure 29

was calculated separately for each muon. The minimum knock-on energy was taken to be 1 Mev. Fortunately the magnetic field was so strong (6kG) that the calculation is very insensitive to this lower limit which is not well known. Only 1.4×10^{-3} of the knock-ons which affected the muon track were less than 2 Mev. Only 16% were less than 5 Mev. The majority of these knock-ons were between 5 and 20 Mev.

Each knock-on was given a polar angle relative to the muon momentum in accordance with two-body kinematics:

$$\sin \theta = \left[\frac{1 - T/T_M}{1 + T/(2m_e)}\right]^{\frac{1}{2}}$$

T = electron kinetic energy

T_M = kinematic maximum knock-on kinetic energy

m_e = mass of electron

The azimuthal angle was chosen randomly. The multiple scattering of each knock-on before leaving a counter was neglected. Since most of the knock-ons had an energy greater than 5 Mev, this is a good approximation.[30] However, the energy loss in leaving a counter was calculated.

The magnetic field was approximated again by a cylindrical grid with two inch radial and vertical spacing. However, in order to avoid the solution of a transcendental equation for each knock-on, the magnetic field was taken to be vertical at

---

[30] When going through one R counter [.65 g/cm^2] each knock-on undergoes a nuclear multiple scatter of $\sim$.04 radians. It also has a probability of only $\sim$.1 of creating a secondary knock-on greater than one-tenth its energy.

each point but with its proper magnitude. In actuality the vertical component was only ∿90% of the total field so that this treatment results in an error of ∿10% in the turning radius of the electron. It turns out that this also produces an error of ∿10% in the total correction to the charge asymmetry. Note that this error is uniform over the knock-on momentum spectrum unlike an error in the energy spectrum. Since we are unwilling to believe a Monte Carlo to an accuracy better than 10% anyway, this treatment was deemed sufficient.

The variation of the field over the knock-on orbit was neglected. Each knock-on was given a turning radius and hence a final position according to the field at its point of origin. Even though the R counters were between the edges of the pole faces, this approximation is good. The field turned fairly rapidly at this location but the magnitude of the field was constant to about 4% over a typical knock-on orbit. Due to the cylindrical symmetry of the field, the change in the field was nearly zero between initial and final knock-on positions.

In order to study the multiple-track knock-on events in the data, scatter plots were made of the smallest bend angle versus the largest for events with just two tracks containing different R bins only. The events having the 3-bin configuration of Figure 29 were included also. Thus all types of events in Figure 29 except the 1-bin-shift variety are included in the plots. Table II shows the scatter plot of the asymmetric events while Table III shows the corresponding plot of the number of events. Only NCC events are included. The charge asymmetry in each bin is the ratio of the asymmetric events to the events.

Table II

ASYMMETRIC EVENTS

With Two Tracks Having Different R Bins Only

Smallest Bend Angle

Largest Bend Angle	.00	.06	.12	.18	.24	.30	.36	.42	.48	.54	.60	Sum
.00	0	0	0	0	0	0	0	0	0	0	0	0
.06	0	-5	0	0	0	0	0	0	0	0	0	-5
.12	-83	-196	0	0	0	0	0	0	0	0	0	-279
.18	-808	-738	-46	-35	0	0	0	0	0	0	0	-1627
.24	0	-2839	-2370	-121	-33	0	0	0	0	0	0	-5363
.30	-1361	-613	-2539	-1579	-11	-2	0	0	0	0	0	-6105
.36	-687	-1362	-62	-2117	-452	2	-4	0	0	0	0	-4682
.42	-138	-476	-434	-4	795	545	-4	-2	0	0	0	282
.48	-25	-30	-66	61	-1	3061	92	0	0	0	0	3092
.54	-3	8	18	287	278	-4	4060	-1	0	0	0	4643
.60	0	1	24	65	1059	118	0	2543	0	0	0	3810
.66	-1	11	24	53	154	1600	32	106	848	0	0	2827
.72	0	-5	8	77	372	550	1435	0	75	262	0	2774
.78	3	4	13	23	106	365	482	647	0	50	8	1701
Sum	-3103	-6240	-5430	-3290	2267	6235	6093	3293	923	312	8	1068

Table III

EVENTS

With Two Tracks Having Different R Bins Only

Smallest Bend Angle

Largest Bend Angle	.00	.06	.12	.18	.24	.30	.36	.42	.48	.54	.60	Sum
.00	0	0	0	0	0	0	0	0	0	0	0	0
.06	0	21	0	0	0	0	0	0	0	0	0	21
.12	193	616	0	0	0	0	0	0	0	0	0	809
.18	1558	2166	368	125	0	0	0	0	0	0	0	3,217
.24	0	3367	4490	545	139	0	0	0	0	0	0	10,741
.30	3175	1719	4941	3737	33	18	0	0	0	0	0	13,623
.36	2127	3780	446	5597	3222	6	0	0	0	0	0	15,178
.42	920	1724	1932	28	6537	1587	4	-2	0	0	0	12,130
.48	143	356	616	379	5	6359	212	0	0	0	0	8,070
.54	27	36	170	791	664	0	7350	3	0	0	0	9,041
.60	4	21	48	383	2273	364	0	4419	0	0	0	7,512
.66	5	7	70	211	722	3628	60	154	1526	0	0	6,383
.72	4	1	34	277	1276	1350	3865	0	105	492	0	7,404
.78	3	2	15	59	558	1407	1126	1599	0	82	58	4,909
Sum	8159	15,016	12,530	12,132	15,429	14,719	12,617	6173	1631	574	58	99,038

We see that the charge asymmetries per bin are typically ± 40 % implying that about 40 % of the events are knock-ons. The total charge asymmetry, however, is only 1% indicating that the neutron contamination in the plots is higher than for the corresponding NCC, single-track events. Nevertheless it is still small in terms of the accuracy of the knock-on correction. Hence a method of measuring the knock-on correction is to assume the charge asymmetries in bend-angle bins $\geq .24$ are really zero and the asymmetric events in these bins are entirely due to knock-ons. With this assumption then in terms of the asymmetric events, the knock-on correction to be subtracted from each bend-angle bin greater than or equal to .24 is the corresponding sum in the *last line of Table II*. In Table IV we list these corrections and also show the total number of (NCC) multiple-track asymmetric events in each bin. We see that most of the multiple-track charge asymmetry is due to R-bank knock-ons. Events with the multiple-track R-bank knock-on configuration of Figure 29 total 2% of all multiple-track events.

Similar scatter-plots were made for the Monte Carlo knock-on events with the bend-angle spectrum of the muons corrected so as to agree with the data. The resulting predictions for the knock-on corrections are also presented in Table IV. The statistical errors of the Monte Carlo predictions are negligible compared to the systematic error of about 10%. The measured corrections have no statistical error since they are direct measurements of the events concerned if the assumption of zero charge asymmetry in each bin except for knock-ons is justified. The agreement

TABLE IV
R Knock-On Corrections
in Terms of NCC Asymmetric Events

Bend-Angle Bin	All NCC Multiple-Track Events	Corrections	
		Measured	Monte Carlo
.24	3425	2267	444
.30	7342	6235	4534
.36	5951	6093	6296
.42	3376	3293	3250
.48	922	923	892
.54	290	312	145
.60	45	8	17
.66	14		
.72	44		
.78	5		
Total Multiple-Track	21,414	19,131	15,578
1-bin-shift		4026	3,536
Total		23,157	19,114
$\Delta \hat{G}$ (%)		-0.558	-0.461

XBL7111-4773

between Monte Carlo and measured corrections for bend angles greater than or equal to .36 gives us confidence in the Monte Carlo. However, the agreement near the neutron cut is poor.

The 1-bin-shift knock-ons are especially troublesome since they do not indicate their presence with an extra track. They are believed to be responsible for the increase of the NCC single-track charge asymmetry as a function of bend angle evident in Figure 20. They occur only when the muon goes through a single-counter (odd-numbered) R bin as shown in Figure 29. Since they produce single-track events they shift positive muons toward larger bend angles but negative muons toward smaller bend angles. The positive charge asymmetry of the even-numbered R bins in Figure 28b is caused by the shift of positive muons to an even bin while the corresponding negative muon is lost in the neutron cut. Hence by studying the events in the neutron cut we can measure the number of these lost negative muons. We assume that the neutron-induced charge asymmetry does not depend upon whether the apparent muon goes through an odd or even R bin. Then the measured 1-bin-shift knock-on correction in Table IV is the difference of the asymmetric events with odd and even R bins in the neutron cut. The corresponding Monte Carlo correction is also listed.

The two R knock-on corrections to the charge asymmetry are also given in Table IV. Our final R knock-on correction to the good-NCC events is their average. We take the systematic error to be about half their difference.

$$\Delta\delta_{R\ \text{knock-on}} = -(5.09 \pm 0.50) \times 10^{-3}$$

This correction is reasonably independent of the state of the C-coincidence. The corresponding correction for good events is $\Delta\delta_{R\ \text{knock-on(good)}} = -(5.01 \pm 0.50) \times 10^{-3}$

The corrections for knock-ons in the S and T banks are much smaller than the R correction because the magnetic field was weak enough near the S and T banks that we were able to stop most of the appropriate knock-ons with the placement of 0.5 in. of wood just downstream of these banks. These corrections are opposite in sign to the R correction. The measured 1-bin-shift corrections are:

$$\Delta\delta_{S\ \text{1-bin-shift}} = +(1.7 \pm 0.4) \times 10^{-4}$$

$$\Delta\delta_{T\ \text{1-bin-shift}} = +(2.4 \pm 0.4) \times 10^{-4}$$

We have examined scatter plots similar to those for the R knock-on events for all types of multiple-track events. In particular the measured correction for the S bank multiple-track knock-ons is

$$\Delta\delta_{S\ \text{Multiple-track}} = +(1.4 \pm 0.4) \times 10^{-4}$$

The measured corrections are negligible for all other types of multiple-track events when they are grouped into reasonable categories (such as events with an extra R and an extra S counter). The correction for all knock-ons is

$$\Delta\delta_{\text{all knock-ons}} = -(4.54 \pm 0.51) \times 10^{-3}$$

Having made this correction we feel that we have eliminated all biases on the charge asymmetry caused by the neutron cut

except an effect caused by T randoms asymmetry to be discussed in Section IV-D-3. In particular the effects of extra tracks caused by strong interactions of pions before decay are taken into account by the use of measured knock-on corrections. Such extra tracks are expected to have a positive charge asymmetry and thus cannot be the cause of the observed discrepancy between the Monte Carlo and measured corrections for R knock-ons.

3. Residual Air - Mass Extrapolations in General

This is the first of a series of effects which we will treat through the use of a linear mass extrapolation. The procedure is to add mass in various regions of our apparatus in order to extrapolate the charge asymmetry to the result which would be obtained by a zero-mass detector, the ideal detector to be used for this experiment. The procedure is valid as long as the mass added is much less than an interaction length and as long as the number of events affected by this mass is not too large (so that the mass does not change the denominator in the expression for the measured charge asymmetry). In all our extrapolations we added the same material as used in the detector. Hence we do not need to worry about the differences of various nuclei.

The zero-mass intercept was found by doing a minimum χ^2 fit of the measured points to a straight line. This fit may be solved analytically as indicated below:

δ_i = charge asymmetry at point i

σ_i = statistical standard deviation of point i

m_i = mass at point i

δ_o = charge asymmetry at zero mass

σ_o = statistical standard deviation at zero mass

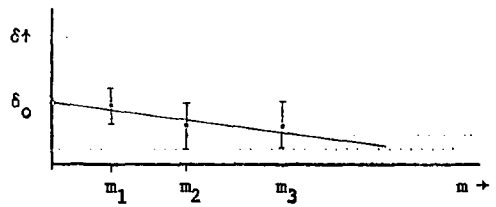

$$\bar{m} = \frac{\sum_i (m_i/\sigma_i^2)}{\sum_i (1/\sigma_i^2)} \qquad m_i' = m_i - \bar{m} \qquad \overline{m'^2} = \frac{\sum_i (m_i'^2/\sigma_i^2)}{\sum_i (1/\sigma_i^2)} \quad \cdots$$

$$\delta_o = \frac{\sum_i (\delta_i/\sigma_i^2)}{\sum_i (1/\sigma_i^2)} - \bar{m} \frac{\sum_i (\delta_i m_i'/\sigma_i^2)}{\sum_i (m_i'^2/\sigma_i^2)}$$

$$\sigma_o = \frac{1}{\sqrt{N}} \sqrt{1 + (\bar{m}^2/\overline{m'^2})}$$

$N = \sum_i (1/\sigma_i^2)$ = total number of events in all points

If we consider such an extrapolation to be a correction, the correction is then

$$\Delta\delta = \delta_o - \delta_1 \pm \sqrt{\sigma_o^2 - \sigma_1^2}$$

In order to do the residual air extrapolation we ran for twenty minutes with the vacuum tank containing air at atmospheric pressure. We accumulated 3180 events with bend angle $\geq .21$ which had a charge asymmetry of -3.5%. Since in this case $m_2/m_1 \geq 10^5$, the correction is negligible.

4. Anti Mass Extrapolation

Figure 30 shows the anti mass extrapolation. The high-mass points of this plot were taken with scintillator (wrapped in paper) hanging just downstream of each of the six separate anti counters. The purpose was to increase the inactive volume of each counter in which neutrons could generate background events. The edge of each piece of scintillator was well aligned ($\pm 1/32$ in.) with the beamside edge of the appropriate counter and the added scintillator extended from this edge at least 9 in. away from the beam. The inactive lengths of A_5 and A_6 were smaller than those of the other counters but this fact is not important since really for each counter only the ratios of the high masses to the low mass are important. The mass added behind A_5 and A_6 was half that added behind the other, thicker counters (the mass value shown in Figure 30). The problems involved in averaging over the six counters were negligible.

The inactive length of each counter was determined with an oscilloscope as follows:

$$\text{inactive length} = \frac{\text{discrimination level}}{\text{minimum-ionizing pulse height}} \times \text{thickness}$$

However, a special problem arose in the anti mass extrapolation due to the fact that more than one charged particle must have been created by any relevant neutron interaction. The multiplicity must have been at least two for any event which triggered both P's. Since neutron interactions often have high multiplicity and the secondaries may have low momentum (high pulse height) we take the average multiplicity to be 3^{+3}_{-1}. The inactive

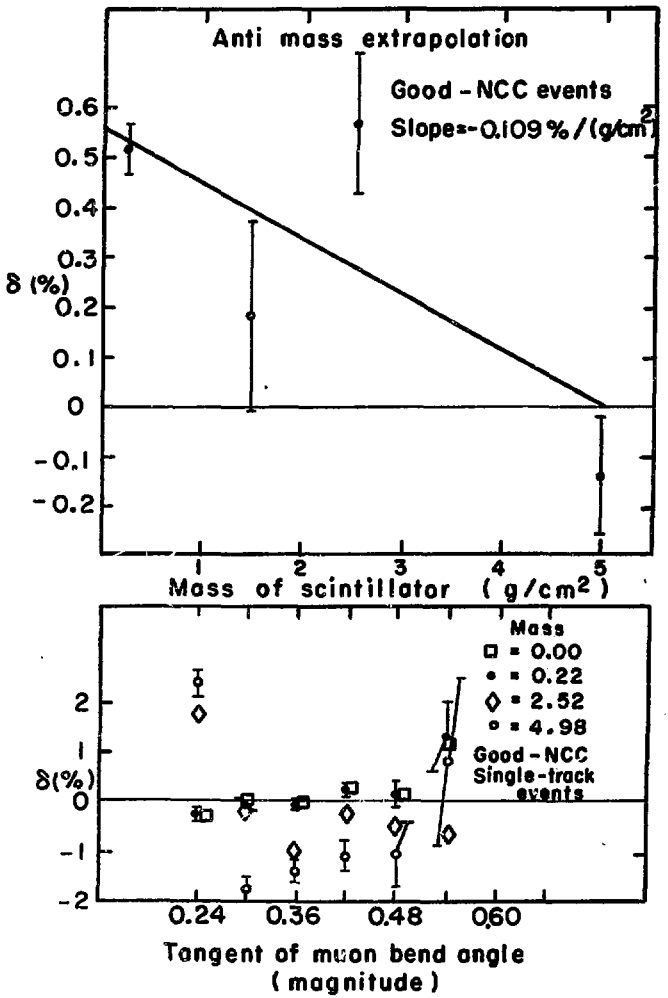
Anti mass extrapolation
Good - NCC events
Slope=-0.109 %/(g/cm²)
δ (%)
0.6
0.5
0.4
0.3
0.2
0.1
0
-0.1
-0.2
1
2
3
4
5
Mass of scintillator (g/cm²)
Mass
□ = 0.00
• = 0.22
◇ = 2.52
○ = 4.98
Good - NCC
Single-track
events
δ(%)
2
1
0
-1
-2
0.24
0.36
0.48
0.60
Tangent of muon bend angle
(magnitude)
XBL7110-4582

Figure 30

length is divided by the multiplicity to obtain the effective inactive length which is the low mass value of Figure 30. The error in the multiplicity then corresponds to an error of $\pm.11$ g/cm^2 in the placement of the origin of the mass axis. The rest of the plot is unaffected.

The confidence level for the straight line fit is only .03 but the correction is small:

$$\Delta\delta = (3.8\pm1.2) \times 10^{-4}$$

The above error is the statistical error of the linear fit. We assign an additional error of 1.2×10^{-4} as a result of the uncertainty in the average multiplicity. Hence the anti-mass correction to the charge asymmetry is

$$\Delta\delta = (3.8\pm1.7) \times 10^{-4}$$

Figure 30 also shows the charge asymmetry per bend-angle bin from .24 through .54 as a function of anti mass. For the sake of clarity, the statistical errors are shown only for the points at .22 and 4.98 g/cm^2. This plot is interesting because it shows the effect of a known source of neutron interactions in these bins. It should be compared with Figure 19 and substantiates our claim that the NCC events in these bins are free of neutrons but that the CC events are not.

D. Randoms

Figure 31 illustrates some of the types of random events we may have accepted. Type 1 represents the real events which we meant to collect while types 2 and 3 represent the random-trigger events which contaminated the real events and which we continuously monitored through the use of delayed-time triggers. Correlated counts are joined by a line representing a particle's trajectory. Uncorrelated counts are not joined. Event type 4 illustrates why randoms subtractions are notoriously unreliable. This type of event is included in the measurement of all of the first three types. Hence, when one subtracts the measured types 2 and 3 from 1, one subtracts type 4 twice, thereby making an error. Events of type 4 cannot be measured by any randoms monitoring technique which uses two time slices. Three time slices are required. Since we actually used three time slices, we could measure events of type 4. However, there are obviously an infinite number of randoms configurations which we could not measure. To do so would require an infinite number of time slices and an infinite amount of equipment.

If we define the "on-time" of a given configuration of counters to be the probability that this configuration is on at any given time, then the on-time for a given type of event is simply the product of the on-times of each uncorrelated track it contains. With this in mind there is a close analogy between a randoms subtraction and a perturbation theory expansion involving an infinite series of Feynman graphs. The number of vertices in

Types of random events

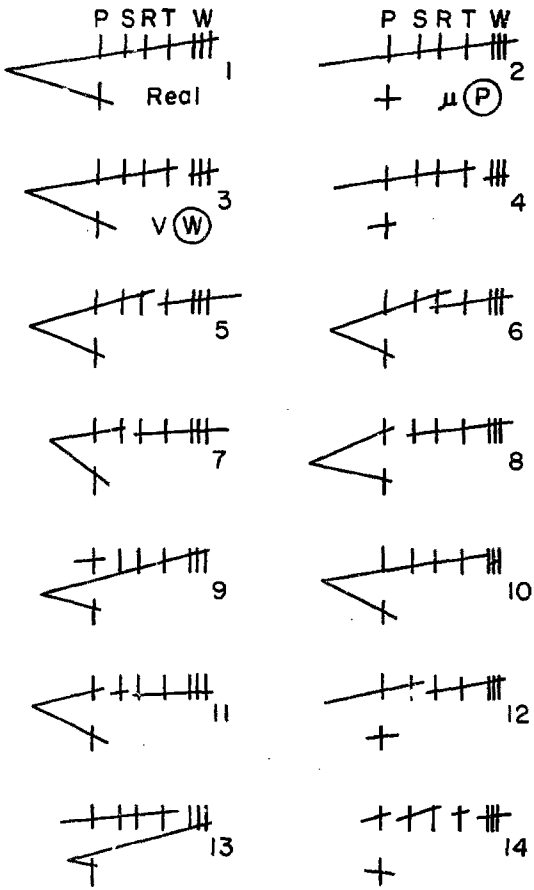

Figure 31

a graph corresponds to the number of uncorrelated tracks in a diagram such as those shown in Figure 31. The coupling constant of the randoms-subtraction series is proportional to the beam intensity. A randoms subtraction thus makes sense only if the beam intensity is sufficiently low that the series can be terminated after the first few terms. Fortunately this is true for this experiment. The on-times of individual counters in our experiment were typically 3×10^{-3} as will be indicated in IV-D-3. The on-time for all W bins combined was $\simeq 2 \times 10^{-3}$.

1. Measured Random Triggers

The randoms subtractions which we have made on the main data sample are listed in Table V. The only problem involved in making the measurements required for these subtractions was to ensure that prompt and delayed time slices were equivalent. Since the separation between time slices was precisely the time of one Bevatron revolution, beam structure was not a problem. The only remaining consideration was to ensure that prompt and delayed time coincidence circuits had equal resolving times. This equality was checked weekly for the strobe circuits (delayed P subtraction) and the resolving times for all such circuits were found to be 37 ± 2 nsec. The equivalence of prompt and delayed MECL coincidence circuits was checked twice for all bits. The resolving times were found to be stable at 60 ± 3 nsec. Hence we believe that these randoms subtractions were measured to a systematic accuracy of 5%. Since measured random triggers account for only 1.8% of the prompt, good-NCC events, the statistical error of the randoms subtractions is negligible (1% of δ). Therefore, the correction for measured random-trigger events is

$$\Delta\delta = (-12.1 \pm 0.6) \times 10^{-4}$$

In order to double check these statements the ($\bar{A}P$) on-time was measured both by the delayed MECL bits and by the strobe logic via the events with two strobes. The ratio of the two on-times was equal to the ratio of the measured resolving times within 2%. This test indicates that both electronics systems worked and in addition that beam structure was not severe since the two time slices had different lengths.

TABLE V

Randoms Subtractions

Type of Events (normal data)	Number of Events	Asymmetric Events	(in %, uncorrected - defined in IV-A) δ	Λ	α
ALL					
prompt	5,569,890	103,477	1.86	-0.57	-0.06
delayed Matrix	161,588	20,686	12.80	-5.13	-0.79
delayed P	66,919	15,255	22.80	-1.14	-0.72
real	5,341,383	67,536	1.26	-0.42	-0.03
GOOD					
prompt	4,834,107	34,991	0.72	-0.32	-0.01
delayed Matrix	80,034	8,562	10.70	-4.56	-0.66
delayed P	39,605	2,710	6.84	-0.66	-0.10
real	4,714,468	23,719	0.50	-0.24	0.01
GOOD-NCC					
prompt	4,224,279	26,904	0.64	-0.30	-0.04
delayed Matrix	43,861	3,604	8.22	-5.68	-0.64
delayed P	30,545	1,892	6.19	-0.45	-0.04
real	4,149,873	21,408	0.52	-0.25	-0.04

2. Unmeasured Random Triggers

As we have indicated a randoms subtraction is easy to measure. The main problem is knowing whether one is subtracting all the necessary random events. Since the T bank was almost never required in the strobe, events of types 5 and 6 (Figure 31) were correctly subtracted with the delayed Matrix events. But events of types 7 and 8 were correctly subtracted only when the R's and S's respectively were not required in the strobe. We studied such events via the S and R TPH analyses. (Figure 26 shows a TPH analysis of the T counters). The timing of the S and R counters in the strobe circuitry (Figure 11) was loose enough that events were accepted with S and R counts up to 4 nsec later than almost all of the real muon events. Hence the events in this time region consist of random events and a small number of real events. The concentration of random events is equal to the concentration under the reals peak. Since the real events have almost no charge asymmetry, the asymmetric events in the late time region must be attributed to random events. Multiplying by the appropriate factor to correct for the different resolving times we find the contribution to the charge asymmetry of random S and R events.

$$\Delta\delta_{(S)} = (0.3 \pm 1.4) \times 10^{-4}$$

$$\Delta\delta_{(R)} = (-1.4 \pm 2.8) \times 10^{-4}$$

With this technique we have measured the contribution to the charge asymmetry of <u>all</u> events with random S and R counts. (Random here means uncorrelated with the strobe, the timing of

which was generally controlled by the muon P count. Events of type 9 are an exception.) Thus the measurements include events of types 7, 8, 11, 12, and 14 in Figure 31.

Events of types 9 and 10 satisfy requirements for a $K^o_{\mu 3}$ signature which are only slightly looser than normal. The M counter randoms are charge symmetric (Section IV-D-3) and random P counts must be charge symmetric since the P counters are upstream of the magnetic field. Hence we accept events of types 9 and 10 as $K^o_{\mu 3}$.

The contribution to the charge asymmetry of events of type 4 is 2×10^{-5}. This measurement was performed by multiplying the delayed P contribution (type 2) by the ratio of the asymmetric muon events of types PSRT$\overline{\text{W}}$/ PSRTW. Events with the pion P and muon W correlated in random time (such as event type 13) make a contribution to the charge asymmetry of less than 10^{-4}.

Hence the randoms subtraction has apparently performed the necessary correction to the charge asymmetry for random events to an accuracy of 2×10^{-4}. We increase the error of the randoms subtraction accordingly.

3. Single-Bin Randoms

In this section we discuss the effects of single-bin randoms on normal $K^{o}_{\mu 3}$ events. The main effect of such randoms is to shift the apparent muon position in a given bank in the same manner as accomplished by knock-ons. Randoms in the 1-bin-shift configuration (Figure29) cause the overpopulation of even S,R, and T bins in Figure 28. (Knock-ons make a contribution in the R bank.) However, randoms are much less dangerous than knock-ons because they are not correlated with the muon track and are charge symmetric in all banks except the T bank. For a given bank we define:

Λ_i = geometric bias (defined in IV-A) of events in bin i

$O_i^{\uparrow}$ = on-time of bin i with the field up

Then a reasonable definition of the effective charge of a random in bin i is Λ_i if the field is up and $-\Lambda_i$ if the field is down. Hence the on-time for asymmetric randoms in bin i is given by:

$$\text{asymmetric on-time of bin i} = \Lambda_i \frac{(O_i^{\uparrow} - O_i^{\downarrow})}{2}$$

The on-time for asymmetric randoms in the entire bank is then the sum of these quantities over all bins i. The asymmetric on-times of the various banks (average of up and down) are given below:

Asymmetric On-Times

(units of 10^{-4})

S	R	T	L	M	N
0 ± 1	1 ± 1	65 ± 3	-2 ± 3	0 ± 3	2 ± 2

As in the case of knock-ons the main danger of randoms is that they may shift the bend angle of events asymmetrically into the neutron cut. Less than about 1/3 of the randoms in an S,R, or T bank are close enough to any particular muon track to affect its bend angle. Hence the effects of randoms in banks other than the T bank are negligible. Because randoms are not correlated with the muon track, we expect the effects of even the T randoms on the charge asymmetry to be small. This expectation is borne out by the T bank scatter plot of asymmetric events (similar to Table II). From this plot we find that the correction to the charge asymmetry due to the asymmetry of T randoms is negligible.

The effects of the T randoms asymmetry can, however, be seen in the outer bins of the T and W banks in Figure 28. Since the positive particles causing the randoms asymmetry generally have a low momentum, the randoms asymmetry is largest in the outer T bins. Hence the excess positive events which become multiple-track events due to the T randoms asymmetry tend to have outer T and W bins. Such multiple-track events are removed from Figure 28 but not from the determination of the charge asymmetry unless they are shifted into the neutron cut. The T bank 1-bin-shift knock-ons also contribute to the

negative charge asymmetry of outer T bins. The excess positive charge asymmetry in the central bins of the T and W banks is due mainly to the exclusion of 1-bin-shift R bank knock-on events in the neutron cut. This cut excludes negative high momentum events leaving a positive charge asymmetry in the T and W bins which tend to be populated by high momentum events.

E. Pion Interactions

If we define

T_s = strong interaction transition operator

χ = any final state

R = rotation of angle π about 2-axis of isospin space

then using the isospin invariance of strong interactions

$$\langle\chi|\ T_s|\ p,\pi^+\rangle = \langle R\chi|\ T_s|\ n,\pi^-\rangle$$

$$\langle\chi|\ T_s|\ n,\pi^+\rangle = -\langle R\chi|\ T_s|\ p,\pi^-\rangle$$

and the corresponding differential cross sections are equal. One can then naively use this line of reasoning to conclude that the asymmetry of pion interactions is due only to the unpaired protons in hydrogen nuclei and the unpaired neutrons in heavy nuclei. The main oversight of this argument is that it neglects the electromagnetic interactions which are important since they cause ionization energy loss, the process by which particles are detected. The electromagnetic interactions also cause a charged particle to turn in a magnetic field. Hence any detection apparatus containing counters and a magnet is expressly non-invariant under isospin rotations of the above reactions. The above argument is reasonably valid in a situation in which strong interactions dominate such as penetration of pions through the lead wall. But in the upstream portion of our system we expect the selective absorbtion of π^- via the reaction

$$\pi^- \ p \rightarrow \pi^0 \ n$$

which has a neutral final state.

1. P Counter Mass Extrapolation

The P mass extrapolation was performed in order to measure the charge asymmetry in the absorption of $K^{o}_{\mu 3}$ pions before they could traverse the inactive length of the relevant P counter. The plot is shown in Figure 32. Differing amounts of wrapped scintillator were placed upstream of P_{up} and P_{down} to provide the two high mass points. The two low mass points represent the portions of the main data with the pion up and down. The two P counters were run with different discrimination levels in order to provide these two points. The inactive lengths were measured as described in section IV-C-4 except that here there is no multiplicity problem. The straight line fit is good and the correction is

$$\Delta\delta = (0.9 \pm 3.6) \times 10^{-4}$$

expressed as a correction to the charge asymmetry of all uncorrected, good-NCC events.

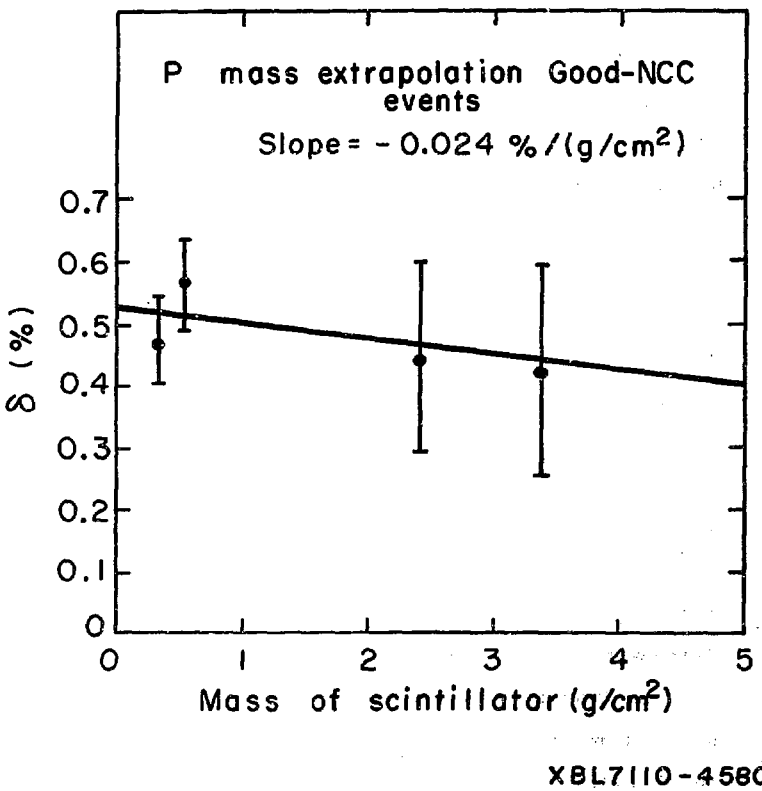
P mass extrapolation Good-NCC events
Slope = - 0.024 %/(g/cm²)
δ (%)
0.7
0.6
0.5
0.4
0.3
0.2
0.1
0
0
1
2
3
4
5
Mass of scintillator (g/cm²)
XBL7110-4580

Figure 32

2. Penetration of Lead Wall

In this section we consider the possiblity that pions penetrated our lead wall without decaying and thus caused us to identify them as muons. (Decay in flight is considered in the next section.) Since this penetration is presumably a small effect, the main danger is that pions may have penetrated the lead wall asymmetrically.

One manner in which this could have occurred is that pions may have gone through a portion of the hole in the lead wall and hence an H counter on their way to the L bank. Events with an H counter on comprise 5.3% of the data of which 3.1% is due to H randoms. If all H events are excluded from the uncorrected, good-NCC events, the charge asymmetry increases by $(2.7 \pm 1.1) \times 10^{-4}$. This change is small but not negligible. However, examination of a scatter plot of W bin versus H counter shows that the H counts causing the above change (which is on the edge of statistical significance) are not correlated with the W bins of their events. Hence we attribute this slight charge asymmetry change to interactions of $K^{o}_{\mu 3}$ pions from normal events which did not penetrate the lead wall. Consequently we make no correction for this effect.

The most direct route for pions to take to the L bank was through the entire lead wall. In section IV-C-1 we showed that some strongly interacting particles (high energy protons) were able to take this path. This is not unreasonable. Since the lead wall was only about five interaction lengths thick (including steel plates), we expect about 0.7% of such protons to have passed through

the wall without having a strong interaction at all. We expect the pions from K_L^o decay, however, to have had a much smaller penetration probability due to their lower momenta. Those pions which reached a momentum less than ∿500 MeV/c while inside the lead wall experienced a sharp decrease in the interaction length due to the onset of the Δ(1236) resonance.

Every cloud has a silver lining, even our cloud of neutrons. The penetration of our lead wall by neutron-induced high energy protons gives us a calibration for an upper limit on the charge asymmetry due to pion penetration. In order to obtain as pure as possible a sample of protons we consider CCSV single-track events in bend-angle bin .12. There are 14,365 such events in the main data sample with a charge asymmetry of 55.8%. Hence the sample is about 55% protons. We find that 2118 CCSV events in bend-angle bin .12 are multiple-track due to the presence of extra W bins only. These events have a charge asymmetry of 72.7%. Taking the ratio of the asymmetric events we find that the efficiency for detecting high energy protons through the presence of extra W bins is 16%. We expect the corresponding efficiency for detection of pions from K_L^o decay to be higher due to their lower average momentum and consequent higher cross section.

A total of 3.2% of the main data sample consists of multiple-track events due to the presence of extra W bins only. A rough calculation shows that essentially all of them are due to knock-ons. The extra tracks must be caused by knock-ons, randoms or strong interactions. The knock-ons and randoms are charge symmetric. (Only single counter randoms need be considered. The charge

asymmetry due to random counts of a whole W bin is negligible.) Hence the charge asymmetry of such events is due entirely to strong interactions. In the good-NCC main data sample there exist -476 ± 365 asymmetric events of this type. Hence, dividing by .16, possibly -2,975 asymmetric events are due to pion penetration. This means that an upper limit on a correction to the chage asymmetry for pion penetration is 7.2×10^{-4}.

Figure 33 shows the total and absorption cross-sections of pions and protons on various nuclei. (The terms "absorption", "reaction", and "inelastic" are synonymous in this context.) The general features are evident from the curves for Carbon. Since we are interested in detecting strong interactions, our main interest is the absorption cross sections. For incident nucleons these cross sections are essentially independent of the nucleon kinetic energy from 200 MeV to 5 GeV. (The proton cross sections have been corrected for Coulomb effects which are negligible in our region of interest, 2 to 5 Gev.) The pion absorption cross section on carbon rises to more than twice the proton cross section at the peak of the $\Delta(1236)$ resonance, falls to about 10% higher than the proton cross section at 1 GeV, and equals the proton cross section at 3 GeV. Few measurements have been made of these pion cross sections on heavy nuclei with incident momenta less than 1 GeV/c. However, Cronin and his collaborators[31] have measured the cross-sections

31. J.W.Cronin et al.,"Cross-Sections of Nuclei for High-Energy Pions", Phys. Rev. 107, 1124 (1957)

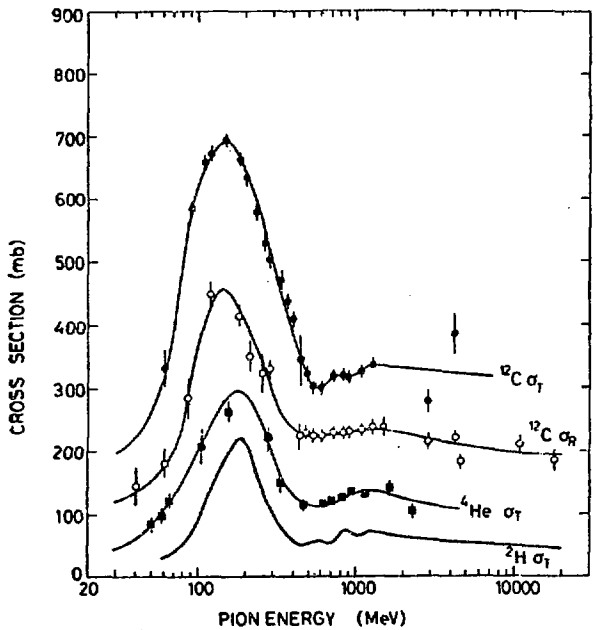

The pion-nucleus interaction; total cross-sections for ^{2}H, ^{4}He and ^{12}C, and the reaction cross-section for ^{12}C.

XBL 7111-1607

from Intermediate Energy Nuclear Physics, by W. O. Lock and D. F. Measday, p. 281, Methuen & Co Ltd, London (1970)

Figure 33a

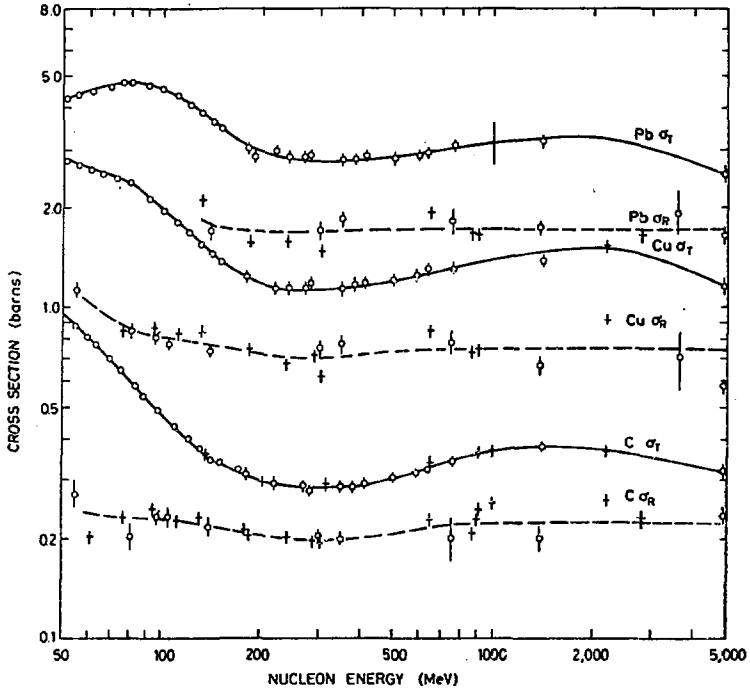

Total and reaction cross-sections for protons (+) and neutrons (0) on the nuclei C, Cu and Pb.

XBL 7111-1606

from Intermediate Energy Nuclear Physics, by W. O. Lock and D. F. Measday, p. 256, Methuen & Co Ltd, London (1970)

Figure 33b

in Table VI. The attenuation cross sections reflect the probability of occurrence of an event in which no charged particles emerge at an angle less than a give value from the beam direction. The minimum permissible angles are given in parentheses next to each cross section value.

We see that the absorption cross sections for negative pions on Cu and Pb are essentially equal to the proton cross sections from Figure 33 at the same energy. This equivalence is also shown by Cronin et al. with one set of experimental apparatus to an accuracy of about 3% for the attenuation cross sections at 1.5 GeV/c.

From the above data we see that the absorption cross sections for pions and protons are equal (± about 10%) on both light and heavy nuclei, and are flat above about 1 GeV. Below 1 GeV the proton cross sections remain flat but the pion cross sections are in the resonance region. Since pions penetrating the lead wall can generally be expected to emerge with energies in the Δ-resonance region, we expect the detection efficiency for pions via multiple W bins to be about twice that of protons from consideration of the absorption cross sections alone. But in addition the diffraction peaks for both elastic and quasi-elastic scattering can be expected to be much broader for the pions than for high-energy protons. We expect the main inelastic reactions to involve nuclear breakup. Therefore we expect the multiplicities of pion and proton inelastic reactions to be about the same. Hence we feel

TABLE VI

Cross Sections (Millibarns) at Indicated Momentum (Gev/c)

	Absorption	Attenuation		
Element	π^- at 1.1	π^- at 1.1	π^- at 1.5	p at 1.5
C	252 ± 13	212 ± 3 (12.95^0)		
Al	442 ± 20	379 ± 7 (13.50^0)	416 ± 3 (9.2^0)	421 ± 14 (9.2^0)
Ca	618 ± 27	492 ± 21 (15.60^0)	490 ± 7 (13.7^0)	486 ± 18 (13.7^0)
Cu	806 ± 35	718 ± 9 (13.70^0)		
Pb	1690 ± 100	1654 ± 34 (13.70^0)	1651 ± 32 (11.8^0)	1695 ± 64 (11.8^0)

XBL7111-4772

justified in dividing the above upper limit by a factor of 2:

$$\Delta\delta_{\text{penetration}} \lesssim 3.6 \times 10^{-4}$$

This conclusion is independent of whether or not the original hadron actually emerges from the lead wall. The arguments apply to the hadron's first strong interaction wherever it occurs.

The credibility of this upper limit is compromised somewhat by the fact that we do not know to high accuracy the relative efficiency for detecting π^+ and π^-. We expect π^- to interact more strongly than π^+ with the excess neutrons in the Pb and Fe nuclei upstream of the L and M banks. We also expect the low energy π^+ to be excluded from nuclei by Coulomb repulsion while their negative counterparts are attracted. However, these two effects are counterbalanced by the charge exchange reaction which tends to decrease the detection efficiency for π^-. If the π^+ and π^- detection efficiencies differ appreciably and there is a significant amount of pion penetration, we would expect to see a charge asymmetry in the events with extra W bins. Again we adopt the attitude that a null result means that there is no effect rather than a cancellation of two effects. Since the observed asymmetry in the events with an extra W bin on is small and is not statistically significant, we make no correction for pion penetration.

3. Decay in Flight

A Monte Carlo calculation predicts that 14 ± 2% of our events are actually due to pion decay in flight. The mechanism is K_L^o decay to a mode yielding two charged particles into our acceptance one of which is a pion which subsequently decays to a muon which in turn penetrates the lead wall. The contributions from the various K_L^o decay modes are as follows:

mode	fraction of events (%)	charge asymmetry after decay
K_{e3}^o	7.8	$-(3.22 \pm 0.29) \times 10^{-3}$
$K_{\mu 3}^o$	5.4	$-(2.1 \pm 1.0) \times 10^{-3}$
$K_{\pi 3}^o$	0.5	0
Total	13.7	

The ± 2% error includes our estimate of the possible systematic uncertainties in the Monte Carlo calculation. The largest source of uncertainty is lack of precise knowledge of the K_L^o momentum spectrum. This uncertainty can affect the result through the fact that muons from pion decay in flight have a momentum spectrum which is different from that of ordinary $K_{\mu 3}^o$ muons. The fact that the Monte Carlo successfully predicts the number of double penetration events (IV-B) gives us confidence in this calculation.

Since decay in flight accounts for a significant fraction of the data, two corrections are necessary in order to remove the effects of such events. First, the magnitude and error of the charge asymmetry must be appropriately increased to take into account the number of real $K_{\mu 3}^o$ decays. This correction will be applied after all other corrections have been made. Second, the asymmetric events resulting from decay in flight must be subtracted

from the total number of asymmetric events. This latter correction will be considered in the remainder of this section.

The charge asymmetries of the pions in each mode after K^o_L decay are listed above. The K^o_{e3} result has been published.[32] The asymmetry in $K^o_{\mu 3}$ decay is the result of this experiment. These pion charge asymmetries change as the pions interact while traversing the system. In calculating the charge asymmetry due to these interactions, the isotopic spin argument presented above is valid——if used with care. In this section we are concerned with penetration mechanisms in which the particle penetrating the lead wall is not strongly interacting and therefore is a muon. The only feasible ways in which muons can be produced are decay in flight of π and K mesons. Since π^+ and π^- are isospin conjugates, only unpaired nucleons can cause a charge asymmetry via pion decay in flight. However, this is <u>not</u> true if K^+ mesons are produced. The isospin conjugate of the K^+ is the K^o which does not produce muons readily by decay.

We approximate the cross sections of pions on light nuclei (hydrogen, carbon and aluminum) by the sum of the corresponding cross sections on free nucleons. Since the relevant pion momenta are above 1.2 Gev/c before these interactions, this approximation is reasonable.[33] For heavy nuclei (iron and lead) we divide the sum of the nucleon cross sections by $A^{1/3}$ to take into account

---

[32] See reference in footnote 27.

[33] C. J. Batty, "The Scattering of High Energy Nucleons by Complex Nuclei," Nuclear Physics <u>23</u> (1961), P. 567.

nuclear screening. This latter procedure is necessary only for the K^+ production cross sections since the pion absorption cross section in lead has been measured (Table VI). Even more importantly the charge asymmetry of this cross section has also been measured[34] for 1.1 Gev/c pions:

$$\frac{\sigma(\pi^-) - \sigma(\pi^+)}{\sigma(\pi^+)} = 0.017 \pm 0.012$$

The main cause of charge asymmetry in pion decay in flight is preferential absorption of one charge over the other. Extensive data exist on the π-nucleon cross sections.[35] We take the absorption cross section on a nucleon to be the difference of the total and elastic cross sections:

$$\sigma_a = \sigma_{total} - \sigma_{elastic}$$

If a pion suffers an inelastic collision it is very likely to lose so much energy that its decay muon can not penetrate the lead wall. With this definition in mind we find that

$$\sigma_a(\pi^- p) - \sigma_a(\pi^+ p) = 5 \pm 2 \text{ mb}$$

for incident pions in the momentum range of interest (1.2 to 2.5 Gev/c). The mass which was in the path of the pions upstream of the T bank for most of the running consists of the following components:

	aluminum	$12.0 g/cm^2$
taken to be CH	scintillator	5.2
	wood	1.3

---

[34] A. Abashian et. al., "Neutron and Proton Distributions in Pb," Phys. Rev. 104, 855 (1956).

[35] See for example G. Giacomelli et. al., "A Compilation of Pion-Nucleon Scattering Data," CERN/HARA 69-1.

If we calculate the contribution to the charge asymmetry from pion interactions with the hydrogen nuclei using the above cross section difference, we find

$$\Delta \delta_{\text{hydrogen}} = 6 \times 10^{-5}$$

The corresponding calculation for the unpaired neutron in each aluminum nucleus yields

$$\Delta \delta_{\text{aluminum}} = -5 \times 10^{-5}$$

Both corrections are negligible and they nearly cancel. The weakest link in this calculation is neglect of nuclear screening in aluminum. If such screening is included in the calculation, the aluminum correction becomes even smaller.

Pion interactions in the lead wall and steel plate near the T counters produce similarly small changes in the charge asymmetry. More pion interactions occur but the available path length for decay is shorter. We take the absorption cross section for pions on iron to be 12.6 mb/nucleon in agreement with the measured absorption cross section on copper (Table VI). We use the simple isotopic spin arguments to calculate the charge asymmetry of pion absorption on iron:

$$\frac{\sigma(\pi^-) - \sigma(\pi^+)}{\sigma(\pi^+)} = -0.018$$

The magnitude of this asymmetry agrees with that of the measured asymmetry on lead but the sign causes the two numbers to mildly disagree (by three statistical standard deviations of the measured value). With these assumptions we calculate that the change in the charge asymmetry due to interactions in the steel plate is also negligible.

$$\Delta \delta_{\text{steel}} = -7 \times 10^{-5}$$

Using the measured cross sections for lead we find

$$\Delta \delta_{lead} = +6 \times 10^{-5}$$

As we have indicated, the signs of these two changes are somewhat inconsistent but both changes are small.

The conservation of strangeness and baryon number in strong interactions causes K^+ associated production followed by $K_{\mu 2}$ decay to be completely charge asymmetric. The relevant reactions are

$$\pi^+ n \rightarrow K^+ \Lambda^0 \text{ or } K^+ \Sigma^0$$

$$\pi^+ p \rightarrow K^+ \Sigma^+$$

$$\pi^- p \rightarrow K^+ \Sigma^-$$

The last reaction seems especially dangerous but is in fact negligible since it produces K^+ mainly backwards in the center of mass. The relevant K^+ production cross sections have been published.[36] Even though the above reactions are 100% asymmetric, the change in the charge asymmetry is again negligible

$$\Delta \delta_{K^+} = 5 \times 10^{-5}$$

thanks to the fact that the production cross sections are small and appreciable energy is expended in the associated production and subsequent decay.

Hence the correction for the asymmetric events caused by decay in flight is entirely due to the decay asymmetry.

$$\Delta \delta = +(3.7 \pm 0.6) \times 10^{-4}$$

The results of this section are in apparent contradiction with the charge asymmetry found for the events in Figure 7a. In section IV-C we attributed this charge asymmetry to the positive

---

[36] Orin I. Dahl et. al., "Strange-Particle Production in π^-P interactions from 1.5 to 4.2 Bev/c II. Two-Body Final States," Phys. Rev. 163, 1430 (1967).

charge asymmetry of pion interactions. This asymmetry is apparently due to reactions such as

$$\pi^- n \rightarrow \pi^0 p$$

where we detect the proton while the isospin-conjugate reaction has a neutral final state. The results of this section depend on the fact that the proton does not decay.

F . Muon Interactions

1. Wide-Angle Scattering

Differences in the wide-angle scattering of 300 MeV electrons and positrons have been observed on Cobalt and Bismuth.[36] These differences are in good agreement with partial-wave calculations based on the Dirac equation.[37] The differences can be understood by noting that electrons scatter from a potential valley while positrons scatter from a potential hill. Hence the electron wavelength is decreased in the region of the nucleus and its diffraction pattern is consequently contracted, whereas the diffraction pattern of the positron is broadened. As might be expected from this picture, the differences become large only at low incident momenta. We define

$\sigma_{\pm}$ = differential cross-section of $e^{\pm}$

$R(\theta) = (\sigma_- - \sigma_+) / (\sigma_- + \sigma_+)$

Then the behavior of R is as follows:[36]

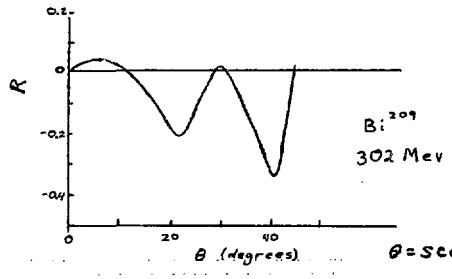

36. Goldemberg et al.,"Scattering of 300 MeV Positrons from Cobalt and Bismuth," Phys. Rev. 132, 406 (1963).
37. Herman et al., "Scattering of Electrons and Positrons from Cobalt and Bismuth:Calculations", Phys. Rev. 132, 414(1963)

Michael A. Paciotti[38] has investigated the importance of these differences for a previous $K^0_{\mu 3}$ charge-asymmetry experiment with a Monte Carlo technique. He considered the scattering from $5^o \pm 3^o$, $20^o \pm 5^o$, and $40^o \pm 5^o$ regions separately (scaled to the appropriate incident momentum and momentum transfer as the muon moved through his system). He found, as might be expected, that the contribution of the 5^o region to the charge asymmetry was greatly reduced by multiple-scattering. Hence in spite of the $\sin^{-4}(\theta/2)$ dependence of the Mott cross section, a reasonable interpretation of his results is that the contributions of the 5^o and 20^o peaks to the charge asymmtery were about equal and opposite at 5×10^{-5}. The contribution of the 40^o region was negligible by comparison. In order to estimate the effects of these differences in our own system, we multiply the above number by (2/3) to take into account the fact that very few muons in our system could induce an incorrect charge determination by scattering in the lead wall. Then even if we multiply by (6) to take into account the fact that our muons had lower momentum than those of the previous experiment, we find

$$|\Delta\delta| \lesssim 2 \times 10^{-4} \quad .$$

from either the 5^o region or the 20^o region. The effects of these two regions probably cancel to a large extent. Hence we make no correction for wide-angle scattering differences of μ^+ and μ^- in this experiment.

---

38. Michael A. Paciotti, "Charge Asymmetry in the Muonic Decay of the K_2^{0}", Ph.D. dissertation, University of California, Berkeley (1970), p. 52

The approximations used in the above treatment are invalid at low energy[39]. However, the charge asymmetry due to the events in the tails (outer nine bins on each side) of the scattering-angle plot (Figure 27c) is only (-3×10^{-4}) and is probably due at least in part to mu-mesonic X-rays as will be discussed in Section IV-F-3.

39. S.D.Drell and R.H.Pratt, "Extrapolation to Cuts and the Scattering of Electrons and Positrons", Phys.Rev.125,1398(1962)

2. Range Difference of μ^+ and μ^-

There are several possible reasons why positive and negative particles might have different rates of energy loss in matter. The most obvious cause is the fact that positive particles attract electrons while negative particles repel them. This effect should be important only at low incident energies. Heckman and Lindstrom[40] find differences in the rate of energy loss for positive and negative π mesons in emulsion at incident energies less than 2 MeV. This results in a range difference in emulsion of 6 microns. Since this energy-loss difference occurs only in the last 100 microns, it is not obvious that μ^+ and μ^- would affect our counters differently at all as a result of this effect. The total energy deposited would be the same for both. However, even if we interpret this range difference as being completely detectable by our counters, the resulting change in the charge asymmetry is only 5×10^{-6}.

Heckman and Lindstrom showed that at momenta greater than about 20 MeV/c the energy-loss rates for π^+ and π^- are equal to within 1%. Other authors [41,42] find that this equality holds up to momenta of 10 GeV/c for μ^+ and μ^- within 1%. A difference in μ^+ and μ^- energy-loss rates could arise at high energies from two-photon exchange to atomic electrons. Our result would be sensitive to any such differences as small as 0.1 %. If such differences are found, our result would be in need of correction.

40. Harry H. Heckman and Peter J. Lindstrom, "Stopping Power Differences Between Positive and Negative Pions at Low Velocities", Physical Review Letters 22,871(1969)
41. A.Crispan and P.J.Hayman, "Ionization Loss of Muons in Plastic Scintillator",Proc.Phys.Soc. 83, 1051 (1964)
42. Bellamy et al., "Energy Loss and Straggling of High-Energy Muons in NaI(Tl)", Phys. Rev. 164, 418 (1967)

3. End-of-Range Differences of μ^+ and μ^-

Positive and negative muons behave quite differently at the end of their range. We are most interested in the muons which stopped in the 2 in. steel plate between the L and M counters but which originated from a $K^o_{\mu 3}$ decay which satisfied all $K^o_{\mu 3}$ signature criteria upstream of the M bank. The ratio of the number of such muons to the number of muons associated with events which passed all signature criteria is 0.30 ± 0.03 according to the Monte Carlo. Secondaries associated with the muons which stopped in this plate could have reached the M bank, thereby completing the signature requirements. A bias on the charge asymmetry results from asymmetric completion of these requirements.

When a μ^+ stops in the above plate it simply decays to an e^+ with a lifetime of 2.2 microseconds.[43] A μ^-, however, cascades into the lowest Bohr orbit around an iron nucleus, where it is subject to capture as well as decay. The decay probability of the μ^- in a bound state is nearly the same as that of a free muon.[44] However, due to the large capture probability, the lifetime of a μ^- in the first Bohr orbit about an iron nucleus is only 200 nsec.[45]

The net effect of $\mu^\pm$ decaying to $e^\pm$ is negligible. From Figure 9 we see that the sensitive time for accepting these decay leptons is only 15 nsec. Consequently, only about 2.5×10^{-4} of our events are due to these decays. About 6% of

---

43. A.O. Weissenberg, Muons (North-Holland Publishing Company, Amsterdam, 1967), p. 15
44. Ibid., p. 177
45. Ibid., p. 163

the e^+ are lost due to annihilation, but the number of μ^- decaying in 15 nsec is about 4% lower than the corresponding number of μ^+ due to the difference in lifetimes. Hence these $\mu^\pm$ decay events are symmetric within our required precision.

The main bias on the charge asymmetry caused by end-of-the-range effects is due to mu-mesic X-rays produced during the cascade into the first Bohr orbit. Essentially all stopping μ^- produce such an X-ray well within our 15 nsec sensitive time.[46] The energies and relative intensities of these X-rays have been measured[47] and are listed below:

X-ray	Energy (MeV)	Relative Intensity
K_α	1.26	0.71
K_β	1.53	0.08
K_ν	1.70	0.21

(Here K_α, K_β, K_ν refer to the $2P \rightarrow 1S$, $3P \rightarrow 1S$, and $nP \rightarrow 1S$ transitions where $n > 3$). The efficiencies for detecting these X-rays in our M counters were calculated from the Klein-Nishina formula as given by Rossi.[48] The main source of uncertainty in this calculation is the lack of exact knowledge of the threshold of our M counters. This threshold was determined to be 0.8 ± 0.1 MeV from the known pulse heights for minimum-ionizing particles. The detection

46. C. Scott Johnson et al., "Mu-Mesonic X-Rays in the Iron Region", Phys. Rev. 125, 2111 (1962)
47. D. Quitmann et al., "Study of Mu-Mesonic X-Rays: Elements from Sulphur to Molybdenum", Nuclear Physics 51, 609 (1964)
48. Bruno Rossi, High Energy Physics, p. 78

efficiency for the K_α X-ray is particularly sensitive to this threshold value. The absorption lengths of the cascade X-rays in iron were also calculated from the Klein-Nishina formula. The results of the calculations are presented in the following table:

X-ray	(in %) Detection Efficiency	Fraction of μ with γ reaching M bank (%)	Correction $\Delta\delta$ (10^{-4})
K_α	$1.3^{+0.2}_{-0.6}$	1.50 ± 0.30	$1.95^{+0.49}_{-0.98}$
K_β	2.2 ± 0.3	0.20 ± 0.04	0.44 ± 0.11
K_ν	2.8 ± 0.3	0.55 ± 0.11	1.55 ± 0.36

The total correction to the charge asymmetry from cascade X-rays is then

$$\Delta\delta_{\text{X-rays}} = +(3.94\ ^{+0.96}_{-1.45}) \times 10^{-4} \quad .$$

The mean numbers of gamma rays[49] and neutrons emitted from an iron nucleus after μ^- capture are not well known. The absorption length of a neutron (3 to 30 Mev) in iron is about the same (35 g/cm^2) as the absorption length for a 1.5 MeV gamma ray but the detection efficiency for such neutrons in our M bank is only about 0.7 %. A reasonable assumption is that about 1 neutron and about 1 gamma ray are emitted after each μ^- capture. This is the equivalent of about 1.3 gamma rays. A correction for secondaries emitted from the nucleus after μ^- capture would then be

$$\Delta\delta \sim 1.3 \times \frac{15 \text{ nsec}}{200 \text{ nsec}} \times 3.9 \times 10^{-4} = 4 \times 10^{-5} \quad .$$

This correction is negligible but in order to take its uncertainty into account we symmetrize the error of correction

49. A.O.Weissenberg, Muons, p. 175

for X-rays:

$$\Delta\delta_{\text{end-of-range}} = + (3.9 \pm 1.5) \times 10^{-4} \quad .$$

The cascade X-rays from stopping μ^- are probably responsible for the negative charge asymmetry of events for which the muon has a large scattering angle in the lead wall. This negative asymmetry has been observed in the scattering-angle plot (Figure 27c) and in bins 37-42 of the W distribution (Figure 28e).

V. The Asymmetry

The $K^{o}_{\mu 3}$ charge asymmetry is determined as follows (in units of 10^{-4}).

	Value	Errors Statistical	Errors Systematic
after neutron cut	δ = +51.6	± 4.9	± 5.0
knock-ons	$\Delta\delta$ = -45.4		± 5.1
anti mass	$\Delta\delta$ = +3.8	± 1.2	± 1.2
randoms	$\Delta\delta$ included		± 2.0
P mass	$\Delta\delta$ = +0.9	± 3.6	
$\pi^{\pm}$ penetration	$\Delta\delta$ = none		
decay in flight			
asymmetry	$\Delta\delta$ = +3.7		± 0.8
dilution	$\Delta\delta$ = +2.9	± 2.5	± 0.4
$\mu^{\pm}$ range difference	$\Delta\delta$ = none		
$\mu^{\pm}$ end of range	$\Delta\delta$ = +3.9		± 1.5
TOTAL	δ = +21.4	± 6.7	± 7.7

Since we know of no correlations among the above corrections, the errors have been combined in quadrature. The systematic errors are to be interpreted as one standard deviation. Using this interpretation, the total statistical and total systematic errors are combined in quadrature to yield:

$$\delta = (21.4 \pm 10.1) \times 10^{-4}$$

This number should be compared to the previous result

for the $K^o_{\mu 3}$ charge asymmetry[50], the best value of the K^o_{e3} charge asymmetry[51], and the superweak prediction.[52]

previous $K^o_{\mu 3}$: $(49. \pm 16.) \times 10^{-4}$

best value K^o_{e3} : $(32.2 \pm 2.9) \times 10^{-4}$

superweak : $(28.0 \pm 0.7) \times 10^{-4}$

Our result tends to support the superweak prediction but our error is too large to allow us to make a decisive statement.

---

50. M. A. Paciotti, Ph. D. Thesis, University of California, Berkeley, California (1969). This is a reanalysis of the data of D. Dorfan et al., Phys. Rev. Letters 19, 987(1967).

51. J. Marx et al., Physics Letters 33B,222(1970)

52. See Section I.

Acknowledgements

I would like to thank R. J. Budnitz for his tireless efforts in behalf of this experiment from the stages of earliest planning until now. He even typed a portion of this thesis. The sound judgment of D. H. Miller was an important asset to the experiment. I am grateful for the large measure of trust which he placed in me. J. H. Brewer's PDP-9 program was vital to our effort but I will remember best his poetry. R. M. Graven is to be commended for building our electronics system and keeping it in top condition throughout the course of the experiment. The contributions of W. N. Ross and A. C. Entis during the construction and data-taking phases of the experiment respectively were also important. M. A. Paciotti made many helpful suggestions.

We owe thanks to the Bevatron crew and especially to the riggers. We probably had the heaviest experiment in the history of the Bevatron.

The University of Chicago has waited patiently for me to finish this thesis. Mrs. Bette Berry of the Enrico Fermi Institute typed most of it.

I owe special thanks to Bob and Jean Graven, and Jess and Susie Brewer for providing me with a place to stay and transportation during my five week stay in Berkeley while finishing this thesis. My wife Betty and son Michael remained in Chicago. I am grateful for their boundless tolerance and eagerly anticipate seeing them again.

Appendix 1: Definitions and Applications of C, P, $\vec{T}$[1]

Notation: $I \equiv$ identity operator

$\vec{I} \equiv$ operation of complex conjugation

$A^\dagger \equiv$ Hermitean adjoint of A

$|\bar{a}\rangle \equiv$ antiparticle state relative to $|a\rangle$

C, P and $\vec{T}$ are symmetry transformations on the Hilbert space of particle states. C and P are unitary

$$C^\dagger C = I \qquad P^\dagger P = I$$

but $\vec{T}$ is antiunitary.

$$\vec{T} = T\vec{I} \qquad T^\dagger T = I$$

We also require that two applications of C or P result in no effect.

$$CC = I \qquad PP = I$$

Thus $C = C^\dagger \qquad P = P^\dagger$

C and P are Hermitean. Hence they are observables and their eigenvalues are <u>real</u>. The actions of C, P and $\vec{T}$ are defined on plane wave states of the form

$$|a_\mu(\underline{p})\rangle$$

where μ is the helicity and $\underline{p}$ is the three momentum of this (improper) state of particle a. C is the particle-antiparticle conjugation operator. It maps particle states onto the corresponding antiparticle states.

$$C\,|a_\mu(\underline{p})\rangle = \eta_{aC}\,|\bar{a}_\mu(\underline{p})\rangle$$

P is the parity operator. It maps particle states onto the

---

[1] In my treatment of the operators C, P, $\vec{T}$ I use many ideas gleaned from Professor Eyvind H. Wichmann.

corresponding states with the three spatial coordinates inverted.

$$P\,|a_\mu(\underline{p})\rangle = \eta_{aP}\,|a_{-\mu}(-\underline{p})\rangle$$

$\vec{T}$ is the time reversal operator. It maps particle states onto the corresponding states with the time coordinate inverted.

$$\vec{T}\,|a_\mu(\underline{p})\rangle = \eta_{\mu aT}\,|a_\mu(-\underline{p})\rangle$$

For a suitable definition of these states, the phase factors η_{aC} and η_{aP} are independent of μ and $\underline{p}$. They depend only on the type of particle. However, $\eta_{\mu aT}$ depends on the helicity as well as the type of particle.[2] The conditions $CC = I$ and $PP = I$ restrict η_{aC} and η_{aP} to be real. In the special cases that $|a_\mu(\underline{p})\rangle$ is an eigenstate of the relevant transformation the phase factor is observable and can, at least in principle, be determined by experiment. Except for these restrictions, however, the phase factors are arbitrary. We choose them as follows:

$$C\,|K^o(\underline{p})\rangle = -|\bar{K}^o(\underline{p})\rangle$$

$$P\,|K^o(\underline{p})\rangle = -|K^o(-\underline{p})\rangle$$

$$\vec{T}\,|K^o(\underline{p})\rangle = |K^o(-\underline{p})\rangle$$

---

[2]Let $\hat{e}_1$, $\hat{e}_2$, $\hat{e}_3$ be a set of orthogonal right-handed unit vectors. Then if $R(\psi\hat{e}_3)$ is a rotation of angle ψ about $\hat{e}_3$ and if $V(\underline{p})$ is a velocity transformation relating the rest state of the particle under consideration to the state with momentum $\underline{p}$, we define

$$|a_\mu(\underline{p})\rangle \equiv \frac{m}{\sqrt{m^2 + \underline{p}^2}}\, R(\psi_p\hat{e}_3)\, R(\theta_p\hat{e}_2)\, V(|\underline{p}|\hat{e}_3)\, |\alpha_\mu(0)\rangle$$

where $\underline{p} = |\underline{p}|(\sin\theta_p\cos\psi_p\hat{e}_1 + \sin\theta_p\sin\psi_p\hat{e}_2 + \cos\theta_p\hat{e}_3)$

Here m is the mass of the particle under consideration and $|\alpha_\mu(0)\rangle$ is the state of this particle with $\underline{p} = 0$ and 3-component of spin $= \mu$. This definition results in the dependence

$$\eta_{\mu aT} = \eta_{aT}e^{i\pi\mu}$$

where η_{aT} is independent of μ. It results in η_{aC} and η_{aP} being independent of μ as indicated.

$$C\,|\pi^{\alpha}(\underline{p})\rangle = |\bar{\pi}^{\alpha}(\underline{p})\rangle \qquad \alpha = +,\ 0,\ -$$

$$P\,|\pi^{\alpha}(\underline{p})\rangle = -|\pi^{\alpha}(-\underline{p})\rangle$$

$$\vec{T}\,|\pi^{\alpha}(\underline{p})\rangle = |\pi^{\alpha}(-\underline{p})\rangle$$

Due to non-conservation of C and P in weak interactions we cannot define the operations C and P acting separately on neutrinos but the products CP and $CP\vec{T}$ are well defined

$$CP\vec{T}\,|\nu_{\mu}(\underline{p})\rangle = e^{i\theta_{\mu}^{\nu}}\,|\bar{\nu}_{-\mu}(\underline{p})\rangle$$

For muons we have a similar equation.

$$CP\vec{T}\,|\mu_{\beta}(\underline{p})\rangle = e^{i\theta_{\beta}^{\mu}}\,|\bar{\mu}_{-\beta}(\underline{p})\rangle$$

As indicated above, the phase factors depend only on the helicity and type of particle.

Now in reality, of course, the states we deal with in the laboratory are not plane wave states. They are instead superpositions of plane wave states. Thus if

$$|K_2^o(\underline{p},s)\rangle \equiv \frac{1}{\sqrt{2}}\left(|K^o(\underline{p},s)\rangle - |\bar{K}^o(\underline{p},s)\rangle\right)$$

then the physical K_2^o state is of the form

$$|\psi_{K_2^o}\rangle = \int_{-\infty}^{\infty} d^3\underline{p}\ \Phi(\underline{p}) \int_0^{\infty} \frac{ds}{\sqrt{2E}}\, B(s,M_K^2)\ |K_2^o(\underline{p},s)\rangle$$

Here $\Phi(\underline{p})$ is the momentum space wave function and $B(s,M_K^2)$ is the mass distribution of the K_2^o. The quantity s is the square of the K_2^o energy in the frame with $\underline{p} = 0$ so that $B(s,M_K^2)$ is very strongly peaked at $s = M_K^2$. (M_K is the K_2^o mass.) We use the normalization conditions

$$\langle K_2^o(\underline{p}',s')|K_2^o(\underline{p},s)\rangle = \delta^3(\underline{p}' - \underline{p})\ \delta(E' - E) \qquad E = \sqrt{s + \underline{p}^2}$$

$$\int d^3\underline{p}\ |\Phi(\underline{p})|^2 = 1 \qquad \int_0^{\infty} ds\ |B(s,M_K^2)|^2 = 1$$

Thus

$$CP\,|\psi_{K_2^o}\rangle = \int_{-\infty}^{\infty} d^3\underline{p}\ \Phi(\underline{p}) \int_0^{\infty} \frac{ds}{\sqrt{2E}}\, B(s,M_K^2)\ (-1)\,|K_2^o(-\underline{p},s)\rangle$$

$$= -\int_{-\infty}^{\infty} d^3\underline{p}\ \Phi(-\underline{p}) \int_0^{\infty} \frac{ds}{\sqrt{2E}}\, B(s,M_K^2)\ |K_2^o(\underline{p},s)\rangle$$

So, strictly speaking, the physical K_2^o state is not an eigenstate of CP unless $\Phi(\underline{p}) = \Phi(-\underline{p})$.[3] Nevertheless, the normal heuristic arguments made from the K meson rest frame are valid. Consider the decay to two pions. After the decay the overall momentum distribution and mass distribution must remain unchanged. Hence the final state is of the form

$$|\psi_{\pi\pi}\rangle = \int_{-\infty}^{\infty} d^3\underline{p}'\ \Phi(\underline{p}') \int_0^{\infty} \frac{ds'}{\sqrt{2E'}}\, B(s',M_K^2)\ |\pi\pi(\underline{p}';s')\rangle$$

so that if we define the Lorentz invariant amplitude $\mathcal{M}$ by

$$\langle\pi\pi(\underline{p}',s)|H_w|K_2^o(\underline{p},s)\rangle = -i(2\pi)^4\,\delta^3(\underline{p}-\underline{p}')\,\delta(E-E')\,\frac{\mathcal{M}\left(\pi\pi|H_w|K_2^o(\underline{p},s)\right)}{\sqrt{(2\pi)^9\ 2E_K 2E_{\pi_1} 2E_{\pi_2}}}$$

then

$$\langle\psi_{\pi\pi}|H_w|\psi_{K_2^o}\rangle$$

$$= \int_{-\infty}^{\infty} d^3\underline{p}\ |\Phi(\underline{p})|^2 \int_0^{\infty} ds\ |B(s,M_K^2)|^2\ (-1)(2\pi)^4\,\frac{\mathcal{M}\left(\pi\pi|H_w|K_2^o(\underline{p},s)\right)}{\sqrt{(2\pi)^9\ 2E_K 2E_{\pi_1} 2E_{\pi_2}}}$$

$$= \int_0^{\infty} ds\ |B(s,M_K^2)|^2\,\mathcal{M}\left(\pi\pi|H_w|K_2^o(0,s)\right) \int_{-\infty}^{\infty} d^3\underline{p}\,\frac{|\Phi(\underline{p})|^2\ (-1)(2\pi)^4}{\sqrt{(2\pi)^9\ 2E_K 2E_{\pi_1} 2E_{\pi_2}}}$$

---

[3] This condition is satisfied in the rest frame of a Gaussian wave packet (as defined by the average momentum and position) but is obviously not true in general.

We have used the fact that $\mathcal{M}$ is Lorentz invariant to evaluate it in the frame where $\underline{p} = 0$. Thus we see that the physical matrix element is rigorously proportional to the plane wave invariant amplitude evaluated in the frame with the K momentum equal to zero. Hence decays forbidden by the CP invariance arguments using plane wave states are rigorously forbidden. In fact, to more accuracy than we would probably ever need

$$\langle \psi_{\pi\pi} | H_w | \psi_{K_2^0} \rangle = -i\,(2\pi)^4 \frac{\mathcal{M}\left[\pi\pi | H_w | K_2^0(0, M_K^2)\right]}{\sqrt{(2\pi)^9\, 2E_K 2E_{\pi_1} 2E_{\pi_2}}}$$

where the energies have been evaluated at $s = M_K^2$ and $\underline{p} = \underline{p}_0$ the average momentum of $\Phi(\underline{p})$.

Finally we wish to find the CP eigenvalue of the $\pi^+\pi^-$ state with $\underline{p} = 0$, energy $= M_K$, total angular momentum ℓ with third component m. If $\pi_+^\dagger(\underline{q})$ is the creation operator for a π^+ meson of momentum $\underline{q}$ this $\pi^+\pi^-$ state is

$$|\pi^+\pi^-(0, M_K)(\ell, m)\rangle = \frac{\omega^2 |\underline{q}|}{M_K} \int d\Omega_{\underline{q}} Y_{\ell m}(\Omega_{\underline{q}}) \pi_+^\dagger(\underline{q})\, \pi_-^\dagger(-\underline{q}) |\text{ vacuum}\rangle$$

where $\omega = \sqrt{m_\pi^2 + \underline{q}^2}$ and $M_K = 2\omega$. So

$$\begin{aligned}
CP|\pi^+\pi^-(0, M_K)(\ell, m)\rangle &= C \frac{\omega^2 |\underline{q}|}{M_K} \int d\Omega_{\underline{q}} Y_{\ell m}(\Omega_{\underline{q}}) \left(-\pi_+^\dagger(-\underline{q})\right)\left(-\pi_-^\dagger(\underline{q})\right) |\text{vacuum}\rangle \\
&= C \frac{\omega^2 |\underline{q}|}{M_K} \int d\Omega_{\underline{q}} Y_{\ell m}(\Omega_{-\underline{q}}) \pi_+^\dagger(\underline{q}) \pi_-^\dagger(-\underline{q}) |\text{vacuum}\rangle \\
&= (-1)^\ell \frac{\omega^2 |\underline{q}|}{M_K} \int d\Omega_{\underline{q}} Y_{\ell m}(\Omega_{\underline{q}}) \pi_-^\dagger(\underline{q}) \pi_+^\dagger(-\underline{q}) |\text{vacuum}\rangle \\
&= (-1)^\ell \frac{\omega^2 |\underline{q}|}{M_K} \int d\Omega_{\underline{q}} Y_{\ell m}(\Omega_{-\underline{q}}) \pi_+^\dagger(\underline{q}) \pi_-^\dagger(-\underline{q}) |\text{vacuum}\rangle \\
&= (-1)^{2\ell} |\pi^+\pi^-(0, M_K)(\ell, m)\rangle
\end{aligned}$$

Thus $CP = (-1)^{2\ell} = +1$ for any ℓ.

Appendix 2: Implications of CP Invariance for the K Meson States

Theorem: If CP is absolutely conserved in nature, the neutral K meson states with definite lifetimes must be eigenstates of CP.[1]

Proof:

Absolute CP conservation means

$$[CP,H] = 0$$

where H is the total Hamiltonian of the universe.

$$\left([CP,H] \equiv CPH - HCP\right)$$

Schrodinger's equation for the time evolution operator U(t) is

$$i\frac{\partial U}{\partial t} = HU \qquad\qquad U(0) = I$$

But if CP is conserved,

$$i\frac{\partial}{\partial t}\left(CPU(CP)^{-1}\right) = H\left(CPU(CP)^{-1}\right) \qquad\qquad CPU(0)(CP)^{-1} = I$$

U and $CPU(CP)^{-1}$ satisfy the same Schrodinger equation and same initial condition. Hence

$$U = CPU(CP)^{-1}$$

or $$[CP,U] = 0$$

and states of definite CP will remain eigenstates with the same value of CP.

The neutral K meson system is observed to decay in two components K_S^0 and K_L^0 with definite but unequal lifetimes

---

[1] I would like to thank Donald Brandschaft for some of the ideas involved in this proof.

τ_S and τ_L.[2]

Thus

$$|K_S^o(t)\rangle = U(t)|K_S^o(0)\rangle = e^{-im_S t} e^{-\frac{t}{2\tau_S}} |K_S^o(0)\rangle + \sum_j c_j^S(t)|j_S\rangle$$

$$|K_L^o(t)\rangle = U(t)|K_L^o(0)\rangle = e^{-im_L t} e^{-\frac{t}{2\tau_L}} |K_L^o(0)\rangle + \sum_j c_j^L(t)|j_L\rangle$$

$$CP|K_L^o(t)\rangle = U(t)CP|K_L^o(0)\rangle = e^{-im_L t} e^{-\frac{t}{2\tau_L}} CP|K_L^o(0)\rangle + \sum_j c_j^L(t)CP|j_L\rangle$$

where the states $|j_S\rangle$ and $|j_L\rangle$ represent decay products. We see that $CP|K_L^o\rangle$ and $|K_L^o\rangle$ have the same lifetime. Now the state $CP|K_L^o\rangle$ is a neutral K meson state. We assume $|K_L^o\rangle$ and $|K_S^o\rangle$ form a basis for the neutral K meson system (no third neutral K meson) so that

$$CP|K_L^o\rangle = \alpha|K_L^o\rangle + \beta|K_S^o\rangle$$

for some α and β. But the term $\beta|K_S^o\rangle$ has the wrong lifetime. Hence $\beta = 0$ and

$$CP|K_L^o\rangle = \alpha|K_L^o\rangle$$

and similarly for some β

$$CP|K_S^o\rangle = \beta|K_S^o\rangle$$

The states of definite lifetimes are eigenstates of CP.

The corresponding theorem for the $CP\vec{T}$ transformation is not true due to the antiunitary nature of this transformation (and the i in Schrodinger's equation).

---

[2] $\tau_S = (.865 \pm .009) \times 10^{-10}$ seconds from Hill et. al., Phys. Rev., 171, 1418 (1968). $\tau_L = (5.154 \pm 0.044) \times 10^{-8}$ seconds from Vosburgh et. al., Phys. Rev. Lett. 26, 866 (1971).

Appendix 3: Relationship Between δ and ε

If we define the invariant amplitudes

$$f_{ij}(D) \equiv \mathcal{M}(\pi^- \mu_i^+ \nu_j | \mathcal{H}_w | K^0) \qquad \Delta S = \Delta Q$$

$$g_{ij}(D) \equiv \mathcal{M}(\pi^- \mu_i^+ \nu_j | \mathcal{H}_w | \overline{K^0}) \qquad \Delta S = -\Delta Q$$

as functions of the Dalitz plot variables D and lepton helicities i and j, and if we assume that $K^0_{\mu 3}$ decay proceeds by CP$\overset{+}{\text{T}}$-invariant first-order weak interactions only, then the charge asymmetry is

$$\delta(\mathcal{R}_D) = 2\,Re\,\varepsilon\left[\frac{1 - \langle x^+x\rangle}{(1+|\varepsilon|^2)(1+\langle x^+x\rangle) - 2(1-|\varepsilon|^2)Re\langle x\rangle - 4\,Im\,\varepsilon\, Im\langle x\rangle}\right]$$

for a given region of the Dalitz plot $\mathcal{R}_D$. We define the matrix X and its average value by

$$g = x f$$

$$\langle x \rangle = \frac{\sum_{\mathcal{R}_D} Tr(f^+ x f)}{\sum_{\mathcal{R}_D} Tr(f^+ f)}$$

So to first order in ε we obtain

$$\delta(\mathcal{R}_D) = 2\,Re\,\varepsilon\left[\frac{1 - \langle x^+x\rangle}{1 - 2\,Re\langle x\rangle + \langle x^+x\rangle}\right]$$

If we then assume X is equal to a number X_N times the unit matrix, the charge asymmetry is given by

$$\delta(R_D) = 2\,Re\,\varepsilon\left[\frac{1 - |X_N|^2}{|1 - X_N|^2}\right]$$

We note that the above assumption that the decay proceeds by first-order weak interactions only is invalid in the presence of electromagnetic final state interactions.

Appendix 4: Correlated Tracks Not Forming a Vertex

One type of event which we may have accepted possessing correlated tracks not forming a vertex is indicated below:

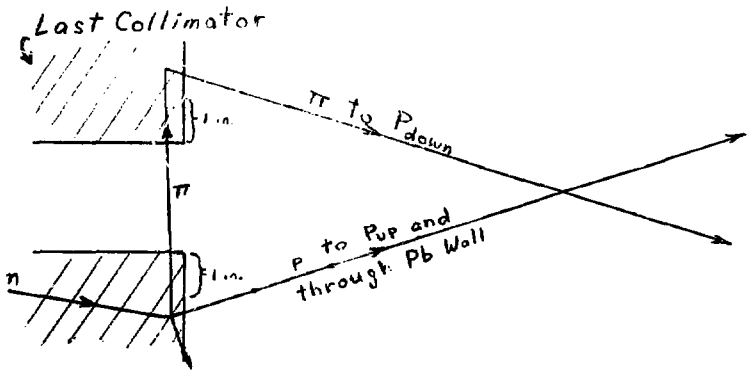

A neutron produces a high energy proton in the collimator which simulates a muon, and the neutron also produces a low momentum pion which passes into the other face of the collimator. In order to trigger our system the pion must pass 1 inch into the other face and then backscatter into the P_{down}. If we do not require the pion P in the signature criteria, we find that

$$\frac{\text{muon tracks}}{K^{o}_{\mu 3}} = 1.2 \qquad \delta_{\text{muon tracks}} = 0.13 \quad .$$

Thus the asymmetric muon tracks which we accept number 15% of our $K^{o}_{\mu 3}$ events. If we assume <u>all</u> these muons are associated with a pion passing into the opposite face of the collimator and that this pion scatters isotropically when it reaches a point 2 inches into the other face, the net bias on the charge asymmetry is

$$\Delta\delta = 0.15 \times 2/3 \times (1.4 \times 10^{-5}) = 1.4 \times 10^{-6} \quad .$$

absorption of pion ↑ ; solid angle of P_{down} ↑

The above type of event is probably the most dangerous type not originating from a vertex since it produces a low momentum pion and thus would probably not appear in the vertex distribution (Figure 7) because the pion would not reach the R bank.